Experimental Investigation of the Al-Ca-Zn system

Shabnam Konica

A Thesis
in
The Department
of
Mechanical and Industrial Engineering

Presented in Partial Fulfillment of the Requirements
for the Degree of Master of Applied Science (Mechanical Engineering) at
Concordia University
Montreal, Quebec, Canada

January 2013

CONCORDIA UNIVERSITY
School of Graduate Studies

This is to certify that the thesis prepared

By: **Shabnam Konica**

Entitled: **Experimental investigation of the Al-Ca-Zn system**

and submitted in partial fulfillment of the requirements for the degree of

Master of Applied Science in Mechanical Engineering

complies with the regulations of the University and meets the accepted standards with respect to originality and quality.

Signed by the final examining committee:

Dr. Hoi Dick Ng Chair

Dr. Zhigang Tian Examiner

Dr. Rolf Wüthrich Examiner

Dr. Mamoun Medraj Supervisor

Approved by _____
Chair of Department or Graduate Program Director

_____
Dean of Faculty

Date May 14, 2013

ABSTRACT

Experimental Investigation of the Al-Ca-Zn System

Shabnam Konica

In this work, the isothermal section of the Al-Ca-Zn system has been investigated at 350°C using 5 diffusion couples and 26 key alloys. The actual compositions of the alloys are measured by inductively coupled plasma technique. Phase relations and solubility limits of the binary and ternary compounds have been determined by means of electron probe microanalysis and X-ray diffraction. In the current work, five ternary compounds have been found, three of which are reported for the first time: ternary intermetallic IM1 with the formula $Al_xCa_{8.5}Zn_y$ ($26\leq x\leq 29$, $62\leq y\leq 65$at 350ºC), ternary intermetallic IM3 with the formula $Al_{3-x}CaZ_x$ ($2\leq x\leq 2.2$ at 350^{o}C) and ternary intermetallic IM5 with the formula $Al_2Ca_9Zn_3$. The crystal structure information of IM1 has been studied by X-ray diffraction technique. XRD data has shown that IM1 is a solid solution that crystallizes in a cubic structure with $Pm\bar{3}m$ (221) space group having $BaHg_{11}$ prototype. The homogeneity ranges of IM2 and IM4 have been determined at 350^{o}C. Binary compounds $Al_{14}Ca_{13}$, Al_2Ca, Al_4Ca, $CaZn_2$, $CaZn_3$, $CaZn_5$, $CaZn_{11}$ and $CaZn_{13}$ have extended solid solubility into the ternary system. For $Al_{14}Ca_{13}$, Al_2Ca and Al_4Ca, Al-atom is substituted by Zn. For $CaZn_2$, $CaZn_3$, $CaZn_5$, $CaZn_{11}$ and $CaZn_{13}$ Zn is substituted by Al.

ACKNOWLEDGEMENTS

This project would not have been possible without the help of several individuals, who in one way or another contributed their valuable assistance in the completion of this study. First of all, I would like to express my gratitude to my thesis supervisor, Dr. Mamoun Medraj for his constant support, guidance and suggestions.

I would like to thank Research Associate, Dr. Dmytro Kevorkov for his continuous supervision and constructive suggestions both in experimental works and technical writing.

I would like to acknowledge the help of Ms. Ming Wei and Mr. Alain Tessier from the chemistry department of Concordia University in conducting the Inductively Coupled Plasma-Mass Spectrometry measurements. In addition, I want to thank Mr. Lang Shi from McGill University for his help with EPMA experiments.

I am grateful to all of my group members for their support during the research.

Furthermore, financial support from General Motors of Canada Ltd. and NSERC through the CRD grant program is gratefully acknowledged.

TABLE OF CONTENTS

LIST OF ABBREVIATIONS

OM	Optical Microscopy
SEM	Scanning Electron Microscopy
EPMA	Electron Probe Microanalysis
XRD	X-ray Diffraction
ICP	Inductively Coupled Plasma
SSDC	Solid-Solid Diffusion Couple
SLDC	Solid-Liquid diffusion Couple
KS	Key Sample

LIST OF FIGURES

LIST OF TABLES

CHAPTER 1

INTRODUCTION

1.1 Importance of the Al-Ca-Zn system

Aluminum and its alloys are the prime structural material used in aircraft industry. The combination of acceptable cost, good mechanical properties, low density, good creep resistance, structural integrity and ease of fabrication makes them attractive to the automobile industry as well. Aluminum sheet is gradually becoming more reputable in automotive engineering. However, when it comes to formability steel sheets still remains the benchmark material. A theoretical improvement in the formability of aluminum sheet can be achieved using superplastic forming [1, 2].

The Al-Zn and Al-Al_4Ca alloys exhibit superplastic behavior at elevated temperatures [3]. However they are brittle at room temperature and cannot be cold rolled industrially. Interestingly, Al alloys containing both Ca and Zn can overcome this problem [4, 5]. Al-alloy containing 5wt.% Ca and 5wt.% Zn shows superplastic forming behavior at room temperature and can provide the general properties of a superplastic alloy with the inherent advantages of aluminum [4]. Also it can be produced by mass production methods standard in the aluminum industry [4].

Another important application of Al-alloys containing Ca and Zn is as corrosion protector devices. These protective materials are characterized by their high current efficiency and

long service life, which can be successfully used for the protection of underground and underwater pipelines, reservoirs, oil storages, drilling rigs, municipal communications, continental self-structures etc. For the conventional aluminum protectors working in soils, it is necessary to use special activators (solutions of salts) to prevent the formation of passivating films on the surfaces of protectors in the process of operation. Whereas, aluminum based protective materials containing calcium and zinc do not require activating solutions and can overcome that difficulty [6].

Mg-Al based alloys are one of the most important alloys among all the Mg based alloys and are attractive to the automotive manufacturers. Among them, the AZ91 series, Mg-9%Al-1%Zn alloys have a good performance at room temperature but they exhibit poor creep resistance at elevated temperatures because of the precipitation of γ-$Al_{12}Mg_{17}$ phase. However a small amount of addition of Ca in the Mg-Al-Zn alloys can significantly improve the thermal stability and creep resistance and is also able to maintain lower cost compared to other solutions for this problem using the expensive rare earth elements [7]. Therefore, it is important to understand the Mg-Al-Ca-Zn quaternary system. Without in-depth knowledge about the Al-Ca-Zn ternary system, it is not possible to achieve maximum benefit from this quaternary system. Hence it is important to establish the phase relationships in this system experimentally, which is the objective of the present research.

Phase diagram is the base of many fundamental material research fields such as phase transformation, solidification, crystal growth, joining, prediction of the degree of

microsegregation and inclusion (or second-phase) formation, oxidation, etc. It also acts as a guideline for material design and processing conditions to obtain the desired microstructures and mechanical properties [8]. Moreover, to improve the mechanical properties, several elements are often mixed. These multi-component systems have complex phase relationships. Therefore, a phase diagram is indispensable for better understanding of these complex phase relations and predicting the possibility of phase formation. In this work, the experimental Al-Ca-Zn ternary phase diagram will be constructed, which will be helpful to predict the phase relationships and the formation of intermetallics. These details are needed for accurate thermodynamic modeling of the system.

1.2 Challenges of the Al-Ca-Zn system

The Al-Ca-Zn system is challenging for experimental investigation because of the following factors:

1. Calcium is highly reactive in air and therefore special procedures and precautions are required to prepare alloys with relatively high calcium content.
2. The Al-Ca and Ca-Zn binary systems contain 4 and 8 intermetallics, respectively. Naturally, this indicates that the Al-Ca-Zn ternary system will probably contain significant number of binary interactions such as solid solutions and ternary compounds leading to a comparatively complicated phase relation among the phases.

A number of researchers investigated the system from 0 to 33 at.% Ca [4, 9-16]. However their work was mostly limited to the understanding of certain properties of some alloys, such as tensile strength, or to study the crystal structure of certain compounds. To date no extensive study has been performed to understand the complete system, including phase relations and solubility limits of the phases in this system. Phase relations and solubility data are also required for the thermodynamic calculation of the phase diagram. Thus it is evident that the system needs to be thoroughly investigated to obtain the missing information. This will be performed during the current work.

1.3 Objectives

The aim of the present work is to provide experimental information about the thermodynamically stable binary and ternary Al-Ca-Zn phases, their homogeneity ranges, crystal structures and phase relationships. Hence the present work mainly focuses on:

- Determination of the phase relations and solubility limits of the binary and ternary compounds by metallographic examination, SEM, EPMA and X-ray diffraction techniques.
- Analyzing the morphology of diffusion couples in the Al-Ca-Zn system at 350^{o}C
- Studying the crystal structures of the ternary compounds using X-ray diffraction technique.
- Construction of the Al-Ca-Zn isothermal section at 350ºCexperimentally.

CHAPTER 2

LITERATURE REVIEW

2.1The Al-Ca binary system

2.1.1 Phase diagram data

Most of the experimental investigations of the Al-Ca system deal mainly with the Al-rich side, which is technically interesting for the aluminum alloys. Donski [9] carried out the first attempt to construct the Al-Ca system using thermal analysis. Later, Matsuyama [10] investigated the system by thermal analysis, electrical resistance and microscopic examination. The entire Al-Ca system was investigated by Kevorkov and Schmid-Fetzer [11] who used X-ray diffraction, SEM/EDX analysis, metallographic and diffusion couple techniques. They [11] reported four intermetallic compounds; Al_4Ca, Al_2Ca, AlCa and Al_3Ca_8. According to by Matsuyama [10] and Kevorkov and Schmid-Fetzer [11], Al_4Ca decomposes at 700^oC whereas Donski [9] reported the value as 690^oC. Kevorkov and Schmid-Fetzer [11] reported that Al_2Ca melts congruently at 1086^oC compared to Matsuyama's [10] value of 1079^oC, AlCa melts incongruently at 633^oC [11] and Al_3Ca_8 melts congruently at 579^oC [11]. However, Huang and Corbett [12] reported the occurrence of $Al_{14}Ca_{13}$ compound with monoclinic structure instead of AlCa. Nowotny et al. [13] determined the crystal structure of Al_4Ca and Al_2Ca as bct and fcc, respectively. Huang and Corbett [12] investigated the crystal structures of $Al_{14}Ca_{13}$ and Al_3Ca_8 using X-ray analysis and noted that they have monoclinic and triclinic structures,

respectively. According to Kevorkov and Schmid-Fetzer [11], the solubility regions of Ca in (Al) and Al in (Ca) are negligible.

Matsuyama [10] reported two eutectic reactions, one in the Al-rich side and other in the Ca-rich side and determined most of the liquidus lines. According to Matsuyama [10], the eutectic in the Al-rich region occurs at 5.2 at.% Ca and 616^{o}C compared to the value reported by Donski [9] 5.5 at.% Ca and 610^{o}C; whereas Kevorkov and Schmid-Fetzer [11] reported these values at 5.1 at.% Ca and 613^{o}C. The other eutectic is in the Ca-rich side.According to Matsuyama [10], it occurs at 64.5 at.% Ca and 545^{o}C compared to Donski's [9] values at 66.9 at.% Ca and 550^{o}C. However, later Kevorkov and Schimid-Fetzer [11] reported the occurrence of two eutectic reactions instead of one in the Ca-rich side; one at 66.2 at.% Ca and 556^{o}C and the other one at 79.5 at.% Ca and 560^{o}C. The eutectic reactions are given at Table 2.1.1

Table 2.1.1 The eutectic reactions and compositions of the Al-Ca system

Reaction	At.% Ca	Temperature,^{o}C	Reference
L ↔Al-fcc + Al_4Ca	5.50 5.20 5.10	610 616 613	[9] [10] [11]
L ↔$A_{14}Ca_{13}$+Al_3Ca_8	66.9 64.5 66.2	550 545 556	[9] [10] [11]
L↔Ca-bcc+Al_3Ca_8	79.5	560	[11]

2.1.2 Thermodynamic data

The enthalpy of formation of Al_4Ca and Al_2Ca compounds were measured by Notin et al. [14]. They [14] determined the enthalpy of formation of these two compounds at 765^{o}C.

They recorded calorimetric signals that corresponded to the enthalpy change during the addition of the solid Ca in the Al-melt. There is a reasonable agreement with the values of enthalpy of formation for Al_2Ca between Notin et al. [14] and Kevorkov et al. [15]. According to Kevorkov et al. [15], the small difference between them may be due to difference in heat capacity, for the formation reaction between room temperature and 765^{o}C. However, there is no experimental enthalpy of formation data available for $Al_{14}Ca_{13}$ compound due to the peritectic formation and slow kinetic of the phase and thus difficulty of preparing $Al_{14}Ca_{13}$ rich sample [15]. The enthalpy of formation of the Al_3Ca_8 phase was measured using drop solution calorimetry by Kevorkov et al. [15]. Aljarrah and Medraj [16] calculated the enthalpy of formation of these compounds thermodynamically and compared with the experimental results of [14, 15] as demonstrated in Figure 2.1.

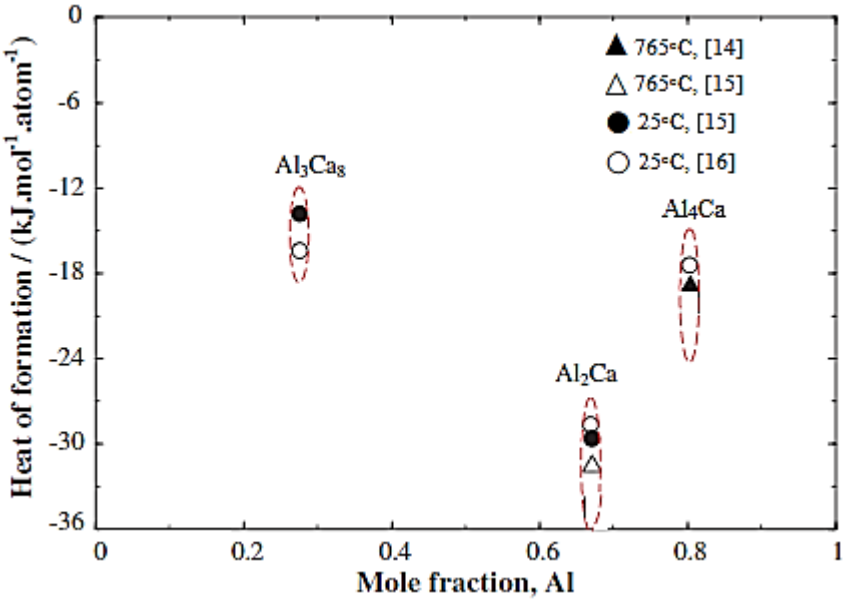

Figure 2.1: Heat of formation against mole fraction of Al for different intermetallic compounds in the Al-Ca system by Aljarrah and Medraj [16]

The enthalpy of mixing of Al and Ca in liquid Al-Ca alloys was measured by Sommer et al. [17] and Esin et al. [18] and their results agree fairly well with each other. The enthalpy of mixing was thermodynamically calculated at 827^{o}C and compared with experimental results by Wasiur-Rahman [19]. The results obtained by [19] are demonstrated in Figure 2.2. The thermodynamic calculation of [19] shows good agreement with the experimental results except in the region of ~0.2at% Ca. The possible deviation could be due to the formation of Al_4Ca phase, the heat of formation decreased due to solidification.

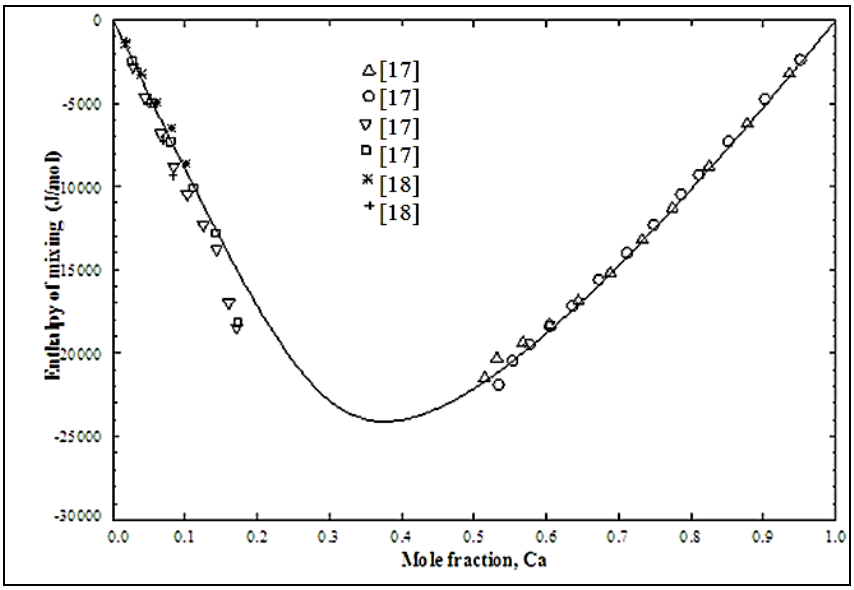

Figure 2.2: Calculated enthalpy of mixing of liquid Al-Ca alloys at 827^{o}C by Wasiur-Rahman [19] in comparison with the experimental results [17, 18]

Jacob et al. [20] determined the activity of the components in the Al-Ca liquid using Knudsen effusion method for alloys in the compositional ranges less than 38 at.% and greater than 44 at.% Ca at 1100^{o}C. Schürmann et al. [21] measured the activity of Ca in the liquid alloys using boiling point determination technique. The results of Jacob et al. [20] and Schürmann et al. [21] agree reasonably well. Wasiur-Rahman [19] calculated the

activity of the components in the liquid Al-Ca alloys thermodynamically. The activity of the Al-Ca alloys calculated by Wasiur-Rahman [19] shows deviation from the experimental works as depicted in Figure 2.4. However, he mentioned that better agreement was not achievable without deteriorating the liquidus curves [19].

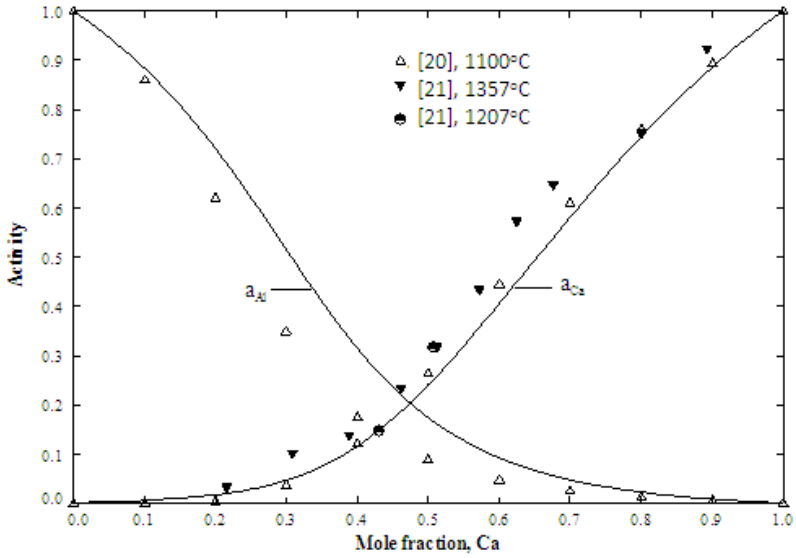

Figure 2.3 Calculated activity of Al and Ca in the liquid at 1100°C [19] in comparison with experimental works [20, 21]

Kevorkov and Schimid-Fetzer [11] calculated the phase diagram of the Al-Ca system using random solution model. In order to adjust the liquidus around Al_2Ca, their calculated enthalpy of mixing deviated from experimental data by shifting the liquidus line of Al_2Ca to a higher temperature. Ozturk et al. [22] used both random and associate model to re-optimize the Al-Ca system. They found that while the random solution model gives better agreement with experimental phase diagram, the associate model agrees well with the experimental thermodynamic data [22]. Later, Aljarrah and Medraj [16] executed critical evaluation of all the available experimental works in the literature and re-optimized the system. They [16] used the modified quasichemical model for the liquid

phase in order to account for the presence of short range ordering. Nevertheless, there was a little deviation of some of their [16] calculated invariant points with experimental results. This was improved by Wasiur-Rahman and Medraj [23] who also used the modified quasichemical model for the liquid phase. In their work [23], they made some adjustments in the values of the composition dependent coordination numbers and the excess Gibbs energy parameters to increase the consistency with the experimental results. In the present work, the results of Wasiur-Rahman and Medraj [19, 23] will be mostly considered. The calculated Al-Ca phase diagram based on the optimization of Wasiur-Rahman [19] is demonstrated in Figure 2.4.

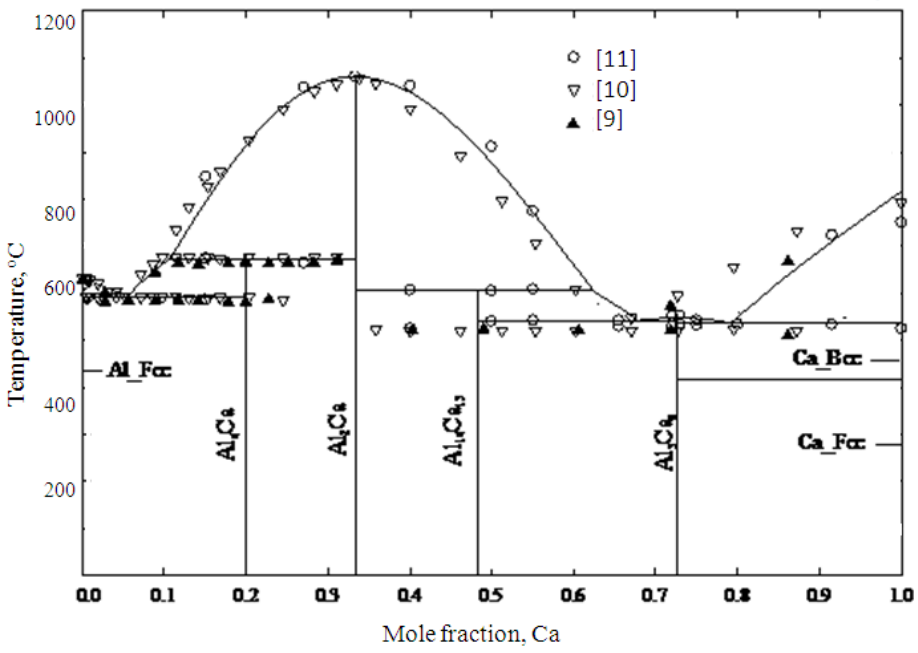

Figure 2.4: The Al-Ca phase diagram based on the optimization of Wasiur-Rahman [14] in comparison with the experimental results [9-11]

2.2 The Ca-Zn binary system

2.2.1 Phase diagram data

Donski [9] studied the Ca-Zn system using thermal analysis. But the alloys were prepared in open glass tubes using materials which were impure by modern standards [19]. Paris [24] investigated the system by thermal and micrographic analysis. Later, the Ca-Zn system was investigated by Messing et al. [25] using differential thermal analysis supplemented by X-ray diffusion and vapor effusion measurement. They reported eight compounds in the system: Ca_3Zn, Ca_7Zn_4, CaZn, $CaZn_2$, Ca_7Zn_{20}, $CaZn_5$, $CaZn_{11}$ and $CaZn_{13}$. According to their thermal analysis, the compounds $CaZn_2$, $CaZn_5$ and $CaZn_{11}$ melt congruently at 704^{o}C, 695^{o}C and 724^{o}C, respectively. The other compounds Ca_3Zn, Ca_7Zn_4, CaZn, Ca_7Zn_{20} and $CaZn_{13}$ undergo peritectic decomposition at 394^{o}C, 414^{o}C, 439^{o}C, 642^{o}C and 669^{o}C, respectively. Itkin and Alcock [26] revised the phase diagram, replacing Ca_7Zn_4 and Ca_7Zn_{20} listed by Messing et al. [25], with Ca_5Zn_3 and $CaZn_3$, respectively, based on the crystallographic data in the literature [27, 28]. Messing et al. [25] reported 3 eutectic reactions occurring at 27.4 at.% Zn and 394^{o}C, at 76.4 at.% Zn and 638^{o}C and at 86.4 at.% Zn and 690^{o}C. The eutectic reactions and phase compositions are given in Table 2.2.1.

The crystal structure data and lattice parameters of the phases in the Ca-Zn system (Table 2.2.2) were determined in a number of studies using X-ray analysis [27-36]. Ketelaar [29] discovered the crystal structure of $CaZn_{13}$ with fcc structure and lattice parameter a=12.13Å. This result was confirmed in the work of Iandelli and Palenzona [30] who reported the value of lattice parameter, a=12.185Å. Iandelli and Palenzona [30] also

determined the crystal structure of $CaZn_{11}$ as $BaCd_{11}$ prototype with a=10.699Å. Haucke [31] determined that the compound $CaZn_5$ has a hexagonal lattice, with parameters a= 5.405 and c= 4.183Å. Messing et al. [25] assumed that $CaZn_5$ has a narrow homogeneity range, but they did not define it accurately. Recently, Wendroff and Röhr [32] reported that the binary compound $CaZn_5$ has a continuous variation in the range 14.3-16.7 at.% Ca, corresponding to the change of the stoichiometry from 1:5 to 1:6 with a continuous structural change from $CaCu_5$ to $TbCu_7$. The orthorhombic structure of $CaZn_2$ was reported by Schulze and Wieting [33] with the lattice parameters a=4.591, b=7.337 and c=7.667Å. The formula of the compounds Ca_7Zn_4 and Ca_7Zn_{20} reported by Messing et al. [25] were revised [27, 28]. Bruzzone et al. [27] prepared an alloy of the composition Ca_5Zn_3 by melting 99.99 wt.% Ca and 99.99 wt.% Zn in sealed iron crucibles, followed by slow cooling and annealing. The result showed a single homogeneous phase with a tetragonal structure of the Cr_5B_3 type and parameters a=7.954 and c=15.443Å. The formula Ca_5Zn_3 was recommended instead of Ca_7Zn_4 [27]. Fornasini and Merlo [28] prepared the compound $CaZn_3$ by melting 99.9 wt.% Ca and 99.999 wt.% Zn in sealed tantalum crucibles, with subsequent annealing at 550^{o}C and found that $CaZn_3$ compound had a hexagonal structure and it exhibited a small homogeneity range from 74 to 75 at.% Zn at 550^{o}C with lattice parameters varying from a=9.157 and c=7.297Åto a=9.168 and c=7.327 Å. Fornasini and Merlo [28] analyzed the crystal structure of $CaZn_3$ using single crystal x-ray diffractometer and described the structure of $CaZn_3$ as a random mixture of two types of elementary cells with the same symmetry and dimensions, but in different composition and atomic arrangement; two thirds of total number of cells is nearly identical to $BaLi_4$, whereas the rest have an arrangement similar to $CeCu_2$. The structures

of the compounds CaZn and Ca_3Zn were identified by Fornasini et al. [34]. Both compounds have the orthorhombic structure. The lattice parameters for CaZn is, a=4.202, b=11.61 and c=4.442Å and for Ca_3Zn, a=4.15, b=13.258 and c=11.086Å.

Table 2.2.1Eutectic reactions and compositions of the phases of the Ca-Zn system

Reaction Type	Reaction	Composition (at.% Zn)	Temperature (^oC)	Reference
Eutectic	$L \leftrightarrow Ca_3Zn + Ca_5Zn_3$	27.4	391	[25]
	$L \leftrightarrow CaZn_3 + CaZn_5$	76.4	638	[25]
	$L \leftrightarrow CaZn_5 + CaZn_{11}$	86.4	690	[25]

Table 2.2.2 Crystal structure information of the phases of the Ca-Zn system

Phase	Compo -sition, at.% Zn	Pearson Symbol	Space group	Structure designa -tion	Prototype	Lattice parameters, Å			Ref.
						a	b	c	
β(Ca)	0	cI2	$Im\bar{3}m$	A2	W	4.48	-	-	[35]
α(Ca)	0	cF4	$Fm\bar{3}m$	A1	Cu	5.59	-	-	[35, 36]
Ca_3Zn	25	oC16	Cmcm	$E1_a$	BRe_3	4.15	13.258	11.086	[34]
Ca_5Zn_3	37.5	tI32	I4/mcm	$D8_l$	Cr_5B_3	7.954	-	15.453	[27]
CaZn	50	oC8	Cmcm	B_f	CrB	4.202	11.61	4.442	[34]
$CaZn_2$	66.7	oI12	Imma	-	$CeCu_2$	4.591	7.337	7.667	[33]
$CaZn_3$	74	hP32	$P6_3/mmc$	-	$CaZn_3$	9.157	-	7.297	[28]
$CaZn_5$	83.3	hP6	P6/mmm	$D2_d$	$CaCu_5$	5.405	-	4.183	[31]
$CaZn_{11}$	91.7	tI48	$I4_1/amd$	-	$BaCd_{11}$	10.699	-	-	[30]
$CaZn_{13}$	92.9	cF112	Fm3c	-	$NaZn_{13}$	12.13	-	-	[29]
Zn	100	hP2	$P6_3/mmc$	A3	Mg	0.266	-	0.495	[36]

Itkin and Alcock [26] assessed the Ca-Zn system based mainly on the work of Messing et al. [25].Their calculated Ca-Zn phase diagram is shown in Figure 2.5. Later, in 2002, Brubaker and Liu [37] re-optimized the system based on the same work of [25]. They

assumed the liquid phase as substitutional solution phase and modeled it using sublattice model with all the intermetallic compounds. However, they proposed a new interpretation by reporting the $CaZn_3$ to undergo congruent melting which was reported to be incongruent melting by previous investigators. Moreover, if $CaZn_3$ is a congruently melting compound then the liquidus of the $CaZn_3$ on the Ca-rich side becomes too flat. According to Okamoto and Massaiski [38], this is thermodynamically improbable. Hence, the phase diagram calculated by Brubaker and Liu [37] will not be considered in this work. The Ca-Zn phase diagram was most recently calculated almost simultaneously by two different research groups [39, 40]. Both Spencer et. al. [39] and Wasiur-Rahman and Medraj [40] used the modified quasichemical model considering the short-range ordering in the liquid phase and their results agreed fairly well with each other. Both research groups considered the incongruent melting of the $CaZn_3$ phase. The calculated Ca-Zn phase diagram of [39] is demonstrated in Figure 2.6. In this work, the results of [39, 40] are used to calculate the Al-Ca-Zn phase diagram.

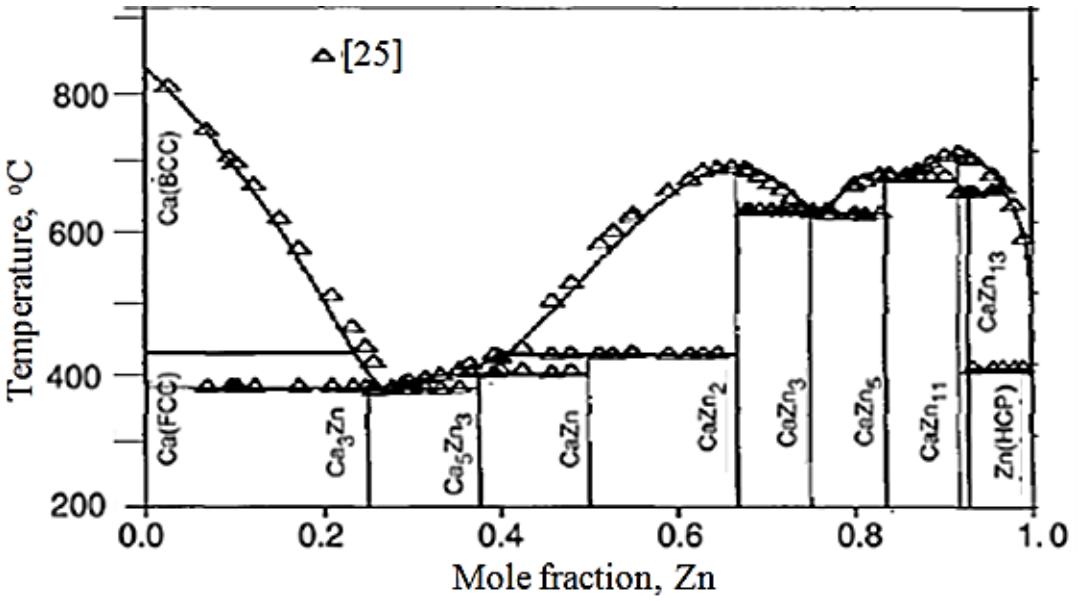

Figure 2.5: Calculated Ca-Zn phase diagram based on the work of Itkin and Alcock [26]

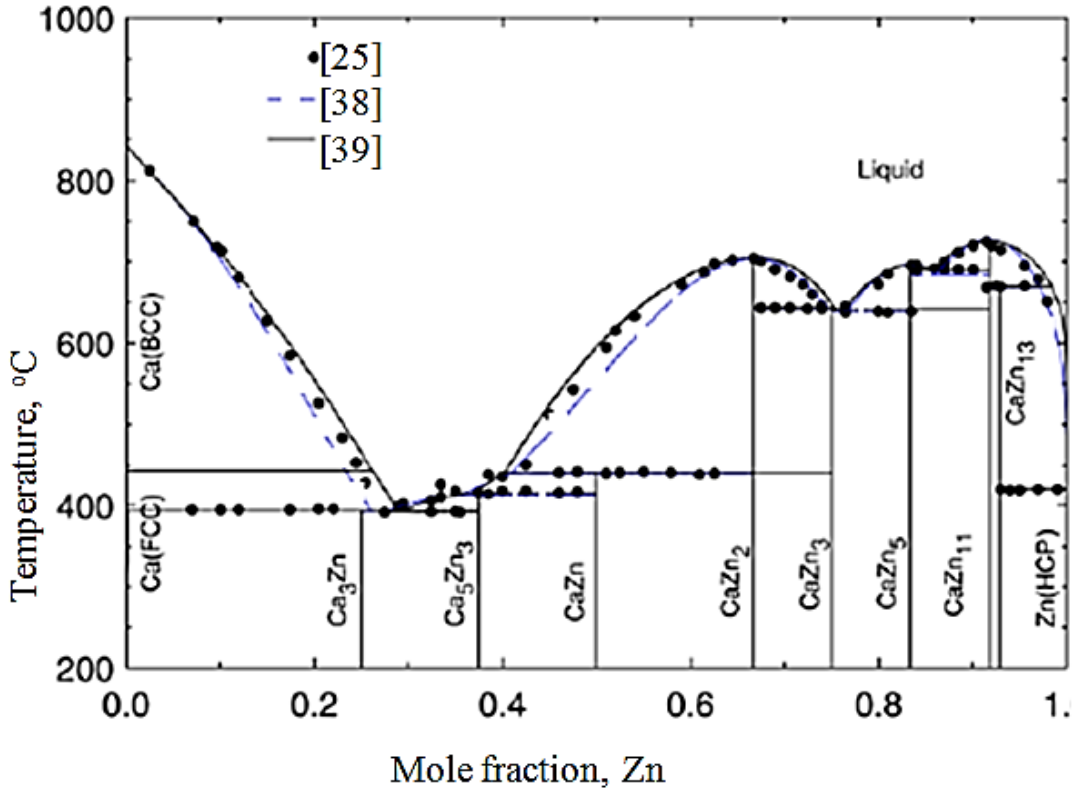

Figure 2.6: Calculated Ca-Zn phase diagram based on the work of Spencer et. al. [39]

2.2.2 Thermodynamic data

The amount of experimental data on the Ca-Zn system both for the solid and liquid states is very limited in the literature. Chiotti and Hecht [41] measured the Zn vapor pressure using the dewpoint method for samples greater than 50 at.% Zn and the Knudsen effusion method for lower Zn concentration. Later, Itkin and Alcock [26] evaluated the activity of Zn at 800°C from the vapor pressure results of [41]. Delcet and Egan [42] determined the activity of Ca at 800°C using EMF measurements on CaF_2 solid electrolyte cells. The calculated value of Spencer et al. [39] and Wasiur-Rahman and Medraj [40] showed

reasonable consistency with the experimental data of [41] and [42] and calculated results of [26]. The activity of Ca and Zn in liquid calculated by Wasiur-Rahman and Medraj [40] is shown in Figure 2.7.

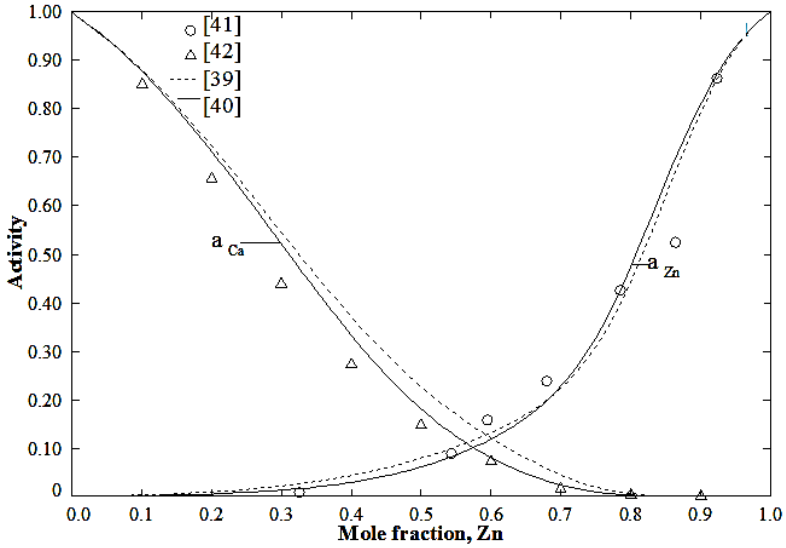

Figure 2.7: Activity of Ca and Zn in the liquid [40]

The enthalpy of formation for all the intermediate phases was calculated by Chiotti and Hecht [41] from the temperature dependence of the experimental Zn vapor pressure data and phase equilibrium condition. These data were compared with the calculated values in the work of Wasiur-Rahman and Medraj [40], and the calculated values are consistent except for Ca_3Zn where the experimental value is lower than the calculation as shown in Figure 2.8.

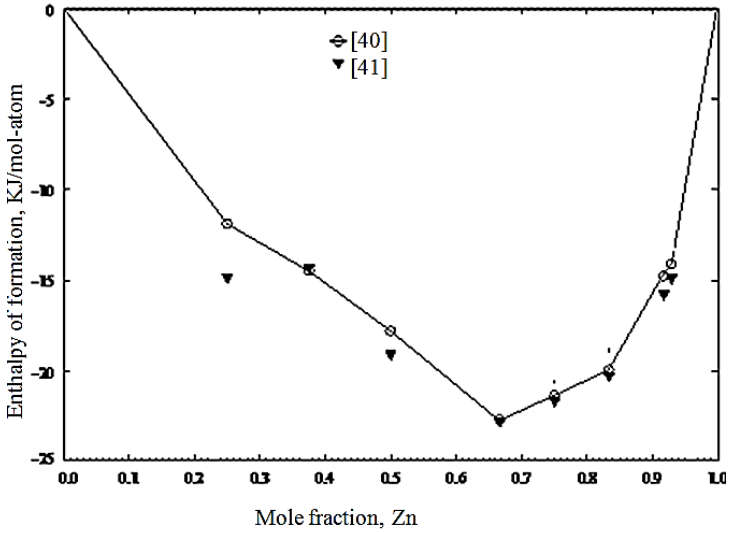

Figure 2.8: Heat of formation of the intermediate phases of the Ca-Zn system

2.3 The Al-Zn binary system

2.3.1 Phase Diagram data

The liquidus and solidus curves of the Al-Zn system were investigated by several researchers [43-52]. Heycock and Neville [43] first investigated the system using thermal analysis and reported one eutectic point in the Zn-rich zone at 380.5^{o}C and 89.5 at% Zn. Later, Isihara [44] studied the system by electrical resistivity, dilatometric method and XRD analysis and determined the eutectic point at 380^{o}C and 88.7 at.% Zn. Similar values were obtained by other researchers [45-47, 49-51]. Morinaga [48] reported a higher eutectic point occurring at 382^{o}C and 90 at.% Zn by heating and cooling of the samples. The liquidus and solidus lines of this system were also studied by Peng et al. [52] using the acoustic emission method. They [52] reported higher liquidus temperatures than other researchers [43-47, 49-51] and concluded that the eutectic reaction occurs at 382^{o}C and 88.7 at.% Zn. They [52] also claimed that their method is more precise than

the conventional thermal analysis because of the absence of the heat hysteresis phenomenon.

The Al-solidus curve was investigated by several researchers [44, 45, 48, 53-56]. Among them Morinaga [48] and Gebhardt [53] used microscopic analysis, Ellwood [54] used high temperature X-ray diffraction and Araki et. al.[55] used electron-probe microanalysis in order to determine the solidus line. Early works [44, 45] showed lower values for solidus temperatures. Isihara [44] and Tanabe [45] found a series of thermal arrests between 440^{o}C and 447^{o}C, which they described as a peritectic reaction, L + (Al) $\leftrightarrow$ solid solution (β). Later, Gayleret al.[46] and Morinaga [48] demonstrated that the thermal effect is the result of segregation. They [46, 48] found no evidence of any kind of phase change and this was supported by later investigators [54, 56].

The fcc miscibility gap has been studied by various groups of investigators [54, 56-61]. Fink and Willey [56] found two aluminum solid solutions in equilibrium at a temperature above 275^{o}C by electrical resistivity method. They [56] reported that the critical temperature occurs at 353^{o}C and 38.5 at.% Zn. Borelius and Larsson [58] reported the eutectoid decomposition at 277^{o}C with an uncertainty of about $\pm 0.5^{o}$C using electrical resistivity method. Using the same method, Münster and Sagel [59] found that the critical temperature is at 341.5 ± 0.4^{o}C and its composition is 39.5 ± 0.002 at.% Zn. Terauchi et al. [60] reported the critical temperature to be 351^{o}C at 39.16 at.% Zn and eutectoid temperature as 275^{o}C using cooling curve technique which are similar to the values reported by [56].

The solubility of Zn in Al was determined by Tanabe [45], Ellwood [54], Araki et al. [55], Fink and Willey [56] and Borelius and Larsson [58]; the results are in good agreement with each other except in the composition range 10 to 16.5 at.% Zn. The data of [45, 55, 56] for the phase boundary Al-fcc$_2$/ (Al-fcc + Zn-hcp) are consistent in the range 59 to 67 at.% Zn whereas the data of Larsson [62] show more scatter than those of [49, 60, 61].

The experimental works of most of the researchers regarding the solubility of Al in Zn are in good agreement with each other. At first, Peirce and Palmerton [63] measured the solubility of Al in Zn using electrical resistivity supplemented by microscopic analysis. Then Auer and Mann [64] used magnetic susceptibility to measure the same phenomenon. Lattice parameters were measured by Fuller and Wilcox [65], Burkhardt [66], Lohberg [67] and Hofmann and Fahrenhost [68], to detect the Zn solvus line. However, the data of Fuller and Wilcox [65] are not accurate due to impurity in the samples and inaccuracy in the experiment. Afterward, Pasternak [69] also measured the lattice parameters using electrical resistivity and they confirmed the earlier works of [63, 64, 66-68]. The invariant points reported by [45-69] are listed in Table 2.3.1.

Table 2.3.1 The invariant reactions of the Al-Zn system

Reaction Type	Reaction	Composition (at.% Zn)	Temperature (^{o}C)	Reference
Eutectic	L↔ Al-fcc+ Zn-hcp	89.5	380.5	[43]
		88.7	380.0	[44]
		88.7	380.0	[45]
		88.7	380.0	[47]
		90.0	382.0	[48]
Eutectoid	Al-fcc_2↔Al-fcc+Zn-hcp	59.8	282.0	[54]
		-	275.0	[56]
		-	277.0 ± 0.5	[58]
Critical point	Al-fcc↔ Al-fcc_1+Al-fcc_2	39.5 ± 0.002	341.5 ± 0.4	[59]
		39.16	351.0	[60]

The phase equilibrium data were critically assessed by Murray [70], but the calculated phase diagram was not in good agreement with the experimental data available in the literature. The system was later investigated by [19. 71-73]. However, the evidence of short range ordering in the Al-fcc solid solution was reported by Rudman and Averbach [74] during their experimental work on this system and it was not considered in the works of [71-73]. Wasiur-Rahman [19] used the modified quasichemical method to calculate both the liquid phase and the Al-fcc solid solution and Bragg-Williams random solution model to describe the Zn-hcp solid solution. The calculated Al-Zn phase diagram published by Wasiur-Rahman is demonstrated in Figure 2.9, which is used to calculate the Al-Ca-Zn system in the current work.

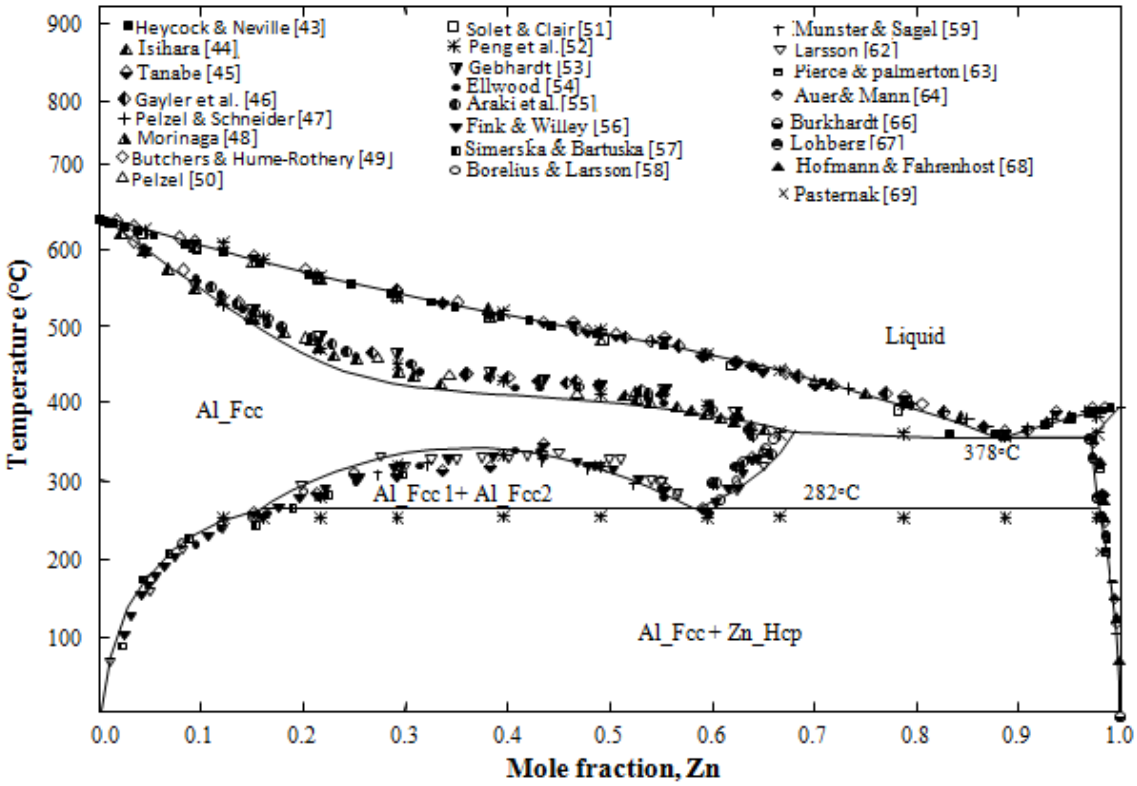

Figure 2.9: Calculated Al-Zn phase diagram [19]

2.3.2 Thermodynamic data

A large number of experimental works are available on the Al-Zn system investigating the thermodynamic properties both in the liquid phase and the extended solid solution of Al-fcc phase. Enthalpy of mixing of the liquid Al-Zn alloys was performed by several researchers [75-79]. Wittig and Keil [75] calculated the enthalpy of mixing values calorimetrically at 680°C. Hilliard et al. [76] and Corsepius and Münster [77] used EMF measurements at 380°C whereas Wittig and Schoffl [78] and Connell and Downie [79] used solution calorimeters at 370°C and 360°C, respectively. Poor agreement has been found between the calorimetric data and those from EMF studies, particularly in the composition range 0 to 40 at.% Zn. Although the agreement is better at compositions

higher than 40 at.% Zn, the trends of the two sets of data are quite different [75-79]. Figure 2.12 illustrates the calculated enthalpy of mixing by Mey [72] both for the liquid and solid phase at 680°C and 370°C, respectively. The curve fits well with the experimental values of [75] in the liquid phase but deviates considerably both in terms of magnitude and trend from the experimental results of [78] and [79] for the Al-fcc solid solution phase.

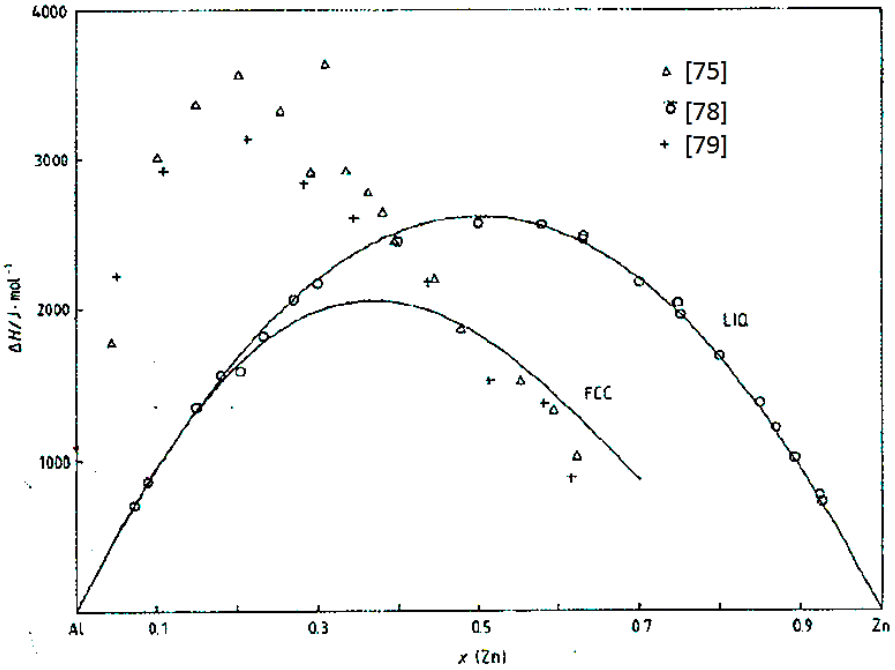

Figure 2.10: Calculated enthalpy of mixing of liquid at 680°C andfcc phase at 380°C [72]

The activity of Al and Zn both in the liquid phase and the solid solutions are measured by several researchers [80-89]. The activity of Al in the Al-Zn liquid alloys was measured by Batalin and Beloborodova [80] at 687°C, Predel and Schallner [81] at 727°C and 827°C and Sebkova and Beranek [82] at 700°C and 800°C. All of them used the EMF method and their results agree fairly well with each other as can be seen from the thermodynamic calculations of Wasiur-Rahman [19] demonstrated in Figure 2.11.

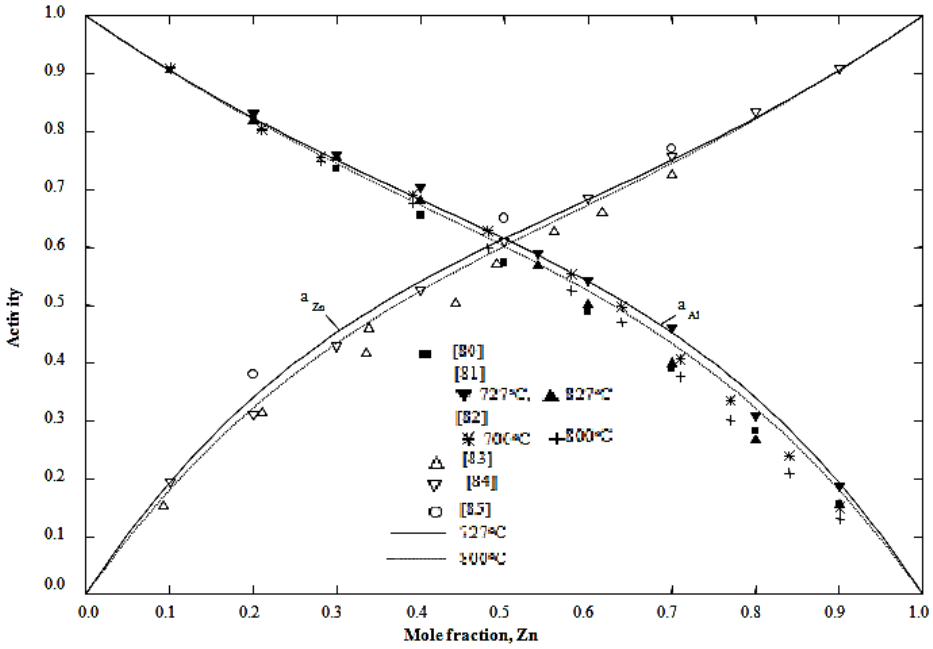

Figure 2.11: Calculated activity of Al and Zn in the liquid state at 727°C and 800°C [19]

Both Hilliard et al. [76] and Corsepius and Münster [77] measured the partial Gibbs energy of Al in the fcc solid solution at 380°Cusing the EMF method; their results show reasonable agreement. In addition, Hilliard et al. [76] determined the partial enthalpy of Al in the solid phase at 380°C.The partial Gibbs energy of Al in the fcc solid solution was calculated by Wasiur-Rahman and Medraj [19] as demonstrated in Figure 2.12. It can be seen form this figure that their calculated results show good consistency with the experimental values except for some disagreements at higher than 50.0 at.% Zn.

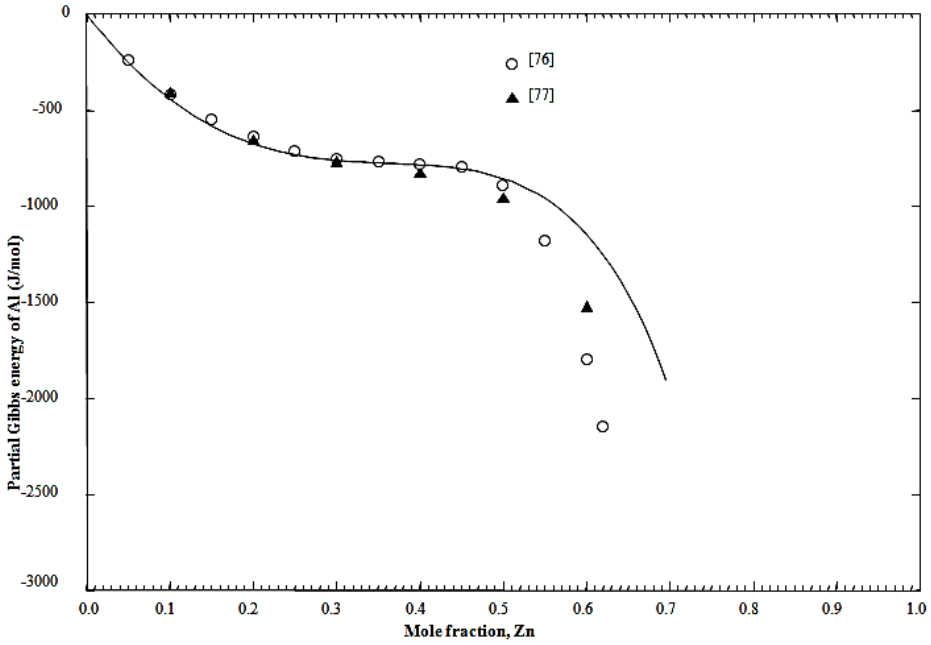

Figure 2.12: Calculated partial Gibbs energy of Al in the fcc phase at 380^{o}C [19]

2.4 The Al-Ca-Zn ternary system

2.4.1 Phase diagram data

The Al-Ca-Zn system has been experimentally investigated from 0 to 33 at.% Ca by several research groups [4, 90-97]. According to these experimental works, the system contains 3 ternary solid solutions, $Al_{2-x}CaZn_x$ ($0.28 \leq x \leq 0.68$at 700^{o}C), Al_2CaZn_2 and $Ca_2(Zn_{1-x}Al_x)_{17}$ (x =0.05-0.17 at 550^{o}C). Among the binary compounds in this system, Al_2Ca, $CaZn_2$, Al_4Ca, $CaZn_3$, $CaZn_5$ and $CaZn_{11}$have extended solubility into ternary system.

The Al-rich corner of the Al-Ca-Zn ternary system is attractive to the researchers due to the interest in superplastic alloys. This was first revealed by Piatti et al. [3] who reported the tensile properties of the Al-Al_4Ca eutectic superplastic alloy. However, these alloys

are brittle at room temperature and cannot be cold rolled industrially. This problem can be overcome by a small addition of Zn in the system which was first determined by Moore and Morris [4]. They [4] first experimentally investigated the Al-Ca-Zn system using metallographic technique, differential thermal analysis, EPMA, TEM and X-ray diffraction techniques and discovered a new ternary compound $AlCaZn_3$ in the Al-rich corner. They reported this compound to be superplastic and have a body centered tetragonal structure. Later, Kono et al. [90] studied the Al-Ca-Zn system and confirmed the presence of the ternary compound $AlCaZn_3$ using micrography, thermal analysis, X-ray diffraction and EPMA analysis. They reported that the binary compound Al_4Ca gradually changes into a ternary compound Al_3CaZn. Almost at the same time Cordier et al. [91] reported the crystal structure of a new ternary compound Al_2CaZn_2 as an ordered ternary variant of Al_4Ba-type structure with lattice parameters a=4.127Å and c=11.671Å. Later, Ganiev et al. [92] investigated the Al-Ca-Zn system using differential thermal analysis, X-ray diffraction and metallographic examination and determined the isothermal section of the Al-Ca-Zn system at 350^{o}C. They reported the congruent melting temperature of the ternary compound Al_2CaZn_2 as 840^{o}C using DTA. The presence of this compound was later confirmed by Gantsev et al. [93]. Recently, Pani et al. [94] reported a wide homogeneity range from Al_4Ca to $Al_{1.88}CaZn_{2.12}$ composition at 550^{o}C. The general formula of this phase was proposed as $Ca(Zn_{1-x}Al_x)_4$ (x=0.47-1.00 at 550^{o}C) with an Al_4Ba-type structure [94], which is consistent with ternary compound Al_2CaZn_2 [91-93]. The lattice parameters plot against *x* in $Ca(Zn_{1-x}Al_x)_4$ reported by Pani et al. [94] is shown in Figure 2.13.The phase boundaries between Al_4Ca and Al_3CaZn as well as Al_3CaZn and Al_2CaZn_2 are not clearly identified in the literature [4, 90-94].

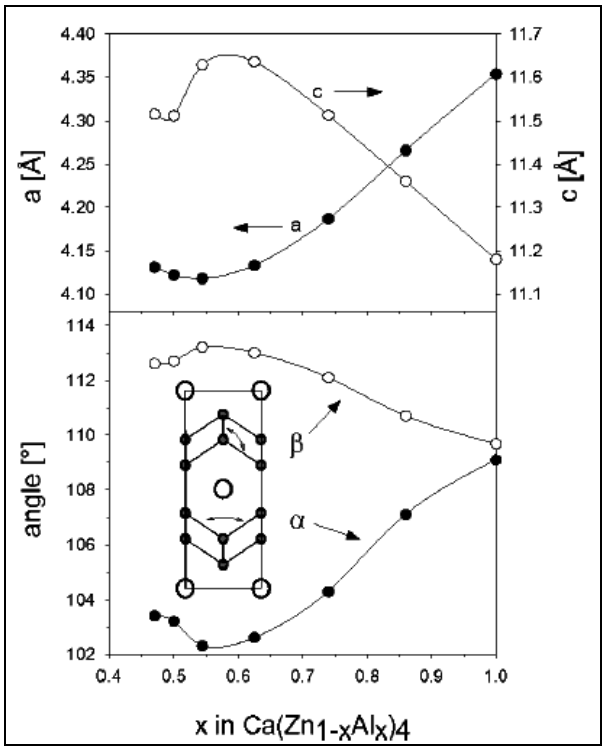

Figure 2.13: Trend of a and c lattice parameters of the $Ca(Zn_{1-x}Al_x)_4$ phases and the variation of α and β bond angles within the Zn/Al structure [94].

A number of researchers [90, 92, 93, 95, 96] studied other ternary compound AlCaZn, but their results were contradictory with each other. Ganiev et al. [92] and Gantsev et al. [93] reported AlCaZn as a congruently melting compound with the melting temperature as 990°C using differential thermal analysis. Later the Al_2Ca-$CaZn_2$ pseudobinary section was studied by Söderberg et al. [95] and Pani et al. [96]. The Al_2Ca-$CaZn_2$ vertical section illustrated by Söderberg et al. [95] is shown in Figure 2.14. Söderberg et al. [95] studied this system in the region below 33 at.% Zn at 700ºC and above 33 at% Zn at 600ºC using X-ray diffraction, transmission electron microscopy and thermal analysis and concluded that AlCaZn is an extended solid solution of the $CaZn_2$ phase.

The binary compound Al_2Ca has a solubility of 6 at.% Zn according to the experimental results of [95, 96]. According to the experimental results of Söderberg et al. [95] Al_2Ca has a solid solubility range up to $Al_{1.82}CaZn_{0.18}$ and the phase forms congruently at 1075^{o}C.

Both Söderberg et al. [95, 97] and Pani et al. [96] reported other new ternary phase, $Al_{2-x}CaZn_x$ ($0.28 \leq x \leq 0.68$) with a C36 Laves phase structure. Söderberg et al. [95, 97] reported that this intermediate phase has a solid solubility range from $Al_{1.72}CaZn_{0.28}$ to $Al_{1.32}CaZn_{0.68}$ and forms peritectically from Al_2Ca and it melts at 954^{o}C. Whereas, Pani et al. [96] reported $Al_{1.406}CaZn_{0.594}$ as $MgNi_2$-type (C36) structure using x-ray diffraction and single crystal diffractometry.

According to the work of Söderberg et al. [95], KHg_2-type phase is a solid solution of binary $CaZn_2$phase extended into the ternary and the maximum ternary solubility is at the composition $Al_{1.07}CaZn_{0.93}$ at 700^{o}C. This solid solution of KHg_2-type forms peritectically from the solid solution of C36-type phase and melts at 839^{o}C [95]. This result was also confirmed by Pani et al. [96] who analyzed the system at 700ºC using EPMA and single crystal x-ray diffraction. The XRD patterns of these phases as depicted by Söderberg et al. [95] are presented in Figure 2.15.

Söderberg et al. [95] also carried out TEM investigation to examine the possibility of occurrence of C14 type phase in the region between stable C36 and KHg_2 type phase. For this purpose they tested $Al_{1.3}CaZn_{0.7}$alloy which constituted of C36 and KHg_2-type phases. The HRTEM (high-resolution transmission electron microscopy) image and ED (electron diffraction) pattern of this sample is illustrated in Figure 2.16. The ED pattern

obtained from $Al_{1.3}CaZn_{0.7}$ sample was compared with simulated patterns of C36 and C14 type structures and the image was only interpretable with C36 type. However, they [95] pointed out that the C36→C14 transition is suppressed in the $Al_{2-x}CaZn_x$ by the too large electronegativity difference between the constituent components. Hence they concluded that there is no C14 type phase present between C36 and KHg_2-type phases [95].

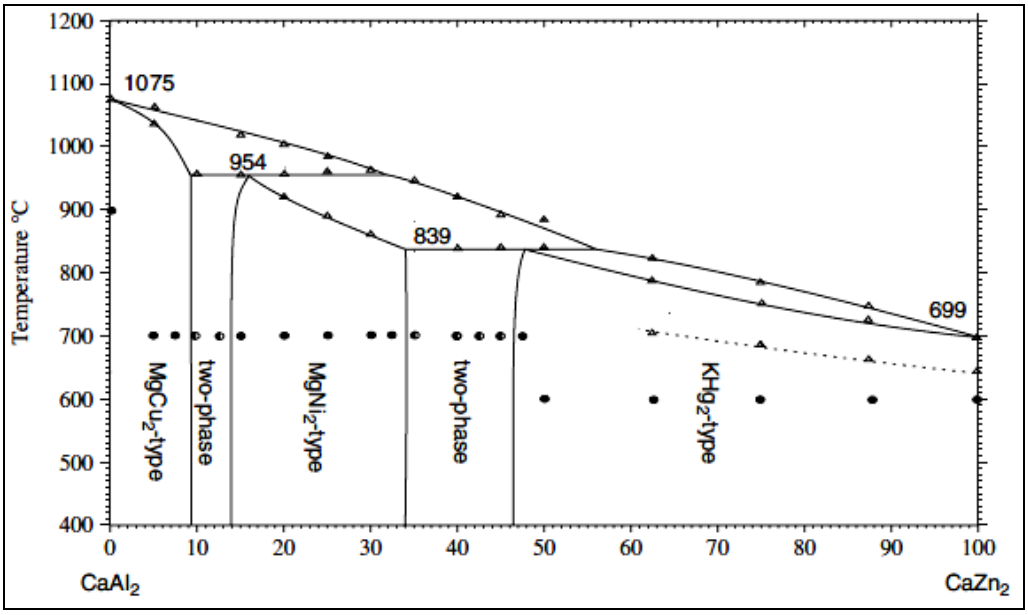

Figure 2.14: The pseudobinary Al_2Ca-$CaZn_2$ phase diagram reported by Söderberg et al. [95], the black circles represent the positions of the key alloys; the broken line is associated with the peritectic formation of the impurity $Al_xCa_{3.33}Zn_{11-x}$.

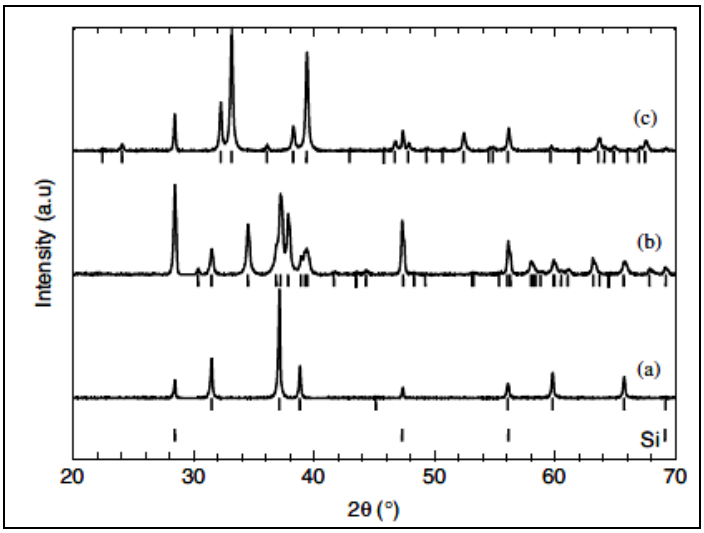

Figure 2.15: X-ray diffraction patterns of three representative $Al_{2-x}CaZn_x$ alloys: (a) x =0.15 (C15 type), (b) x =0.65 (C36 type) and (c) x = 0.95 (KHg_2 type). The vertical bars show the calculated Bragg reflection positions and the vertical bars on the bottom show the reflection positions for silicon, which was used as an internal standard [95]

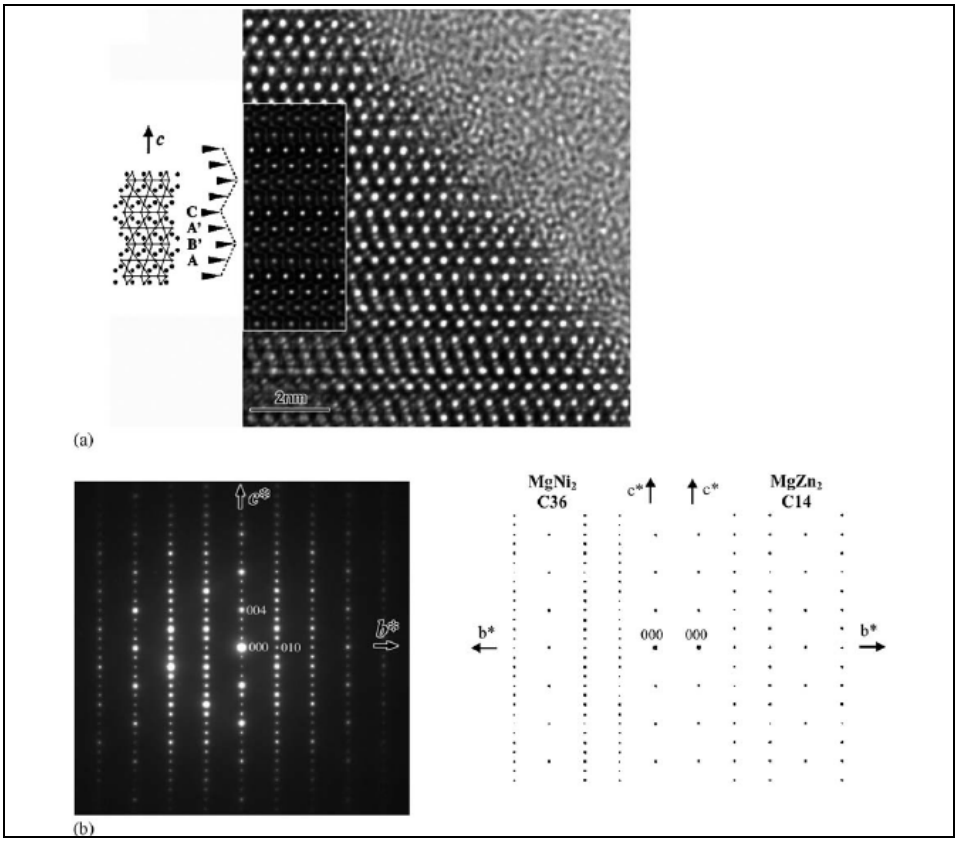

Figure 2.16(a) HRTEM image of $Al_{1.3}CaZn_{0.7}$, (b) ED pattern of $Al_{1.3}CaZn_{0.7}$ along [100] together with simulated patterns for the C36 and C14 structure [95]

Pani et al. [94] investigated the Al-Ca-Zn system from 8 to 33 at% Ca at 550^{o}C by optical and scanning electron microscopy, EPMA and X-ray analysis. They reported several binary solid solutions with their homogeneity ranges and crystal structures. According to Pani et al. [94], the binary phase $CaZn_3$ has an extended solubility in the ternary where the maximum solubility of Al corresponds to the composition $Al_{0.702}CaZn_{2.322}$. The formula for this phase was proposed as $Ca(Zn_{1-x}Al_x)_3$ (x= 0-0.23 at 550^{o}C) [94]. The lattice structure was reported as a=9.157, c= 7.365Å for the nominal composition $Al_{0.3}CaZn_{2.7}$ and a= 9.169, c=7.382 Å for the nominal composition $Al_{0.6}CaZn_{2.33}$ [94].

Wendroff and Röhr [32] reported that the binary compound $CaZn_5$ has a continuous variation in the range 14.3-16.7 at.% Ca, corresponding to the change of the stoichiometry from 1:5 to 1:6 with a continuous structural change from $CaCu_5$ to $TbCu_7$. Pani et al. [94] observed the same phenomena in the ternary system, and reported $CaZn_5$ as a complex solid solution with the formula $Ca_{1-y}(Zn_{1-x}Al_x)_{5-2y}$ (x= 0-0.12 and y= 0-0.12, $CaCu_5$- derived $TbCu_7$ type, 550^{o}C) [94]. The lattice parameter information for $CaZn_5$ solid solution reported by Pani et al. [94] is shown in Figure 2.17. From this figure it can be seen that lowering the Ca content in $Ca_{1-y}(Zn_{1-x}Al_x)_{5-2y}$ results in a decrease in 'a' parameter while increase in 'c' parameter, thus increasing the c/a ratio. On the other hand, when the amount of Ca is kept constant and Zn is replaced by larger Al atom, both lattice parameters increase keeping nearly constant values of c/a [94].

Nominal sample composition	Structure Type	Lattice parameters [Å] *a*	*c*
$CaZn_5$	$CaCu_5$	5.3899(2)	4.2456(1)
$Ca_{0.87}Zn_{5.26}$	$TbCu_7$	5.3338(1)	4.3004(1)
$CaZn_{4.5}Al_{0.5}$	$TbCu_7$	5.410(1)	4.266(1)
$CaZn_{4.80}Al_{0.87}$	$TbCu_7$	5.383(1)	4.304(1)
$CaZn_{5.7}Al_{0.3}$	$TbCu_7$	5.377(1)	4.294(1)
$CaZn_{5.3}Al_{0.7}$	$TbCu_7$	5.385(1)	4.298(1)
$CaZn_{4.32}Al_{0.48}$	$TbCu_7$	5.419(1)	4.255(1)
$CaZn_{4.86}Al_{0.54}$	$TbCu_7$	5.394(1)	4.278(1)
$CaZn_{5.22}Al_{0.58}$	$TbCu_7$	5.374(1)	4.302(1)
$CaZn_{5.58}Al_{0.62}$	$TbCu_7$	5.352(1)	4.329(2)

Figure 2.17: Structure types and lattice parameters for the $Ca_{1-y}(Zn_{1-x}Al_x)_{5-2y}$ phase [94]

Pani et al. [94] also reported one new ternary solid solution, $Ca_2(Zn_{1-x}Al_x)_{17}$ (x =0.05-0.17) with a Th_2Zn_{17} prototype structure. However they mentioned facing some problems regarding finding a good quality single crystal to analyze its crystal information. Figure 2.18 depicts the lattice parameters, unit cell volume and c/a ratio for $Ca_2(Zn_{1-x}Al_x)_{17}$ (x=0.05-0.17) as reported by Pani et al. [94].

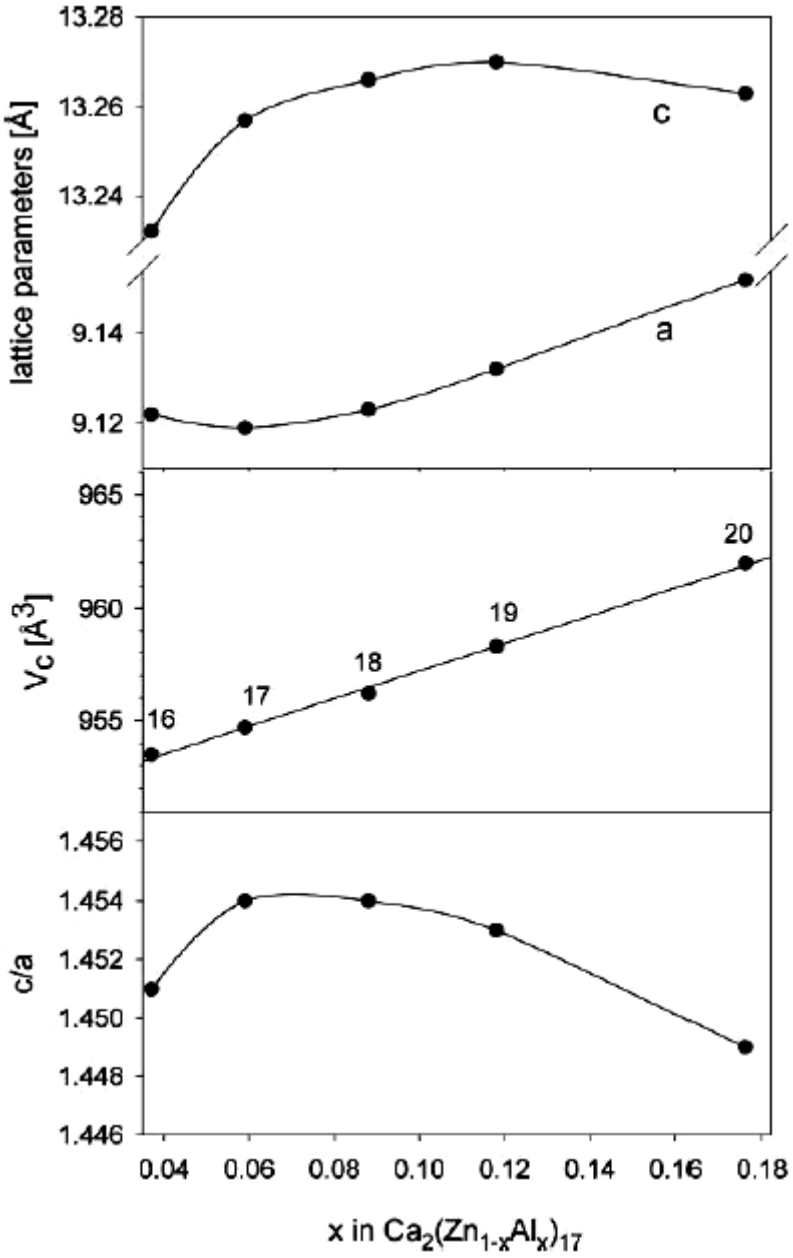

Figure 2.18: Lattice parameters, unit cell volume V_c and c/a ratio, as a function of x, in $Ca_2(Zn_{1-x}Al_x)_{17}$ phases. The points refer to the nominal compositions and lattice parameters obtained by powder diffraction data [94].

Pani et al. [94] reported that $CaZn_{11}$ has a very little solubility at 550^{o}C. The solid solution was formulated as $Ca(Zn_{1-x}Al_x)_{11}$ (x=0-0.018, 550^{o}C) and $BaCd_{11}$ prototype

[94].The lattice parameters values were reported as a=10.706, c=6.851Å for the nominal composition $Al_{0.8}CaZn_{10.2}$ [94].

The liquidus of the Al-Ca-Zn system was studied experimentally by Kono et al. [90] and Gantsev et al. [93]. Kono et al. [9] reported two eutectic points, Al-4.5%, Ca-7.3%Zn and Al-2.4%Ca-57.9%Zn by at.%. Gantsev et al. [93] reported six eutectic reactions with the approximate eutectic compositions and temperatures; these are given in Table 2.4.1 along with the calculated invariant reactions performed by Wasiur-Rahman [19].A liquidus projection had been suggested by Kono et al. [9] as shown in Figure 2.19.

Table 2.4.1: Calculated invariant reactions and special points in the Al-Ca-Zn system based on the thermodynamic modeling of Wasiur-Rahman [19]

Type	Reaction	Composition (at.%)			Temp °C	Reference
		Al	Zn	Ca		
E_1	$L \leftrightarrow Al_2Ca+CaAlZn+CaAl_2Zn_2$	51.8	22.7	25.8	679.0	[19]
E_2	$L \leftrightarrow Al_{14}Ca_{13}+Al_3Ca_8+CaAlZn$	31.5	9.6	58.9	504.2	[19]
E_3	$L \leftrightarrow$ Ca_Bcc+Al_3Ca_8+CaAlZn	19.6	12.4	68.0	479.2	[19]
E_4	$L \leftrightarrow$ AlCaZn+Ca_3Zn+Ca_5Zn_3	4.8	29.5	65.7	375.0	[19]
E_5	$L \leftrightarrow$ $CaZn_5$+AlCaZn+$CaZn_3$	12.9	61.9	25.2	456.9	[19]
E_6	$L \leftrightarrow$ AlCaZn+$CaZn_5$+$CaAl_2Zn_2$	14.8	62.9	22.3	456.5	[19]
E_7	$L \leftrightarrow CaZn_5+CaZn_{11}+CaAl_2Zn_2$	13.4	69.6	18.0	475.8	[19]
E_8	$L \leftrightarrow Zn\_Hcp+Al\_Fcc+CaZn_{13}$	13.6	84.0	2.4	363.4	[19]
		11.22	88.46	0.46	380.0	[93]
U_1	$L+Al_4Ca \leftrightarrow Al\_Fcc+CaAl_2Zn_2$	75.3	11.6	13.1	549.0	[19]

U_2	$L+Al_2Ca \leftrightarrow Al_4Ca+CaAl_2Zn_2$	69.0	14.0	17.0	575.3	[19]
U_3	$L+Al_2Ca \leftrightarrow Al_{14}Ca_{13}+CaAlZn$	35.6	10.6	53.8	550.7	[19]
U_4	$L+Ca\_Bcc \leftrightarrow CaAlZn+Ca\_Fcc$	8.5	19.2	68.3	443.0	[19]
U_5	$L+Ca\_Fcc \leftrightarrow CaAlZn+Ca_3Zn$	8.9	29.6	61.5	357.0	[19]
U_6	$L+CaZn \leftrightarrow CaAlZn+Ca_5Zn_3$	6.2	37.2	56.6	389.2	[19]
U_7	$L+CaZn_2 \leftrightarrow CaZn+CaAlZn$	7.0	40.2	52.8	405.0	[19]
U_8	$L+CaZn_2 \leftrightarrow CaZn_3+CaAlZn$	93.7	61.5	25.8	459.0	[19]
U_9	$L+CaZn_{11} \leftrightarrow CaAl_2Zn_2+CaZn_{13}$	13.4	76.5	10.1	494.0	[19]
U_{10}	$L+CaAl_2Zn_2 \leftrightarrow Al\_Fcc+CaZn_{13}$	21.6	73.5	4.9	347.0	[19]
m_1	$L \leftrightarrow Al_2Ca+CaAl_2Zn_2$	53.0	22.0	25.0	689.0	[19]
		48.8	24.8	26.4	710.0	[93]
m_2	$L \leftrightarrow Al_2Ca+CaAlZn$	18.0	50.0	32.0	807.0	[19]
		15.2	51.5	33.3	850.0	[93]
m_3	$L \leftrightarrow Al_3Ca_8+CaAlZn$	29.0	10.6	60.4	506.0	[19]
m_4	$L \leftrightarrow CaAlZn+Ca\_Bcc$	15.7	16.0	68.3	487.3	[19]
m_5	$L \leftrightarrow CaAlZn+CaZn_2$	9.9	57.0	33.1	513.0	[19]
		7.6	59.1	33.3	375.0	[93]
m_6	$L \leftrightarrow CaAlZn+CaZn_5$	13.8	62.8	19.4	437.0	[19]
		-	-	-	380.0	[93]
m_7	$L \leftrightarrow CaAl_2Zn_2+CaZn_5$	13.8	67.9	18.3	475.5	[19]
m_8	$L \leftrightarrow CaZn_{11}+CaAl_2Zn_2$	13.3	74.1	93.5	502.5	[19]
m_9	$L \leftrightarrow CaAlZn+CaAl_2Zn_2$	37.0	37.0	26.0	740.0	[19]
		36.4	36.4	27.2	650.0	[93]

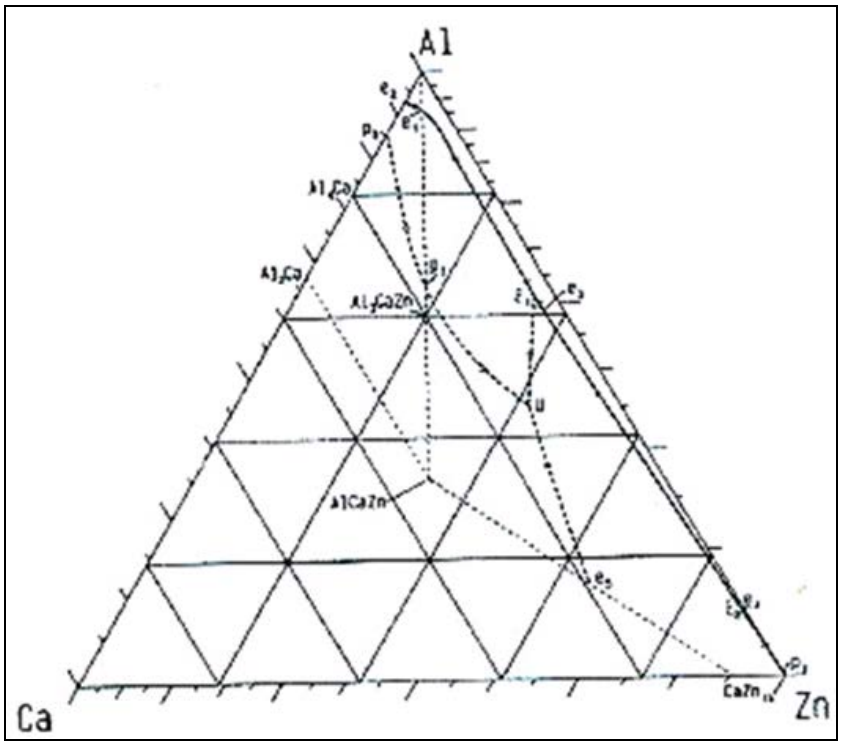

Figure 2.19: Liquidus projection of Al-Ca-Zn ternary system [90]

The Al-Ca-Zn ternary system was optimized by Wasiur-Rahman and Medraj [23] on the basis of the experimental data of [4, 90-93] and their optimization of the three related binary systems. In the work of Wasiur-Rahman and Medraj [23], they considered two ternary compounds, AlCaZn and Al_2CaZn_2 melting congruently. The modified quasichemical model was used to model the liquid phase. Eight ternary eutectic, ten quasi-peritectic and nine maximum points were reported in their work. These invariant reactions are given in Table 2.4.1 [19, 23]. The liquidus projection calculated by Wasiur-Rahman and Medraj [23] is shown in Figure 2.20. However, they [23] did not consider the latest works of Söderberg et al. [95, 97] and Pani et al. [94, 96] in their optimization. Moreover, according to invariant reactions as given in Table 2.4.1, the lowest temperature is at U_{10} corresponding to the temperature 347^{o}C, but from the liquidus

projection depicted by [23] as shown in Figure 2.20, the lowest temperature is corresponding to the point E_8,which is 380°C.

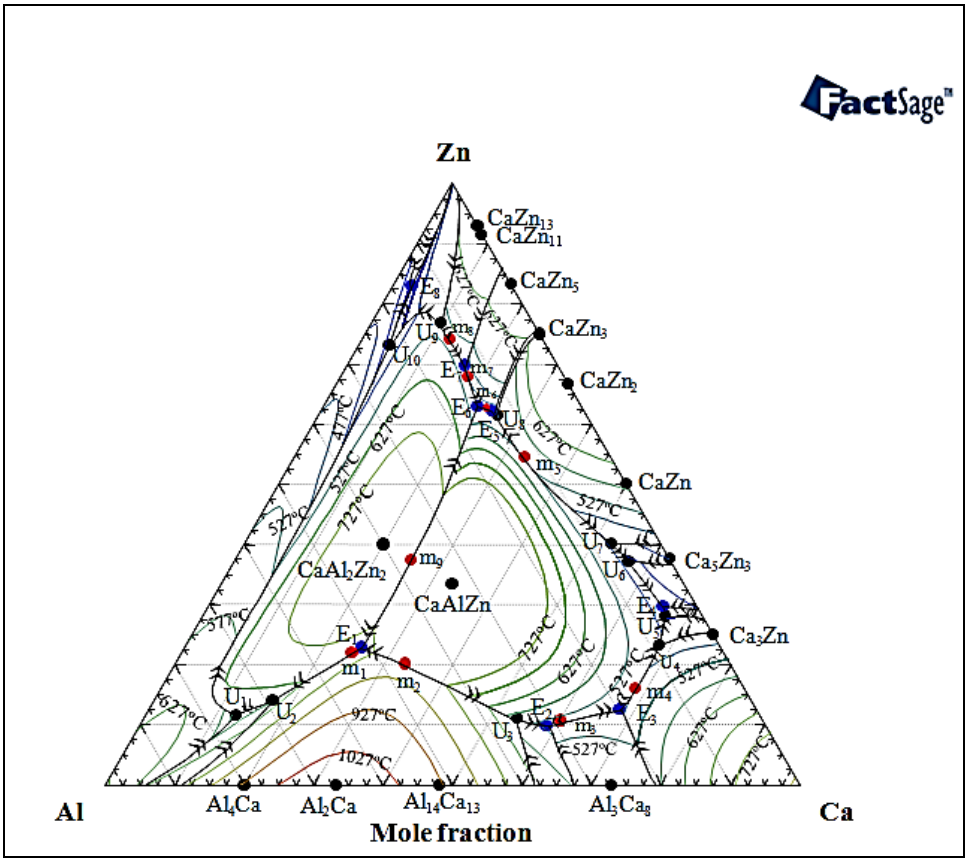

Figure2.20: Liquidus projection of the Al-Ca-Zn ternary system [19, 23]

The isothermal section of the Al-Ca-Zn system at 350°C is calculated based on the work of Wasiur-Rahman and Medraj [23] as demonstrated in Figure 2.21. The homogeneity ranges of the binary and ternary compounds obtained from the literatures [90-97] are also included in the Figure 2.21. From the above discussion it is evident that more information is required to understand the Al-Ca-Zn system fully regarding the solubility of the binary and ternary phases, crystal structure information, the fcc miscibility gap and phase relations. In this work it is attempted to understand the system more elaborately with a diffusion couple approach and key alloy analysis.

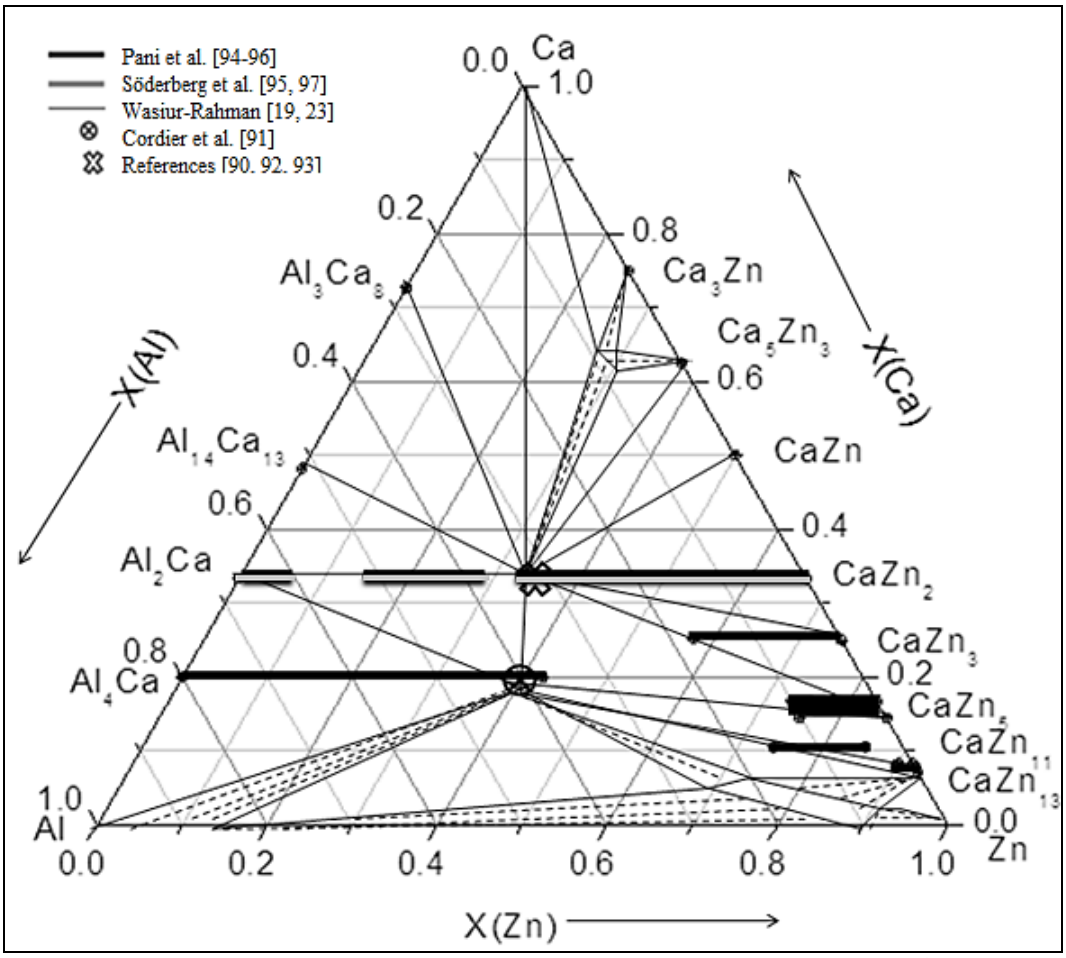

Figure 2.25: The isothermal section of the Al-Ca-Zn system at 350°C based on the thermodynamic model of Wasiur-Rahman [23] and the experimental results reported by [90-97].

2.5. Diffusion couple technique

The diffusion couple technique is a powerful and viable experimental method to map the ternary phase diagrams [98]. There are several types of diffusion couples, but solid-solid diffusion couples and solid-liquid diffusion couples are the most popular ones to study the phase diagrams. To prepare solid-solid diffusion couples, the bonding faces of the couple components are grinded and polished flat, clamped together. Then the samples are annealed at the temperature of interest [98]. Quenching of the sample is desirable to

freeze and keep the high temperature equilibrium [98]. The advantage of solid-solid diffusion couple is that no melting or powder contamination incorporated with this technique and equilibrium phases are formed by interdiffusion reaction [98]. However, sometimes solid-solid diffusion couples are not successful due to certain inherent problems associated with the terminal compositions, such as brittleness of the alloys. In such cases, solid-liquid diffusion couple can be a good alternative, where instead of clamping, the lower melting point alloy or pure metal is molten on top of the high-melting component. Although diffusion couple technique is a powerful tool in phase diagram determination, it is not invincible. When diffusion couple method is used to determine phase relationships, one must always consider for the likelihood of missing phases [98, 99]. The possible reason for the missing phase can be the slow nucleation of the phase, and due to the sluggish nature of the phase formation, the layer of this phase could be too thin to be identified by EPMA. This phenomenon will ultimately give erroneous tie line compositions for phase relations due to the difficulty of extrapolating the interface based on a few data points [98]. The possible solution can be considered by preparing other diffusion couples with different end members [99] or a combination of diffusion method with an investigation of selected equilibrated alloys [99]. In this work, the Al-Ca-Zn system has been studied with diffusion couple technique in conjunction with key alloys.

CHAPTER 3

EXPERIMENTAL PROCEDURE

The Al-Ca-Zn system has been studied experimentally by preparing 5 diffusion couples and 26 key alloys annealed at 350^{o}C based on the thermodynamic model of Wasiur-Rahman [19, 23].The starting materials are 99.999% pure Al, 99.99% pure Zn and 99% pure Ca supplied by Alfa-Aesar. The key alloys have been prepared in an arc-melting furnace with water-cooled copper crucible in an argon atmosphere using a non-consumable tungsten electrode. All the samples have been re-melted 5 times in the arc-melting furnace to ensure the homogeneity of the samples. The samples have been annealed at 350^{o}C. The annealing temperature has been chosen at 350^{o}C for the following reasons,

1. The lowest temperature on the liquidus of the Al-Ca-Zn system was found to be 380^{o}C from the thermodynamic calculation of Wasiur-Rahman and Medraj [19, 23]. So the annealing temperature should be below 380^{o}C.
2. The annealing temperature should be high enough to ensure the interdiffusion and the formation of the phases at a comparatively faster rate to avoid extremely long annealing time.

3.1 Solid-solid diffusion couples

The solid-solid diffusion couples have been prepared with a piece of ternary alloy and a piece of Zn as end members. The faces of the end members of the diffusion couples have

been pre-grinded up to 1200 grit using SiC paper and polished up to 1µm using diamond suspension and 99% ethanol as lubricant. The pieces are then pressed together using clamping rings and wrapped in a tantalum foil, sealed in a quartz tube under protective argon atmosphere. Finally the diffusion couples are annealed at 350^{o}C for 5 weeks and quenched in cold water.

The actual compositions of the end members of the solid-solid diffusion couples are:

SSDC-1: $Al_{66.3}Ca_{26.9}Zn_{6.8}$-Zn

SSDC-2: $Al_{69.6}Ca_{12.2}Zn_{18.2}$-Zn

SSDC-3: $Al_{40}Ca_{40}Zn_{20}$-Zn

SSDC-4: $Al_{30}Ca_{37.3}Zn_{32.7}$-Zn

3.2 Solid-Liquid diffusion couples

To investigate the Al-Ca-Zn system, one additional solid-liquid diffusion couple has been prepared with end members Al_2Ca-Zn. To prepare the solid-liquid diffusion couple, the lower melting element Zn was melted on top of the higher melting compound Al_2Ca in the arc-melting furnace under protective argon atmosphere. The sample was then sealed in a quartz tube and annealed for one week at 350^{o}C followed by quenching in cold water.

The end members of the diffusion couples are illustrated in Figure 3.1.

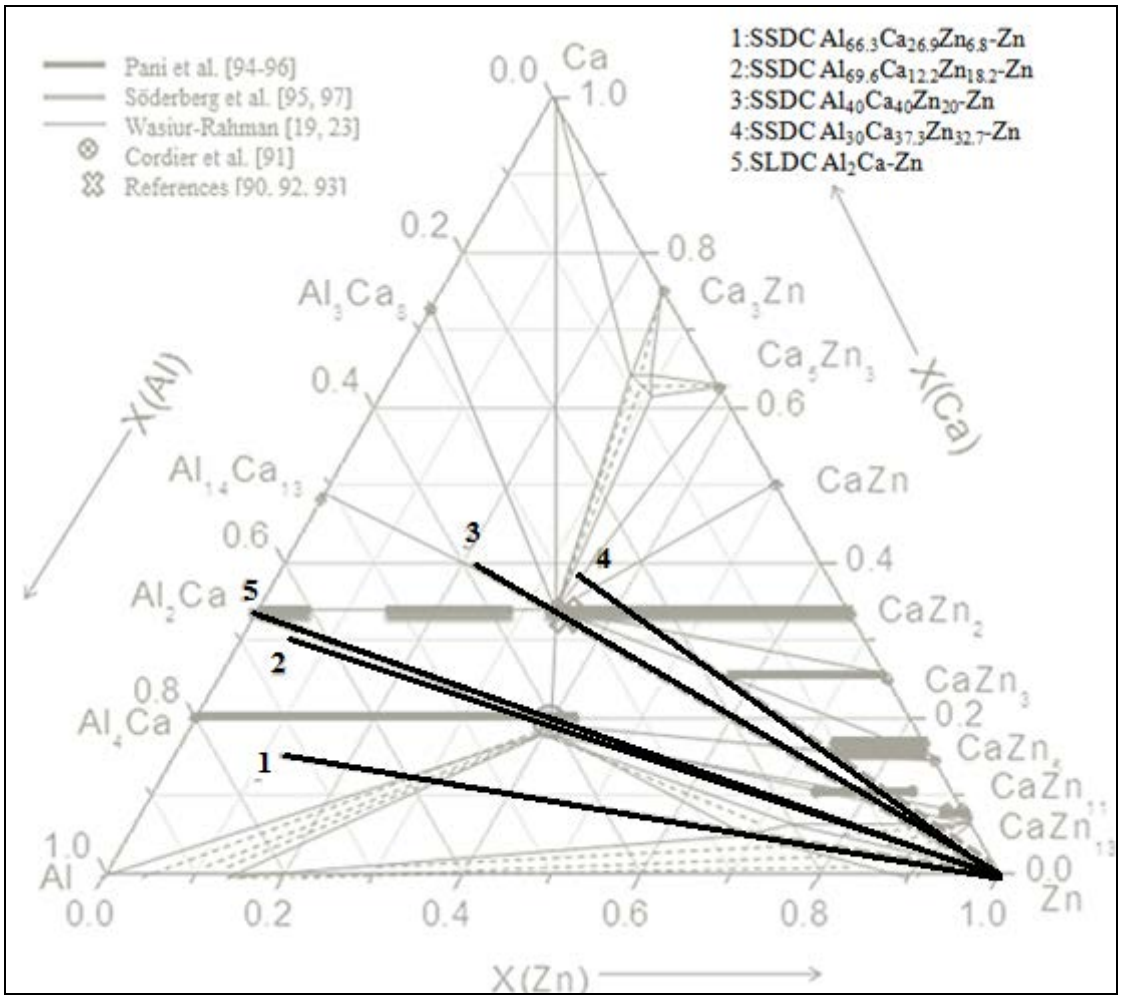

Figure 3.1.Compositions of the end members of the diffusion couples

3.3 Key samples preparation

The key alloys were prepared in an arc-melting furnace with water-cooled copper crucible in an inert argon atmosphere using a non-consumable tungsten electrode. The samples are then enclosed inside a tantalum foil and sealed in a quartz tube filled with argon, then annealed at 350ºC for 4-6 weeks and quenched by cold water. The annealed samples were grinded with 1200 grit paper and polished using 1 micron diamond paste suspension using 99% ethanol as lubricant. The actual composition was measured by Inductively Coupled Plasma-Atomic Emission Spectroscopy (ICP-AES).

3.3.1 Inductively Coupled Plasma technique

Inductively Coupled Plasma-Atomic Emission Spectroscopy (ICP-AES) is an analytical technique for the detection of the trace material. A schematic of a typical ICP-AES is demonstrated in Figure 3.2. The instrument consists of mainly 2 parts: ICP torch and optical spectrometer (monochromator). The sample solution is pumped into the plasma torch in the form of fine spray accompanied by a stream of argon gas. The plasma is a conducting gas constituted of a combination of positively charged ions and their respective electrons. The plasma is initiated by a spark from a tesla coil, and is maintained by a high-frequency electrical current in the induction coil powered by an RF (radio frequency) power supply operating with a power of 0.5 to 2.0 kW at 40.68 MHz. The plasma ionizes and excites the atoms of the sample. Emitted light from the ions in the plasma then passes through the entrance window to the monochromator where it is separated into its various wavelengths (colors). The elements present in the sample are identified by measuring the wavelengths of the light emitted by the sample and the concentration of the element is determined by measuring the amount of the light emitted by a particular element [100].

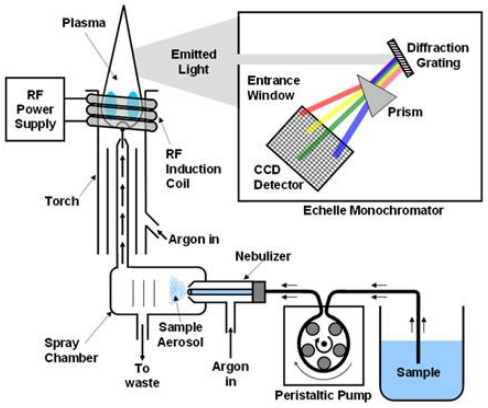

Figure 3.2: Schematic of a typical ICP-AES [100]

3.4 Analysis of the samples

Diffusion couples and key alloys have been analyzed by OM (Optical Microscopy), SEM (Scanning Electron Microscopy), EPMA (Electron Probe Micro-analysis) and XRD (X-ray diffraction). The microstructure of the constituent phases of a sample has been identified by OM and SEM. Phase identification and determination of the phase compositions have been performed with EPMA. XRD method has been incorporated for phase identification and crystallographic information.

3.4.1 Electron Probe Micro-analysis (EPMA)

An electron microprobe is a microbeam instrument designed for the non-destructive x-ray microanalysis and imaging of small volumes of solid materials. Figure 3.3 shows the schematic diagram of a typical EPMA. Low-energy electrons (typically 5-30keV) are produced from the tungsten filament cathode referred as 'gun'. The electrons are directed to a focused electron beam by passing it through a series of magnetic lenses and apertures. The resulted electron beam (5nm to 10μm diameter) is then bombarded on a micro volume of a sample which causes various effects from the samples such as photon emission, visible light fluorescence, continuum x-ray and characteristic x-ray radiation, secondary electron and back-scattered electron production. The characteristic x-rays are used for chemical analysis. For this purpose, specific x-ray wavelengths are selected and counted either by WDS (wavelength dispersive x-ray spectroscopy) or EDS (energy dispersive x-ray spectroscopy). WDS utilizes Bragg diffraction from crystals to select X-ray wavelengths of interest and direct them to gas-flow or sealed proportional detectors.

In contrast, EDS uses a solid state semiconductor detector to accumulate X-rays of all wavelengths produced from the sample. While EDS yields more information and typically requires a much shorter counting time, WDS is the more precise technique because its superior X-ray peak resolution. Chemical composition is determined by comparing the intensities of characteristic X-rays from the sample material with intensities from known composition (standards) [101]. In this work, a JEOL-JXA-8900 EPMA machine with 2µm probe diameter, 15 kV accelerating voltage and 20nA probe current has been used. The error of the EPMA measurement has been estimated to be ±2 at.%. This value was obtained from the comparison and statistical analysis of the compositions of selected phases from several samples.

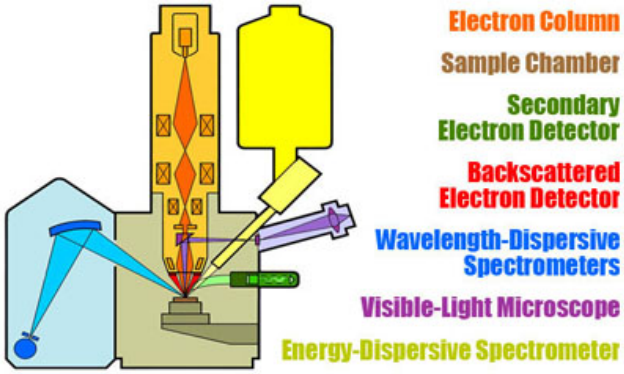

Figure 3.3: Schematic of EPMA [101]

3.4.2 X-Ray Diffraction technique

X-ray diffraction is a non-destructive technique that reveals the chemical composition and crystallographic information of materials. A typical powdered x-ray diffractometer is shown in Figure 3.4. The instrument has 3 basic parts, the x-ray tube, the specimen holder and the detector. Electrons are generated in a cathode ray tube by heating the filaments; a voltage difference is then applied to accelerate the electrons which bombard

the target material. When electrons have sufficient energy to dislodge inner shell electrons of the target material, characteristic x-ray spectra are produced. The x-rays are filtered to produce monochromatic rays which are required for the diffraction. These x-rays are collimated and directed onto the sample. When the geometry of the incident x-rays impinging the sample satisfies the Bragg Equation, constructive interference occurs and a peak in intensity occurs. A detector records and processes this X-ray signal and converts the signal to a count rate which is then output to a device such as a printer or computer monitor [102].

In this work, the XRD patterns were obtained using PANalytical X'pert Pro powder x-ray diffractometer with a CuKα radiation. The XRD spectrum has been taken from 20^{o} to 120^{o} with a step size 0.02^{o} and a scanning time 14s/step. X-ray diffraction study of the samples was done using X'Pert High Score Plus Rietveld analysis software in combination with Pearson's crystal structure database [103].

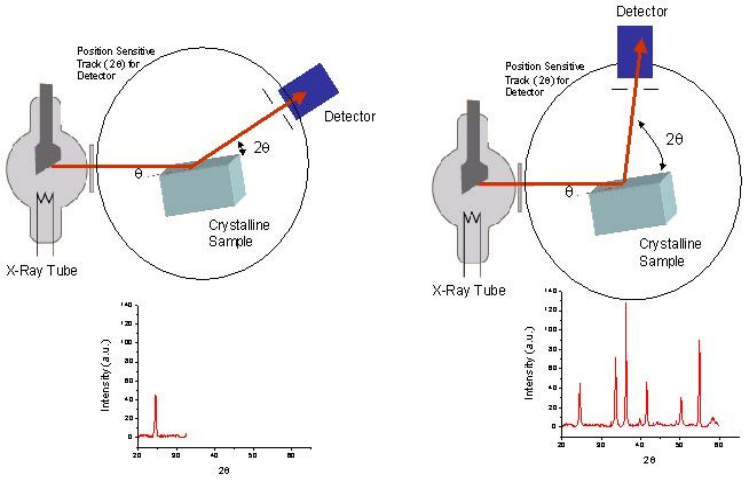

Figure 3.5: Schematic of powder XRD [102]

CHAPTER 4

RESULTS AND DISCUSSIONS

4.1 Isothermal section at 350°C through diffusion couples

The isothermal section of the Al-Ca-Zn system has been studied via 5 diffusion couples and 26 key samples. The analysis has revealed that there are 5 ternary compounds in the system. These ternary compounds have been named as IM1, IM2, IM3, IM4 and IM5 according to the amount of Ca-content in the intermetallics. IM1 is a new ternary solid solution reported for the first time in this work containing approximately 8.5 at.% Ca. The formula of this compound is $Al_xCa_{8.5}Zn_y$ ($26 \leq x \leq 29$, $62 \leq y \leq 65$, 350°C). The crystal structure of IM1 has also been confirmed in this work. IM2 is a ternary compound containing 20 at.% Ca and its formula is $Al_{4-x}CaZn_x$ ($1.2 \leq x \leq 2$, 350°C). IM2 has been studied and reported by a several research groups [90-94]. However, as discussed earlier in the literature review, the homogeneity range of this compound is not clear from the information obtained from the former works. In this work, the equilibrium of IM2 with the binary compound Al_4Ca has been identified using the diffusion couple approach. IM3 is another new ternary compound with approximately 25 at.% Ca-content, the formula for this compound is $Al_{3-x}CaZ_x$ ($2 \leq x \leq 2.2$, 350°C). IM4 is 33 at.% Ca-content ternary solid solution with $Al_{2-x}CaZn_x$ ($0.28 \leq x \leq 0.70$, 350°C) formula, which is similar to the results reported by [94, 95] at 600°C. IM5 is a high Ca-content ternary compound with $Al_2Ca_9Zn_3$formula. Among the binary compounds, Al_4Ca, Al_2Ca, $Al_{14}Ca_{13}$, $CaZn_{13}$, $CaZn_{11}$, $CaZn_5$, $CaZn_3$ and $CaZn_2$ have extended solid solution in the ternary at 350°C.

The detailed discussions of the solid solutions of these compounds and their relationships with other phases have been described in the following sections with the help of diffusion couples and key alloy experiments.

4.1.1 Solid-solid diffusion couples

The Solid-solid diffusion couple SSDC-1 has been prepared with terminal composition $Al_{69.6}Ca_{12.2}Zn_{18.2}$ to pure Zn. Back-scattered electron images of the solid-solid diffusion couple SSDC-1 with increased magnification of the area of interest are illustrated in Figure 4.1 (a), (b), (c) and (d). During heat treatment, extensive interdiffusion among Al, Ca and Zn took place allowing various equilibrium phases to form. EPMA line scan has been carried out to determine the solubility range of IM1, IM2 and $CaZn_{13}$as demonstrated in Figure 4.1(b) and (e). Spot analysis has been carried out for composition detection of smaller grains, for instance those of fcc-Al and ternary eutectic that has been found to have the composition $Al_{90.7}Ca_{3.3}Zn_{6.0}$. Based on the compositional information obtained by EPMA analysis, ternary and binary intermetallic compounds and the solid solubility of the binary compounds extending in the ternary system have been identified. Using the local equilibrium at the interfaces formed between the phases, the sequence of the phases along the diffusion path (from left to right corresponding to Figure 4.1) is: Al_4Ca + IM2+Eutectic→ IM1+ fcc-Al_1(black) → IM1+ fcc-Al_1(black) + fcc-Al_2(grey) → IM1+ fcc-Al_2(grey) + $CaZn_{13}$ → Zn. Two ternary compounds have been detected in this diffusion couple by EPMA spot analysis: ternary intermetallic (IM1) with $Al_{29.8}Ca_{8.6}Zn_{61.5}$formula and ternary intermetallic (IM2) with $Al_{56.0}Ca_{20.4}Zn_{23.6}$formula. The result of the 25μm EPMA line scan of the diffusion couple is shown in Figure 4.1(e). The solubility ranges have been calculated at the boundary between two phases using a

least square approximation method. From Figure 4.1(e), the limiting composition of the solid solution IM2 has been determined to be $Al_{56.0}Ca_{20.3}Zn_{23.7}$at 350^{o}C at the equilibrium with Al_4Ca, but the boundary between Al_4Ca and IM2 has not been identified. The solubility limits of IM1 have been studied at 350^{o}C from SSDC-1 and the compositions are $Al_{29.4}Ca_{8.4}Zn_{62.2}$ at the equilibrium with IM2 and $Al_{26.7}Ca_{8.4}Zn_{64.9}$ at the equilibrium with $CaZn_{13}$, respectively, as illustrated in Figure 4.1(e). The binary compound $CaZn_{13}$ has a maximum ternary solubility of 10.1 at.% Al with the composition $Al_{10.1}Ca_{8.0}Zn_{81.9}$. The least squares approximation has been used to obtain the solubility limits of all the compounds. The deviation from the linearity is about ±1 at.%, which is within the error limits of the EPMA measurements.

The compositions of the phases of ternary alloy have been determined by EPMA spot analysis. The ternary alloy $Al_{69.6}Ca_{12.2}Zn_{18.2}$is composed of a eutectic microstructure with the Al_4Ca+ IM2 matrix. The composition of the eutectic in the Al-rich region has been found by EPMA spot analysis to be approximately $Al_{90.7}Ca_{3.3}Zn_{6.0}$, as shown in Figure 4.1(a). Figure 4.1 (c) presents the fcc-Al miscibility. Two different fcc-Al precipitates have been found: the higher Al-rich phase is named as fcc-Al_1(black) and the Zn-rich phase is named fcc-Al_2(grey). The solubility range offcc-Al_1(black) has been found from pure Al to $Al_{71.2}Zn_{28.8}$ whereas fcc-Al_2(grey) phase has a solubility range from $Al_{52.4}Zn_{47.6}$ to $Al_{39.7}Zn_{63.3}$. The solubility of Zn in Al has been measured to be 7.7 at% Zn at 350^{o}C.

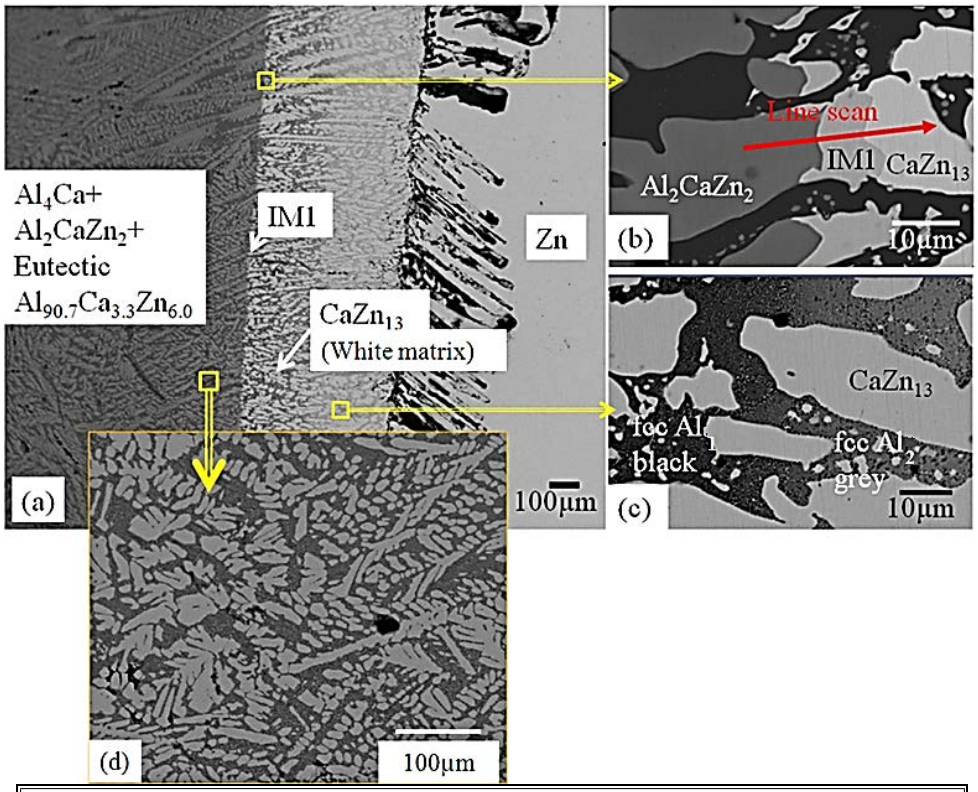

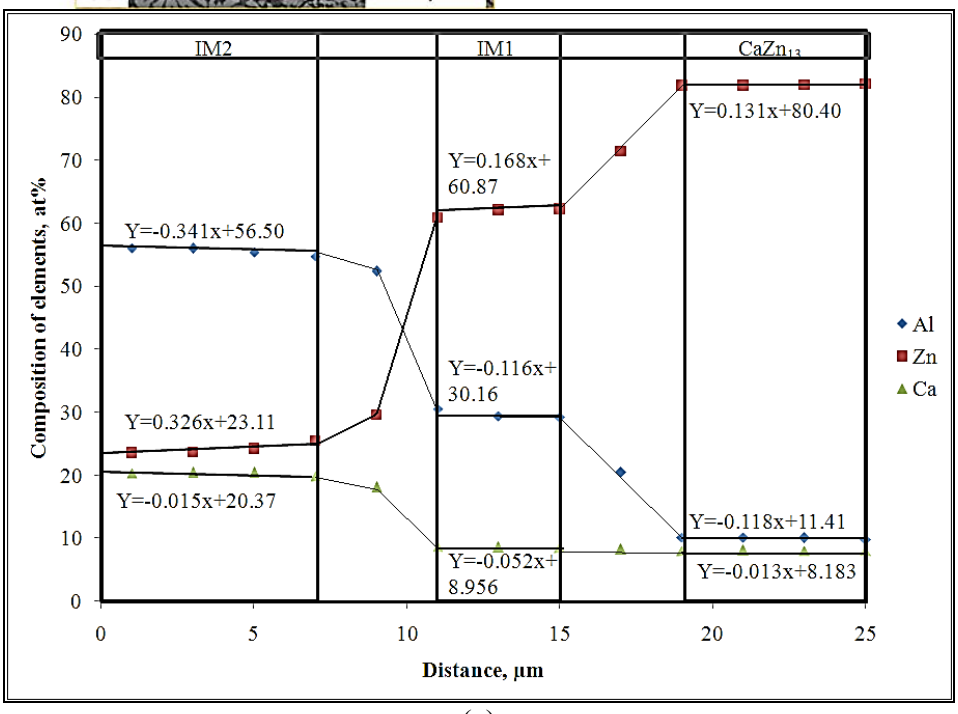

(e)

Figure 4.1: (a), (b) and (c) The back-scattered electron image of SSDC-1 annealed at 350°C for 5 weeks showing all the phases, (d) magnified view of the end member ternary alloy (e) compositional profile of the line scan of Figure 4.1 (b).

SSDC-1 has given the information about the phases that can form in the lower Ca-content region of the Al-Ca-Zn system. However, the results from SSDC-1 are not adequate enough to completely understand the solid solubility information and phase relations in this lower Ca-content region. In order to verify the phase boundary between Al_4Ca and IM2, solid-solid diffusion couple SSDC-2 with $Al_{66.3}Ca_{26.9}Zn_{6.8}$ ternary alloy and pure Zn as end members has been prepared. Back-scattered electron images of the solid-solid diffusion couple SSDC-2 with increased magnification of the area of interest are illustrated in Figure 4.2. The presence of the new ternary compound (IM1) has been confirmed from this diffusion couple. The sequence of the phases along the diffusion path (from left to right according to Figure 4.2) is: $Al_2Ca+Al_4Ca \rightarrow IM2 \rightarrow IM1$ + fcc-Al_1 (black) → IM1+ fcc-Al_1 (black)+ fcc-Al_2 (grey)→ IM1+ fcc-Al_2 (grey)+ $CaZn_{13}$ → Zn. A 45µm long EPMA line scan has been carried out to find the homogeneity ranges of Al_4Ca, IM1, IM2 and $CaZn_{13}$ phases, as demonstrated in Figure 4.2(b) and 4.2(d). The solubility ranges has been calculated at the boundary between two phases using a least square approximation method. On the basis of EPMA line scan, the phase boundary between Al_4Ca and IM2 has been well studied. Al_4Ca is a substitutional solid solution where Al atoms are gradually replaced by Zn atoms and the maximum solubility of Zn has been determined to be $Al_{65.2}Ca_{20.1}Zn_{13.9}$ at 350^{o}Cat the boundary with IM2. The solid solubility limit of IM2 has been identified with the composition $Al_{56.0}Ca_{20.6}Zn_{23.3}$ at the interface between Al_4Ca and IM2, which also verifies the result of SSDC-1. This finding contradicts the data of Pani et al. [94] who reported a continuous solid solution $Ca(Zn_{1-x}Al_x)_4$ (x=0.47-1.00 at 550^{o}C). However, it is possible that the continuous solid solution at 550^{o}C decomposes before reaching 350^{o}C to Al_4Ca and Al_2CaZn_2 phases suggesting

the presence of solid state immiscibility gap. This assumption could be supported by two facts: (i) Al-Zn system demonstrates similar tendency for the Al-fcc phase and (ii) Al_4Ca and Al_2CaZn_2 phases have same Al_4Ba-type crystal structures that can form continuous solid solubility. Additional experimental study is needed to verify this assumption. The composition of IM1 has been determined to be $Al_{29.7}Ca_{8.7}Zn_{61.6}$ at the grain boundary between IM1 and IM2. Binary compound $CaZn_{13}$ has been found to form extended substitutional solid solutions where Al is substituted for Zn up to 10.0 at.% Al having the composition $Al_{10.0}Ca_{7.9}Zn_{82.1}$. The composition is in accord with the results obtained from SSDC-1. Furthermore, the fcc-Al miscibility of the SSDC-2has been examined by EPMA spot analysis, as illustrated in Figure 4.2(c). The solubility limits of fcc-Al_1(black) phase have been determined to be from pure Al to$Al_{72.6}Ca_{27.4}$ and the solubility limits of the fcc-Al_2(grey)phase have been determined from $Al_{54.2}Zn_{45.8}$ to $Al_{37.8}Zn_{62.2}$at 350^{o}C. The results are consistent with the he values obtained from SSDC-1.

The morphology of the diffusion zone evolved in this solid-state SSDC-2 has been studied. The IM2 diffusion layer appears as a continuous layer adjacent to Al_4Ca, as demonstrated in Figure 4.2(b). Then another continuous layer of IM1 appears adjacent to the IM2 layer. The morphology then changes to a three phase region consisting of fcc-Al precipitates embedded in IM1 matrix, which later, enters another three phase region containing IM1, fcc Al-grey and $CaZn_{13}$. Finally, the morphology terminates at the end member Zn.

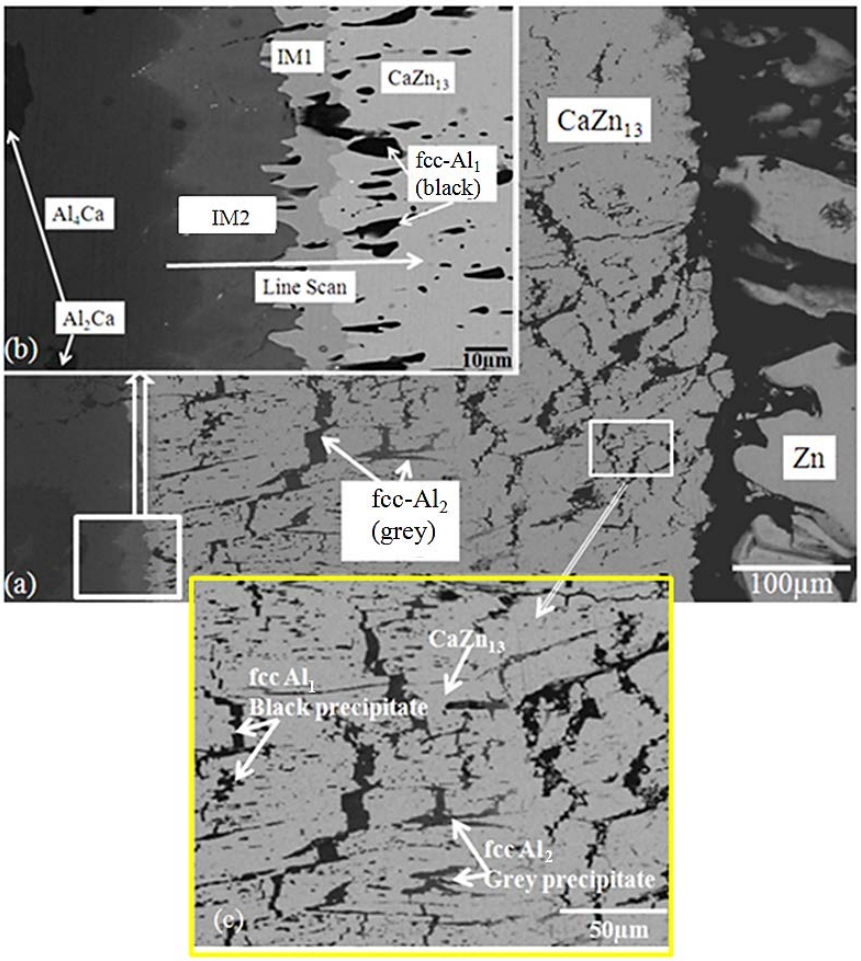

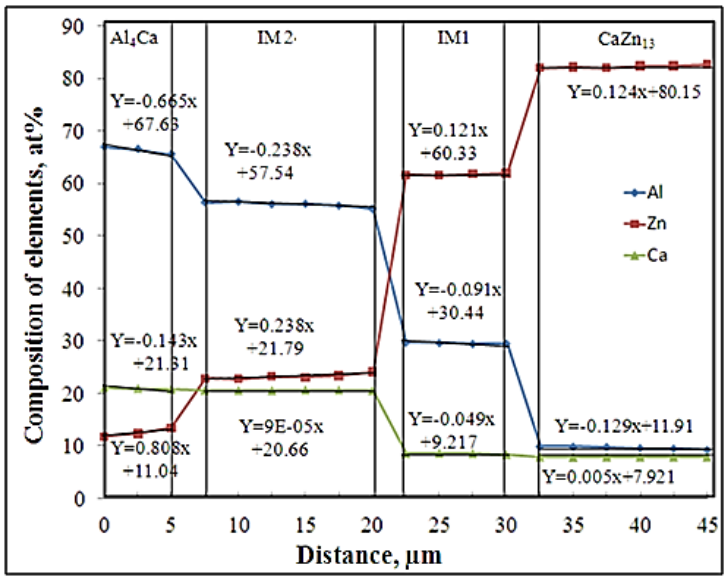

Figure 4.2: (a) and (b) Back-scattered electron image of SSDC-2 at 350°C annealed for 5 weeks, (c) the microstructure of fcc Al miscibility, (d) compositional profile of the line scan performed in Figure 4.2 (b).

Combining the results from SSDC-1 and SSDC-2, a large amount of phase equilibrium information has been obtained from 0 to 30 at.% Ca of the Al-Ca-Zn phase diagram. A partial isothermal section at 350ºC of the Al-Ca-Zn system has been constructed and the phase relations are demonstrated in Figure 4.3. The existence of the ternary substitutional solid solution IM1 has been confirmed in these two diffusion couples. Based on the EPMA analysis the solubility ranges for this compound has been determined with the compositions $Al_{29.4}Ca_{8.4}Zn_{62.2}$to $Al_{26.7}Ca_{8.4}Zn_{64.9}$. The solid solubility limit of IM2 has been identified with the composition $Al_{56.0}Ca_{20.6}Zn_{23.4}$ at the Al-rich region. Al_4Ca is an extensive binary substitutional solid solution and the maximum solubility has been determined with the composition $Al_{64.36}Ca_{20.56}Zn_{15.08}$. $CaZn_{13}$phase has been found to form extended substitutional solid solution where Al atom replaces approximately 10.0 at.% of Zn.

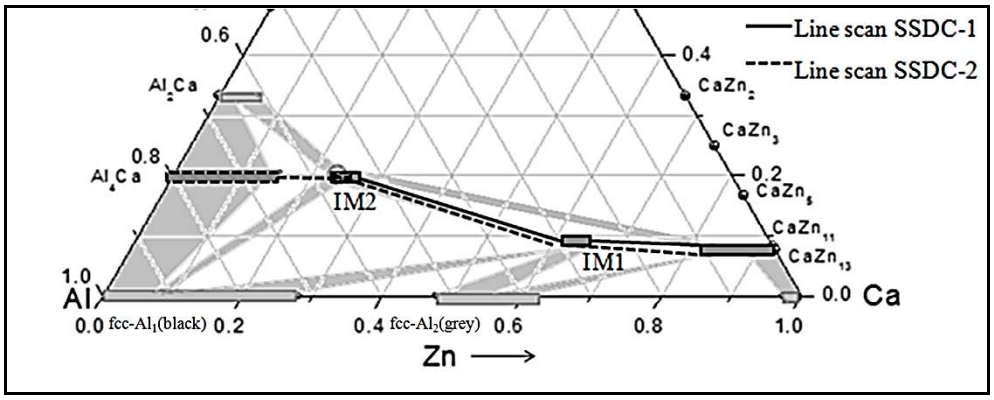

Figure 4.3: Partial isothermal section of the Al-Ca-Zn system from 0 to 30 at.% Ca at 350ºC obtained from SSDC-1 and SSDC-2.

The solid-solid diffusion couple SSDC-3 has been prepared with the terminal compositions $Al_{40}Ca_{40}Zn_{20}$ and pure Zn. Back-scattered electron images of SSDC-3 with increased magnification showing the formation of eight different intermetallics are

illustrated in Figure 4.4. Four ternary compounds have been found in the diffusion couple: IM2, IM3, IM4 and IM5. IM2 is a ternary solid solution with $Al_{4-x}CaZn_x$ ($1.2 \leq x \leq 2$ at 350^oC) formula. IM3 is a ternary compound with $Al_{3-x}CaZ_x$ ($2 \leq x \leq 2.2$ at 350^oC) formula. IM4 is a C36-type ternary solid solution with $Al_{2-x}CaZn_x$ ($0.28 \leq x \leq 0.7$ at 350^oC) formula. On the other hand, IM5 is a high Ca-content ternary compound with $Al_2Ca_9Zn_3$ formula. The binary compounds: $CaZn_2$, $CaZn_5$, $CaZn_{11}$ and $CaZn_{13}$ have extended solid solubility in the ternary. The following three phase triangulations are identified from Figure 4.4: IM2, $CaZn_{11}$ and $CaZn_{13}$; IM2, $CaZn_5$ and $CaZn_{11}$; IM2, IM3 and $CaZn_5$; IM2, IM3 and IM4. From SSDC-3, the homogeneity ranges of several compounds have been studied. The limit of IM2 solid solution has been found with the composition $Al_{40.5}Ca_{20.3}Zn_{39.2}$ in Zn-rich side. The maximum solubility of IM4 has been determined to be at the composition $Al_{57.4}Ca_{33.3}Zn_{9.3}$ in the Al-rich side and $Al_{43.5}Ca_{33}Zn_{23.5}$ in the Zn-rich side. Two new ternary compounds have been found from this diffusion couple by EPMA point analysis: $Al_{20}Ca_{25}Zn_{55}$ (IM3) and $Al_{14.3}Ca_{63.2}Zn_{22.5}$ (IM5). To determine the homogeneity range of IM3, several key alloys have been analyzed and will be further discussed in the key alloys analysis section. IM5 ternary compound has been found with the composition $Al_{14.3}Ca_{63.2}Zn_{22.5}$. Therefore, the chemical formula of IM5 has been derived as $Al_2Ca_9Zn_3$.Among the binary compounds, $CaZn_2$ has a wide range of solubility starting from 31 at.% Al with the composition$Al_{31}Ca_{33}Zn_{36}$. The result is in good agreement with the values reported by [94, 95]. $CaZn_5$ has a solid solution with 11.3 at% Al and the composition is $Al_{11.3}Ca_{17.1}Zn_{71.6}$. $CaZn_{11}$ has a solubility of 1.7 at% Al with the composition $Al_{1.7}Ca_{8.8}Zn_{89.5}$. One new eutectic has been found with the composition $Al_{16.4}Ca_{12.7}Zn_{70.8}$ in the Zn-rich zone.

The morphology of the diffusion zone evolved in this solid-state diffusion couple SSDC-3 has been studied. The $CaZn_{13}$ diffusion layer appears as a continuous layer adjacent to the end member Zn, as demonstrated in Figure 4.4(a). Then the morphology changes to another continuous layer of $CaZn_{11}$ as demonstrated in Figure 4.4(b). After that, the morphology changes to a eutectic structure and IM2. Later, the morphology of the reaction layer changes gradually to another two-phase structure consisting of IM2 and $CaZn_5$. Then the diffusion path enters to another two-phase region consisting of the phases IM2 and IM3. The morphology finally terminates at the ternary alloy end member consisting of IM4, IM5 and $CaZn_2$.

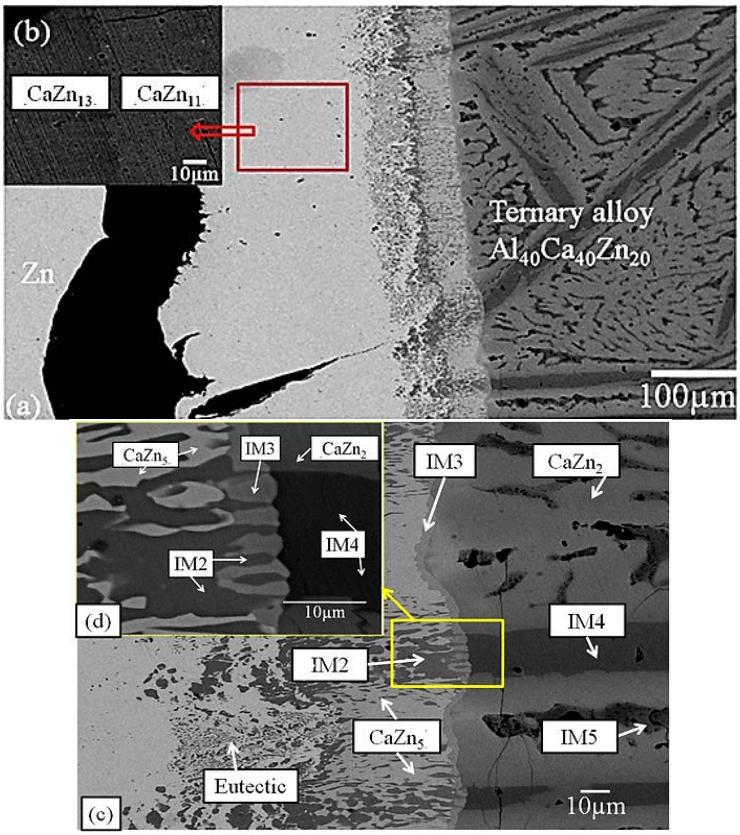

Figure 4.4.: (a), (b), (c) and (d) Back-scattered electron image of SSDC-3 with increased magnification showing 8 different intermetallics.

Back-scattered electron image of SSDC-4 is demonstrated in Figure 4.5 showing the formation of nine different intermetallic compounds. The diffusion couple has been prepared with terminal compositions $Al_{30}Ca_{37.3}Zn_{32.7}$ and pure Zn. Four ternary compounds have been found in this diffusion couple: IM2, IM3, IM4 and IM5. The binary compounds: $Al_{14}Ca_{13}$, $CaZn_2$, $CaZn_5$, $CaZn_{11}$ and $CaZn_{13}$ have extended solid solubility in the ternary. The subsequent six phase-triangulations are identified from Figure 4.5: IM5, $Al_{14}Ca_{13}$ and $CaZn_2$; IM4, $Al_{14}Ca_{13}$ and $CaZn_2$; IM3, IM4 and $CaZn_2$; IM2, IM3 and IM4; IM2, IM3 and $CaZn_5$; IM2, $CaZn_{11}$ and $CaZn_{13}$. The homogeneity ranges of different binary and ternary compounds are detected by EPMA spot analysis. The maximum solubility of IM2 has been found with the composition $Al_{40.5}Ca_{20.3}Zn_{39.2}$ in the Zn-rich side at 350^{o}C. The solubility limit of the C36-type phase IM4 has been determined with the composition $Al_{57.3}Ca_{33.3}Zn_{9.4}$ at 350ºC in the Al-rich corner. The composition of IM3 has been determined to be $Al_{20.4}Ca_{25}Zn_{54.5}$ by EPMA point analysis while the composition of IM5 has been detected as $Al_{14.7}Ca_{62.9}Zn_{22.4}$.Among the binary compounds, $Al_{14}Ca_{13}$ has a solubility limit of 16.6 at% of Zn with the composition $Al_{33.6}Ca_{49.7}Zn_{16.6}$. $CaZn_2$ has a huge extended solid solubility in ternary with the composition $Al_{31}Ca_{33.3}Zn_{35.7}$. The solid solutions of $CaZn_5$ and $CaZn_{13}$ have been determined with the composition $Al_{11.4}Ca_{17.1}Zn_{71.5}$ and $Al_{10.4}Ca_{8.1}Zn_{81.4}$, respectively. The results show a good consistency with other diffusion couples within the error limits of the EPMA measurements.

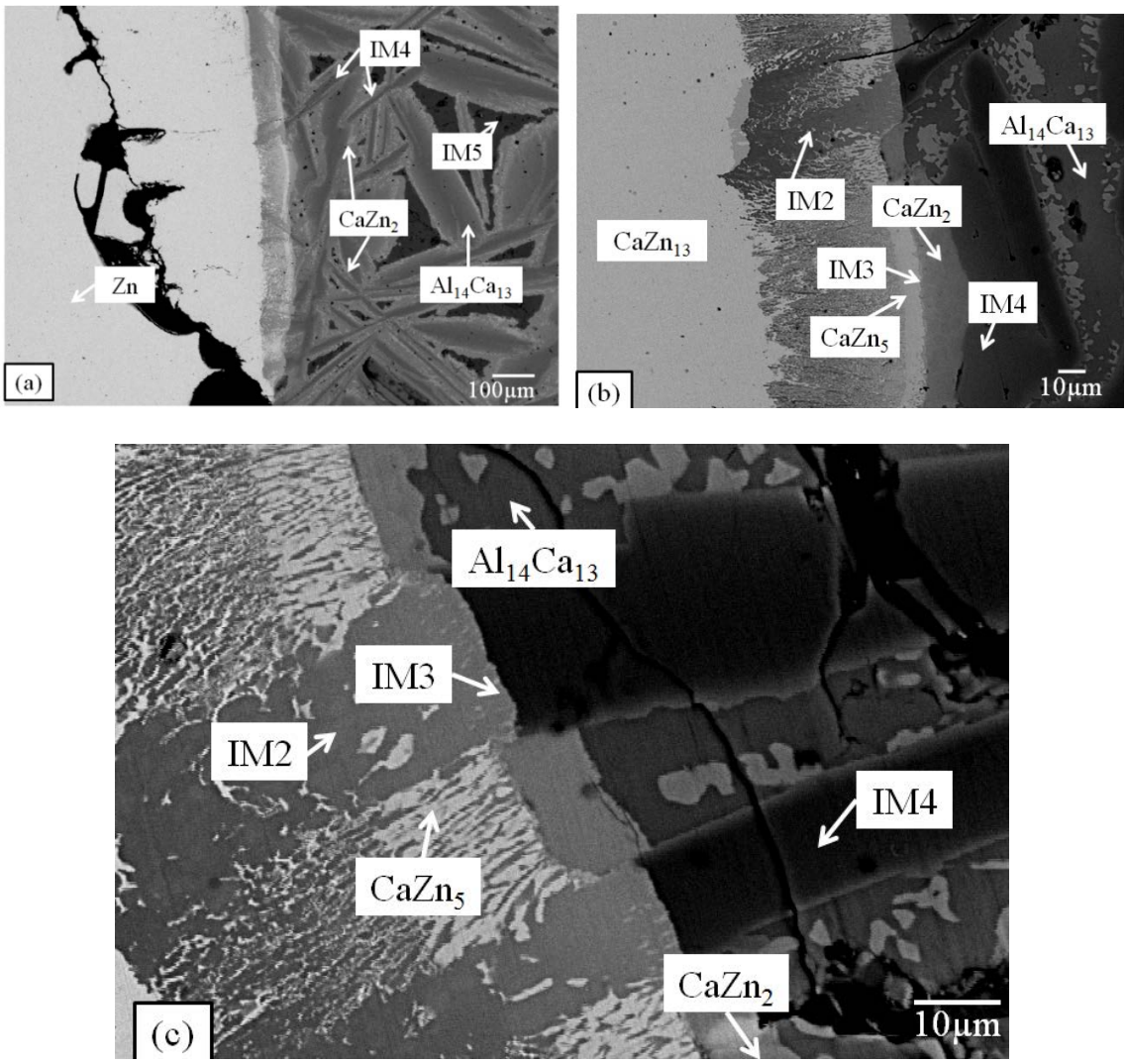

Figure 4.5 (a) Back-scattered electron image of SSDC-4, (b) and (c) magnified view of different phases in SSDC-4.

Combining the EPMA results of the solid-solid diffusion couples SSDC-3 and SSDC-4, a partial isothermal section of the Al-Ca-Zn system at 350ºC has been constructed and the phase relations are demonstrated in Fig 4.6. The existences of IM1 and IM3 ternary compounds have been confirmed by these two diffusion couples. The solubility limits of the C36-type phase IM4 have been determined with the composition $Al_{57.3}Ca_{33.3}Zn_{9.4}$ in the Al-rich corner and $Al_{43.5}Ca_{33}Zn_{23.5}$ in the Zn rich corner, which are similar values compare with the literature at 700ºC [94, 95]. The maximum solubility of IM2 has been determined with the composition $Al_{40.5}Ca_{20.0}Zn_{39.5}$ in the Zn-rich side. $Al_{14}Ca_{13}$ has a

homogeneity range of 16.6 at% of Zn corresponding to the composition $Al_{33.6}Ca_{49.7}Zn_{16.6}$. $CaZn_2$ has a maximum solubility with the composition $Al_{31}Ca_{33}Zn_{36}$. The limit of $CaZn_5$ solid solution has been studied where 11.3 at% of Al substituted for Zn with the composition $Al_{11.3}Ca_{17.1}Zn_{71.6}$. $CaZn_{11}$ has a solubility of 1.7 at% of Al with the composition $Al_{1.7}Ca_{8.8}Zn_{89.5}$.

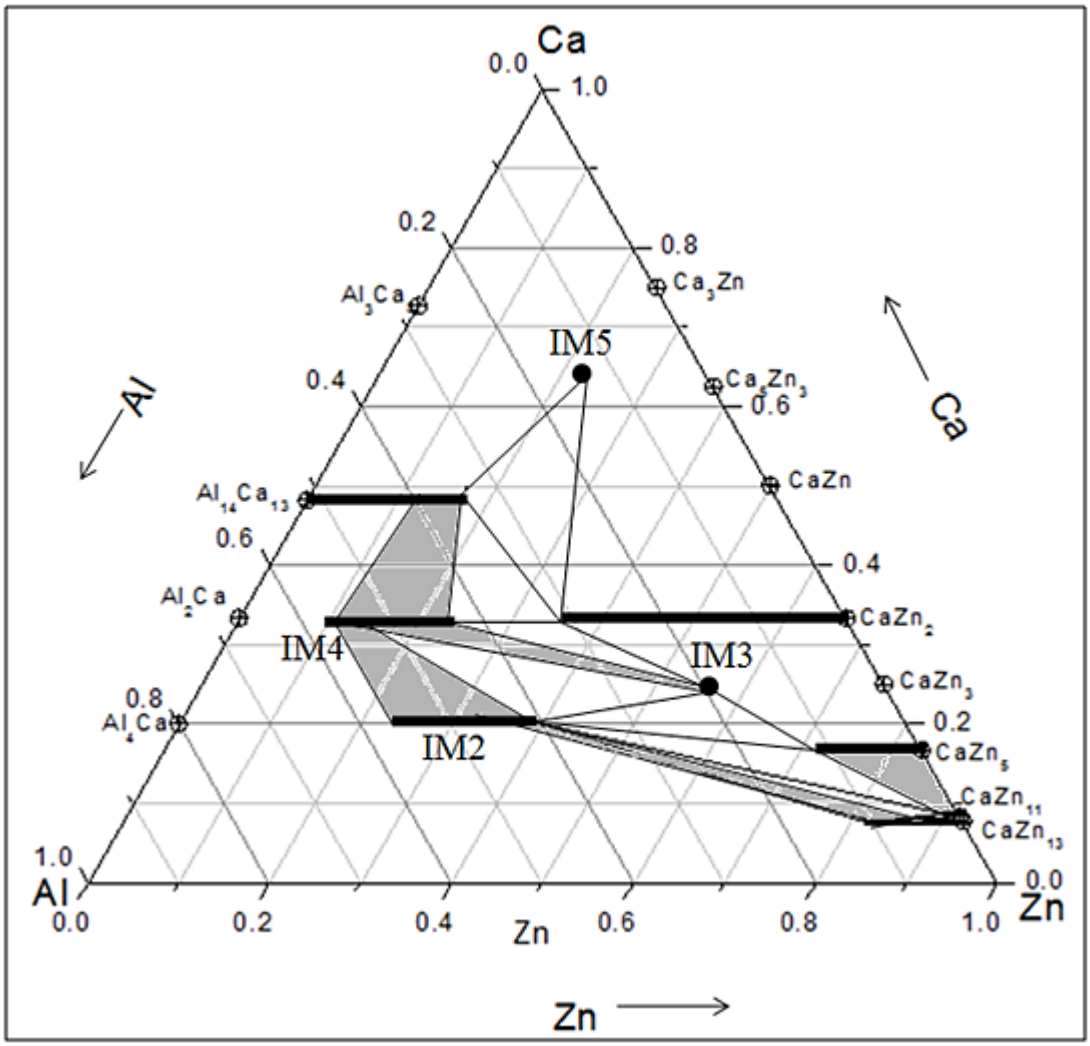

Figure 4.6: Partial isothermal section of the Al-Ca-Zn system obtained from SSDC-3 and SSDC-4 annealed at 350ºC for 5 weeks.

4.1.2. Solid-Liquid diffusion couple

When solid-solid diffusion couples are not successful owing to the fragility and brittleness of the end members, solid-liquid diffusion couple is a feasible technique. In this experiment one solid-liquid diffusion couple has been prepared and analyzed with the end members Al_2Ca and Zn. The back-scattered electron images of solid-liquid diffusion couple Al_2Ca-Zn annealed at 350^oC for 1 week has been demonstrated in Figure 4.7 showing the formation of five intermetallic compounds. On the basis of similar terminal end members of diffusion couples, the sequences of the phases along the diffusion path are the same as the results of SSDC-2. Analysis of the diffusion reaction zone indicates that the sequence of the phases along the diffusion path (Figure 4.7) is: $Al_2Ca \rightarrow Al_4Ca \rightarrow IM2 \rightarrow IM1 +$ fcc-Al_1(black) $\rightarrow$ fcc-Al_1(black) +fcc-Al_2(gray) + $CaZn_{13} \rightarrow Zn$. Two ternary intermetallic compounds have been found from this diffusion couple: IM1 and IM2. Binary compounds Al_4Ca and $CaZn_{13}$ have extended solubility in the ternary. A 100 μm line scan has been performed to determine the solubility limits of the compounds as shown in Figure 4.8. The least square approximation is used to establish the elemental concentration profiles of Al_4Ca, IM1, IM2 and $CaZn_{13}$ compounds. The deviation from the linearity of all phases is ±2 at.%, which is within the error limits of the EPMA measurements. The maximum solubility of Al_4Ca has been found to be at the composition $Al_{64.7}Ca_{19.7}Zn_{15.6}$. The solid solubility limit of IM2 has been determined to be at the composition $Al_{55.9}Ca_{19.6}Zn_{24.5}$ in the Al-rich side. From this solid-liquid diffusion couple the maximum solubility limits of IM1 has been found at the composition $Al_{29.1}Ca_{8.8}Zn_{62.1}$in the Al-rich side and $Al_{26.7}Ca_{8.7}Zn_{64.6}$in the Zn-rich side, respectively. The maximum solubility of $CaZn_{13}$ is at the composition $Al_{9.9}Ca_{8.3}Zn_{81.8}$.On

the basis of this solid-liquid diffusion couple Al_2Ca-Zn, a partial isothermal section at 350°C has been constructed in Figure 4.9.

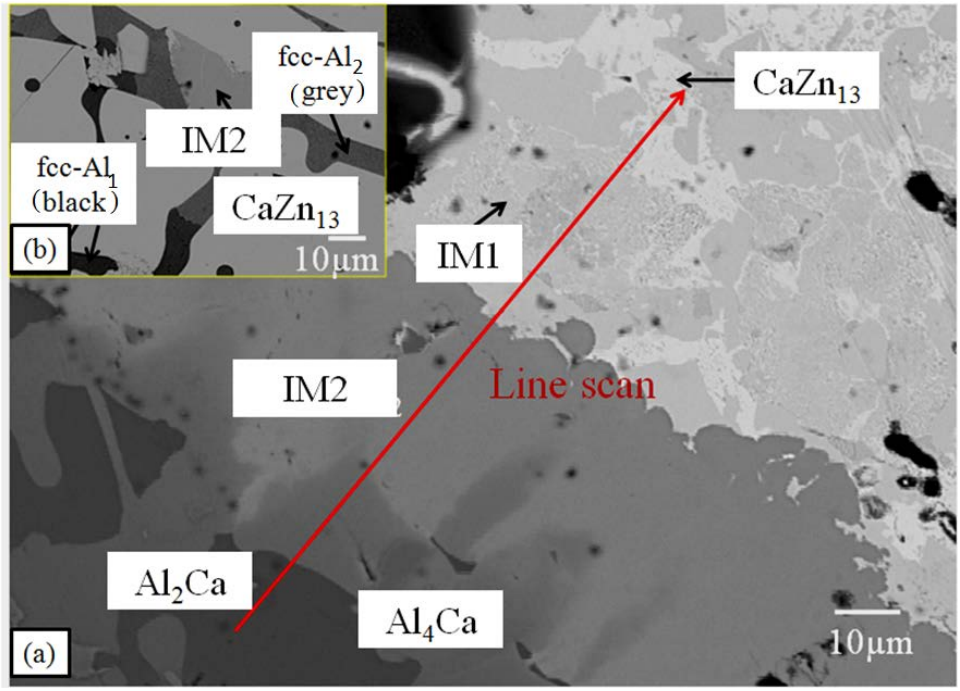

Figure 4.7: (a) Backscattered electron image of solid-liquid diffusion couple Al_2Ca-Zn, (b) The microstructure of the fcc Al miscibility.

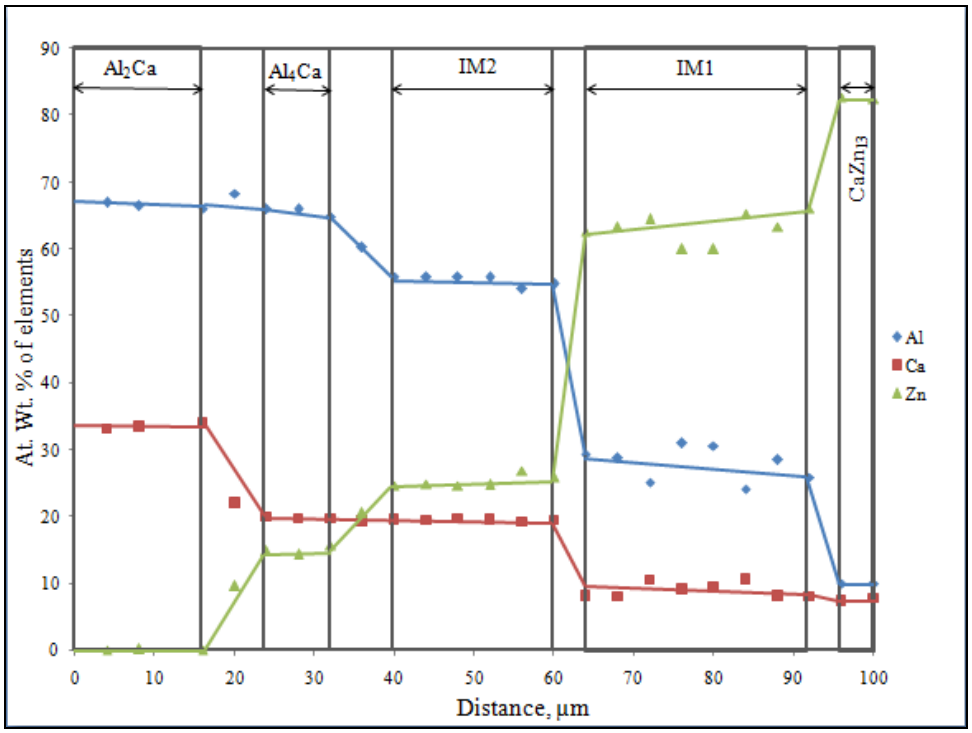

Figure 4.8: Line scan performed on the solid-liquid diffusion couple from Figure 4.7

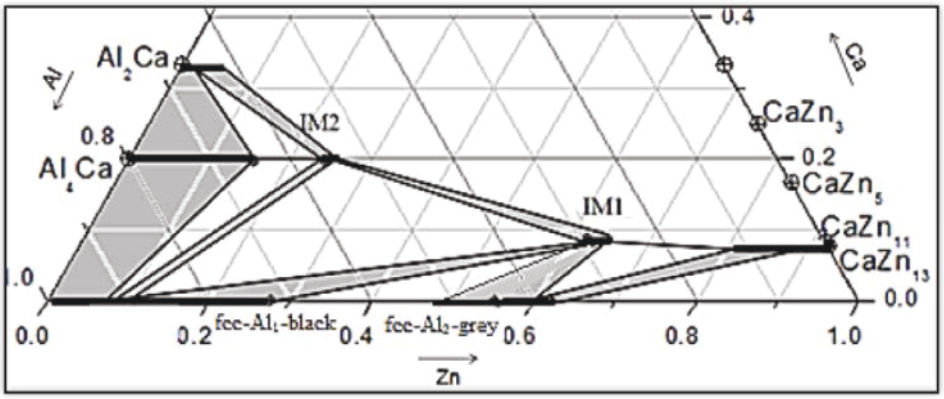

Figure 4.9: Partial isothermal section of the Al-Ca-Zn system from 0 to 30 at.% Ca at 350ºC obtained fromsolid-liquid diffusion couple Al_2Ca-Zn.

Combining the results obtained from four solid-solid diffusion couples and one additional solid-liquid diffusion couple, a partial isothermal section of the Al-Ca-Zn system at 350ºC has been constructed and the phase relations are demonstrated in Figure 4.10. In order to improve the reliability of the information obtained from the diffusion couples, 26 selected key alloys have been used to study the phase relations, phase boundaries and crystallographic information of the ternary compounds in the Al-Ca-Zn system 17 of which will be discussed in the key alloys section.

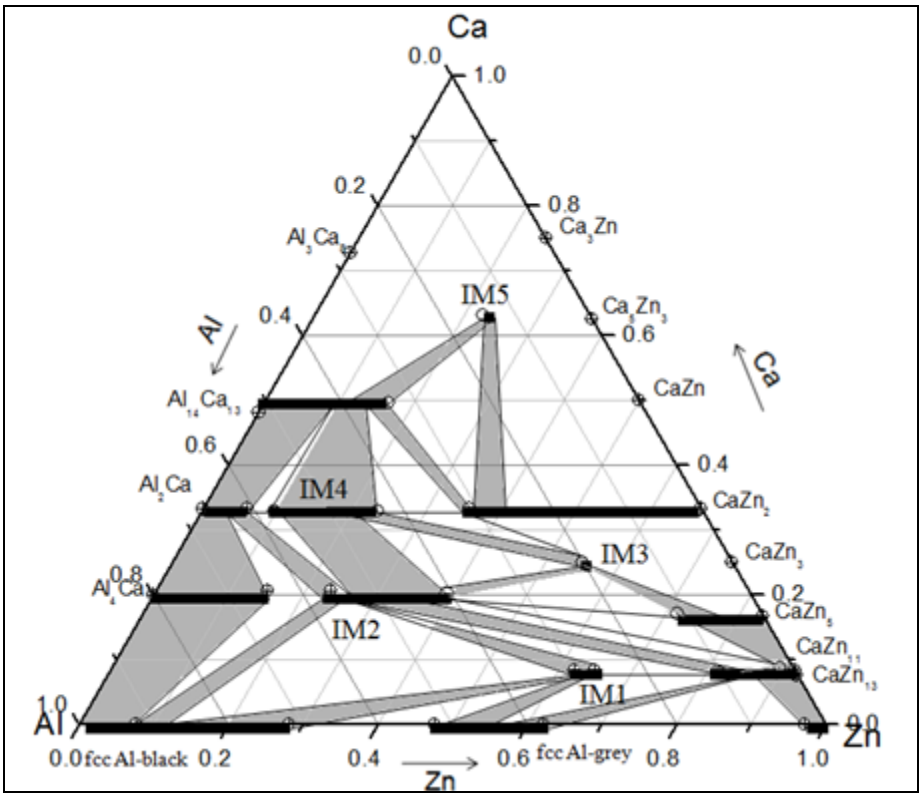

Figure 4.10: Isothermal section of the Al-Ca-Zn system at 350°C based on the results obtained from 4 solid-state diffusin couples and one solid-liquid diffusion couple

4.2. Diffusion couple morphology

The morphology of the diffusion zone evolved in the solid-solid diffusion couple SSDC-2 has been studied. In this diffusion couple the diffusion reaction starts from the two-phase end member Al_2Ca+ Al_4Ca, as demonstrated in Figure 4.2, then the morphology changes to a single phase IM2 layer. Afterwards, the morphology changes to another single layer of IM1 compound. Then the morphology changes to isolated fcc-Al precipitates embedded in the IM1 matrix. Then, the matrix IM1 changes to $CaZn_{13}$ with fcc-Al precipitates. Finally, the morphology terminates at the end member Zn. In order to calculate the interdiffusion coefficients, determination of the volume fraction of phases in the diffusion couple is needed. The volume fraction of the fcc-Al precipitates with layer

$CaZn_{13}$ matrix is considerably higher than the layer IM1 with fcc-Al precipitates, as illustrated in Figure 4.2. A schematic representation of the morphology of SSDC-2 has been depicted in Figure 4.11(a). The morphology of this diffusion couple has been compared with a similar type of diffusion couple with the end members $Ca_{10.3}Mg_{41.4}Zn_{48.3}$-Zn as reported by Zhang et al.[99]. In their work, they reported possible diffusion couple morphology when a pure element is coupled with a three-phase alloy as demonstrated in Figure 4.11(b). Whereas, a pure element coupled with a two-phase alloy has been used in this work and the morphology has been obtained from the current work shows good similarity with [99].

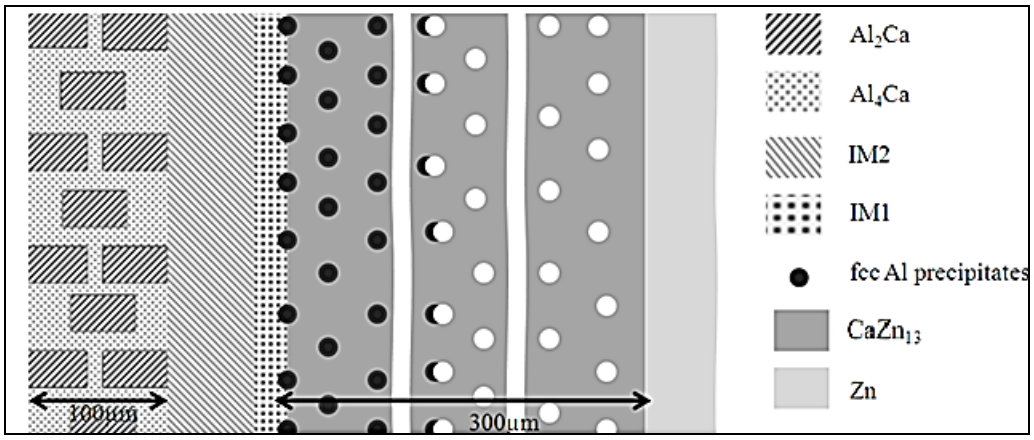

(a)

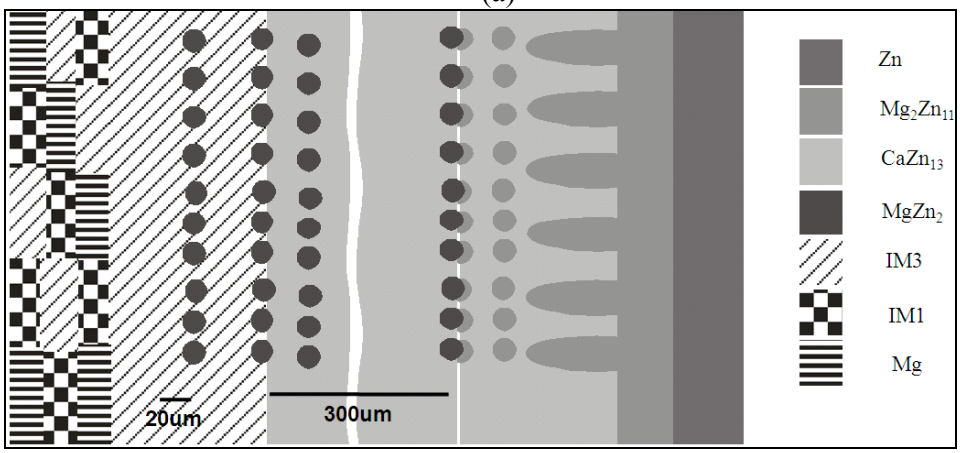

(b)

Figure 4.11 :(a) The morphology of the diffusion zone evolved in the solid-solid diffusion couple SSDC-2 (b) The possible morphologies in solid-solid diffusion couples when a pure element is attached to a three-phase alloy [99].

In the solid-solid diffusion couple SSDC-3, $CaZn_{11}$ and $CaZn_{13}$ phases are the dominant reaction products, as the microstructure in Figure 4.4 exemplifies. Another morphology of the diffusion zone evolved in this diffusion couple is the 'tooth-like' structure, as can be seen clearly in Figure 4.4. This 'tooth-like' morphology has first been demonstrated in the work of Zhang et al.[99]. The morphology of SSDC-3 is rather complex compared to SSDC-1 and SSCDC-2. To understand such complex morphology, the diffusion couple can be divided into several sub-diffusion couples. In the present work, the morphology of the diffusion couple has been studied by considering two micro-diffusion couples; IM4 with $CaZn_{11}$ and $CaZn_2$ with $CaZn_{11}$ as demonstrated in Figure 4.12(a) and (b) respectively. Figure 4.12(a) and (b) is combined to understand the morphology of SSDC-3 as demonstrated in Figure 4.12(c). The diffusion path has followed two different directions during the interdiffusion between IM4 and $CaZn_{11}$ phase as shown by rectangular box 1 and 2 in Figure 4.12(a). For diffusion path-1 the products of interdiffusion between IM4 and ($CaZn_{11}$) are IM2 and ($CaZn_5$) whereas for diffusion path-3 the products of interdiffusion are IM2, IM3 and ($CaZn_5$). On the other hand, IM2, IM3 and ($CaZn_5$) are produced as a result of interdiffusion between ($CaZn_2$) with ($CaZn_{11}$) as illustrated in Figure 4.12(b).

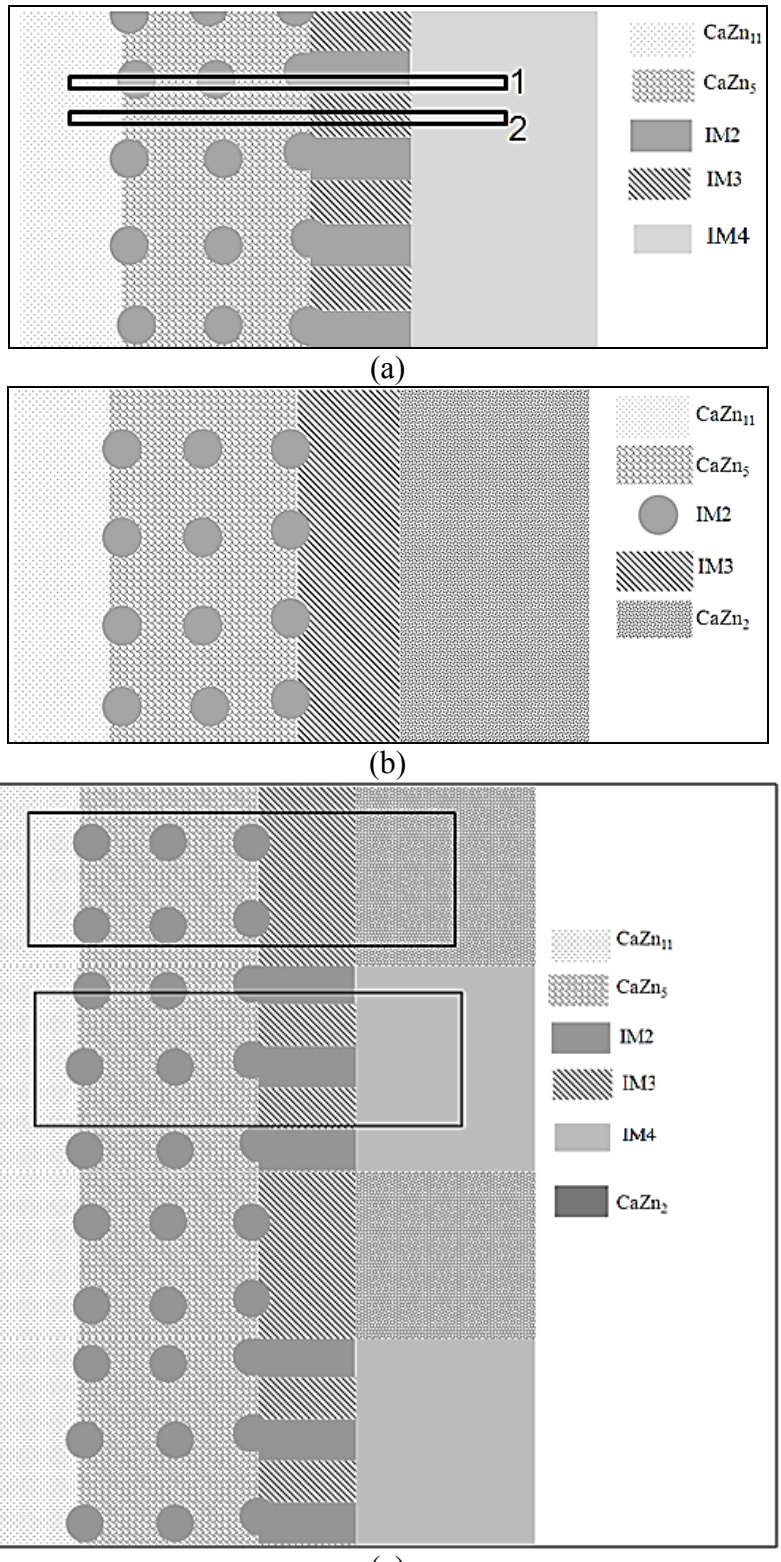

Figure 4.12: (a) Morphology of the micro-diffusion couple IM4-$CaZn_{11}$: the tooth-like morphology and (b) The $CaZn_2$-$CaZn_{11}$ micro-diffusion couple (c) The tooth-like morphology in SSDC-3

4.3 Key alloys analysis

4.3.1 Homogeneity ranges and crystallographic information of IM1and phase relations between IM1, IM2 and $CaZn_{13}$

In order to determine the solubility ranges and crystal structure of IM1, 4 key alloys have been prepared (KS1 to KS4). The microstructures and XRD patterns of these key alloys are illustrated in Figure 4.13. The chemical compositions of phases in these key alloys have been measured quantitatively by EPMA. The composition and phase identifications of these alloys are summerized in Table 4.3.1-1. The actual composition of the alloys has been measured by ICP and used for the analysis.

The microstructure of the key alloy KS1shows the presence of three phases (IM1, IM2 and $CaZn_{13}$) and a ternary eutectic morphology. EPMA point analysis of KS1 has been carried out to determine the compositions and phase equilibriums of the existing phases. As shown in Figure 4.13(a), IM1 is in equilibrium with IM2 and $CaZn_{13}$ phases. The composition of IM1 has been determined as $Al_{29.8}Ca_{8.5}Zn6_{1.7}$. The consecutive composition of IM2 has been found to be $Al_{54.4}Ca_{20.3}Zn_{25.3}$ and the composition of the eutectic has been determined approximately as $Al_{36.2}Ca_{52.7}Zn_{11.1}$. $CaZn_{13}$ phase is in equilibrium with the other two phases with the corresponding composition $Al_{10.3}Ca_{7.9}Zn_{81.7}$. The results obtained from KS1 support the results found from SSDC-1 and SSDC-2. Key alloy KS2 constitutes of IM1, IM2 and Al phases. The compositions of the equilibrium phases are $Al_{30.0}Ca_{8.5}Zn_{61.5}$ for IM1, $Al_{53.3}Ca_{20.5.5}Zn_{26.2}$ for IM2 and $Al_{95.0}Zn_{5.0}$ for the Al solid solution. The results support those obtained from SSDC-1 and SSDC-2. KS3 shows similar results as KS2. In KS3, IM1, IM2 and Al phases are in

equilibrium, as shown in Figure 4.13(d). The compositions of the equilibrium phases are as follows: IM1 ($Al_{30.4}Ca_{8.5}Zn_{61.1}$), IM2 ($Al_{55.5}Ca_{20.5}Zn_{24.0}$) and Al ($Al_{95.1}Zn_{4.9}$). The key alloy KS4 gives homogeneity ranges of IM1 with the composition $Al_{28.9}Ca_{8.5}Zn_{62.6}$ in the Al-rich region and $Al_{26.7}Ca_{8.4}Zn_{64.9}$ in the Zn-rich region. The microstructure of the alloy consists of 2 phases, IM1 and Al and one ternary eutectic. The Al-solid solution has a composition of $Al_{95.4}Zn_{4.5}$ and the composition of the eutectic is $Al_{94.2}Ca_{3.6}Zn_{3.2}$. Several EPMA point analysis have been performed to obtain the compositional range of IM1. The homogeneity ranges of IM1 obtained from KS4 are similar with the result obtained from SLDC. However, other key alloys (KS1, KS2 and KS3) and SSDC-1 and SSDC-2 have not shown any formation of solid solution of IM1. The possible reason for it could be the annealing time, which was not long enough for the full formation of the solid solution of IM1.In this work, the general formula of IM1 has been taken as $Al_xCa_{8.5}Zn_y$ ($26 \leq x \leq 29$, $62 \leq y \leq 65$; 350^{o}C) based on the results obtained from KS4 and SLDC. Nevertheless, more experiments are required for better accuracy of the homogeneity ranges of this ternary compound.

The sample KS1 contains significant amount of IM1 (more than 60%), therefore, this sample has been used to determine the crystallographic information of IM1 compound. This sample contains 3 phases, IM1, IM2 and $CaZn_{13}$ and among them IM1 is the dominating phase, as can be seen in Figure 4.13(a). The Rietveld analysis of the XRD pattern showing the phases IM1, Al_2CaZn_2 and $CaZn_{13}$ phases in KS1is shown in Figure 4.12(b). The XRD pattern of IM1 has been indexed using TREOR90 software and the lattice parameters have been identified. Using these lattice parameters the structure type

of phase has been identified from Pearson's crystallographic database [98]. Then the atoms of the cell have been rearranged using the suggested structure type and Rietveld analysis has been performed to determine the exact positions of the atoms and refine the lattice parameters. The crystal structure information of IM1 is included in Table4.3.1-2. IM1 has been found to have a cubic structure with cell parameter a= 8.49Å, $BaHg_{11}$ prototype (Pearson symbol cP36) and space group $Pm\bar{3}m$ (221) [100].

Table 4.3.1-1: Chemical composition of key alloys from ICP and the equilibrium phases

Key alloys	Composition from ICP (at.%)	Phases from EPMA	Phase composition	Phases from XRD
KS1	$Al_{30.1}Ca_{9.8}Zn_{60.1}$	IM1	$Al_{29.8}Ca_{8.5}Zn_{61.7}$	IM1
		IM2	$Al_{54.4}Ca_{20.3}Zn_{25.3}$	IM2
		$CaZn_{13}$	$Al_{10.3}Ca_{7.9}Zn_{81.7}$	$CaZn_{13}$
		Eutectic	$Al_{36.2}Ca_{52.7}Zn_{11.1}$	-
KS2	$Al_{59.3}$ $Ca_{10.4}$ $Zn_{30.3}$	IM1	$Al_{30.0}Ca_{8.5}Zn_{61.5}$	Not available
		IM2	$Al_{53.3}Ca_{20.5.5}Zn_{26.2}$	
		Al	$Al_{95.0}Zn_{5.0}$	
KS3	$Al_{55.3}Ca_{12.8}Zn_{31.9}$	IM1	$Al_{30.4}Ca_{8.5}Zn_{61.1}$	
		IM2	$Al_{55.5}Ca_{20.5}Zn_{24.0}$	
		Al	$Al_{95.1}Zn_{4.9}$	
KS4	$Al_{79.7}Ca_{5.6}Zn_{14.7}$	IM1	$Al_{28.9}Ca_{8.5}Zn_{62.6}$to $Al_{26.7}Ca_{8.4}Zn_{64.9}$	Not available
		Al	$Al_{95.4}Zn_{4.5}$	
		Eutectic	$Al_{94.2}Ca_{3.6}Zn_{3.2}$	

Table 4.3.1-2: Crystallographic data for the ternary compound IM1

Phase	Crystal structure	Pearson symbol	Space group	Lattice parameters (Å)	Wyckoff symbol
IM1	Cubic	cP36	$Pm\bar{3}m$	8.49	221

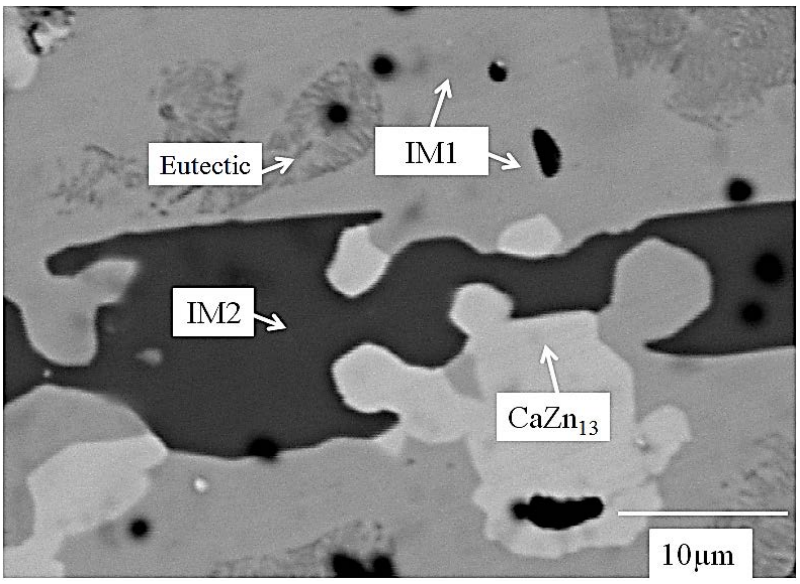
Eutectic
IM1
IM2
CaZn13
10μm

(a)

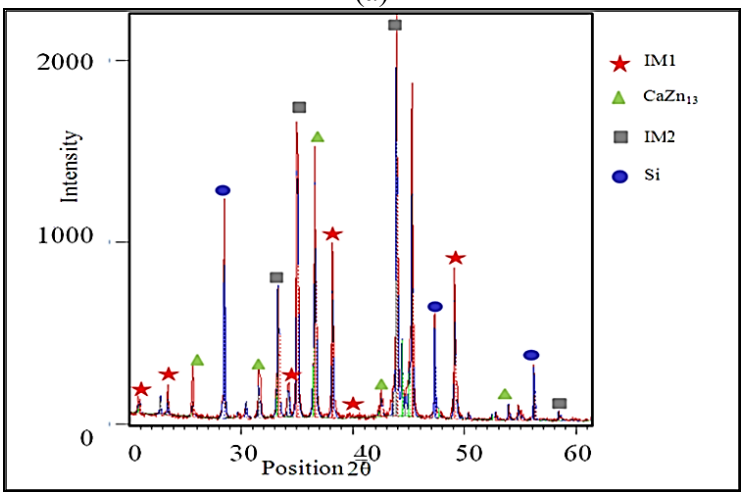
2000
1000
0
Intensity
0
30
40
50
60
Position 2θ
IM1
CaZn13
IM2
Si

(b)

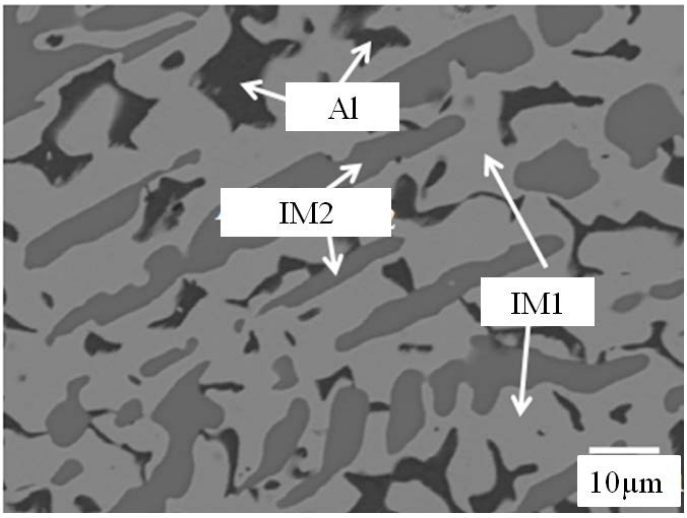
Al
IM2
IM1
10μm

(c)

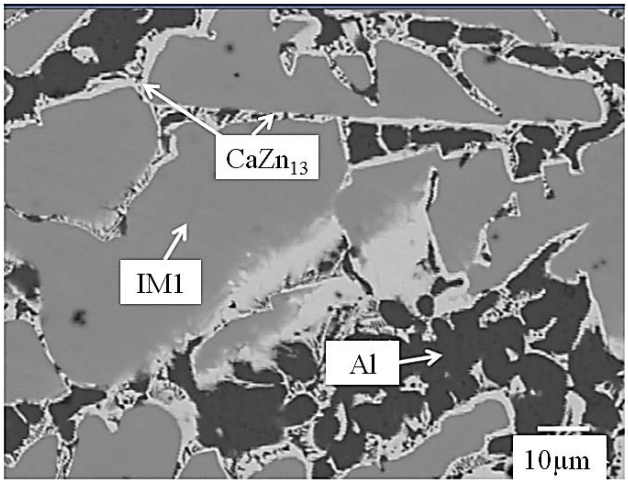

(d)

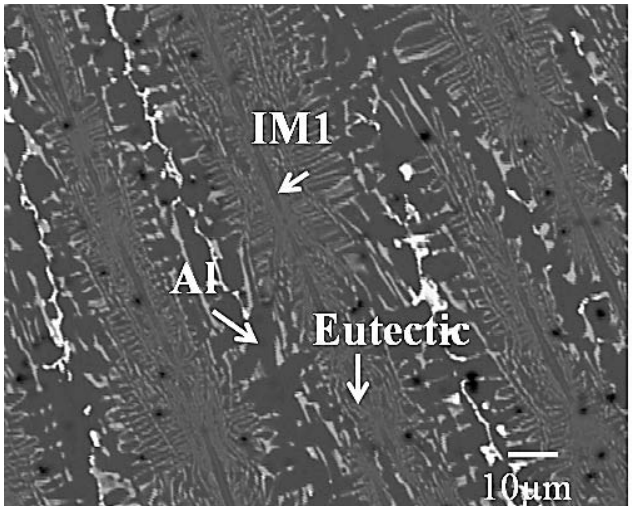

(e)

Figure 4.13: (a) Microstructures of KS1 (b) XRD-pattern of KS1 (c) Microstructures of KS2 (d) Microstructures of KS3 (e) Microstructures of KS4

Combining the EPMA results of the solid-solid diffusion couple and above four key alloys, the actual compositions of IM1 and its complete homogeneity range have been determined. Furthermore, refinement of the XRD patterns has been carried out by Reitveld analysis. The results obtained from the analysis of KS1 to KS4 have been superimposed on the Al-Ca-Zn phase diagram revealing all the existent phasesas shown in Figure 4.14.

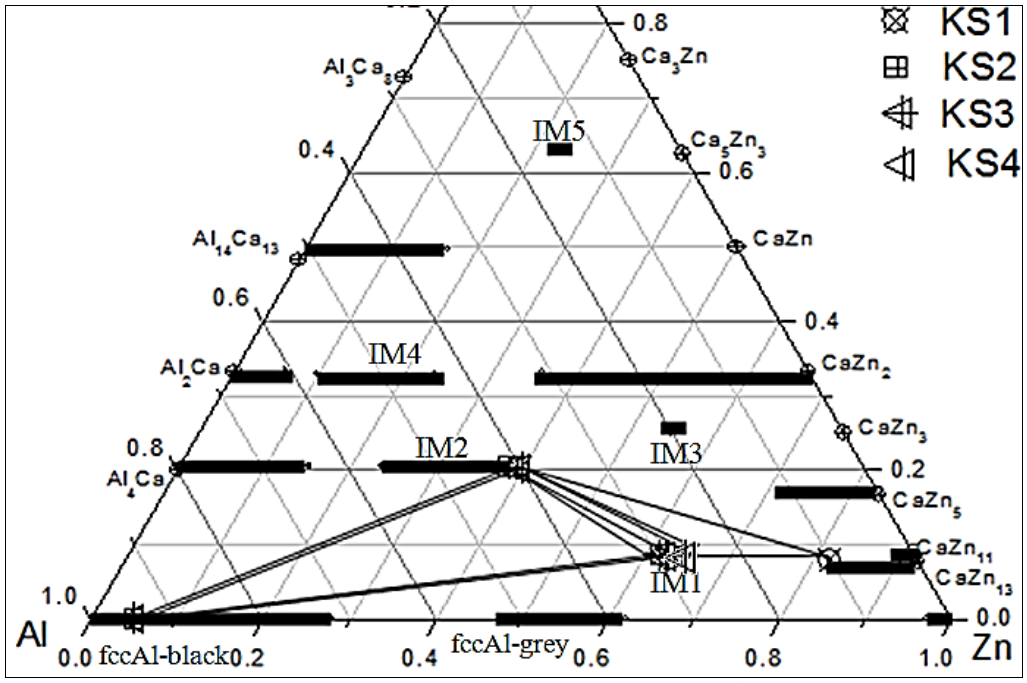

Figure 4.14: The phases of the Al-Ca-Zn system at 350°C showing the results obtained from KS1 to KS4

4.3.2 Homogeneity ranges of IM2, IM3 and $CaZn_5$ and phase relations among IM2, IM3, IM4, $CaZn_2$ and $CaZn_5$ phases

In order to study the phase boundaries of the new ternary compound IM3 and the phase relations among IM2, IM3, IM4, $CaZn_2$ and $CaZn_5$, eight ternary key alloys (KS5 to KS12) have been prepared. The microstructures of these alloys and XRD patterns are illustrated in Figure 4.15. The compositions and phase identification of these samples are summarized in Table 4.3.2-1. The actual chemical compositions of the alloys are measured by ICP and the compositions of IM2, IM3, IM4, $CaZn_2$ and $CaZn_5$ compounds have been measured quantitatively by EPMA. The phase relations obtained from EPMA are consistent with those from XRD.

Back-scattered electron image of sample KS5 annealed at 350ºC for 6 weeks is presented in Figure 4.15. The microstructure of KS5 reveals that the sample contains four phases, which indicates that the sample is not in global equilibrium, which may be due to the peritectic IM3 compound. $CaZn_5$ compound forms congruently at 691ºC. Then IM3 ternary compound forms peritectically from $CaZn_5$. During solidification, $CaZn_5$ solid solution precipitates as a primary phase. After heat treatment at 350ºC for 6 weeks, $CaZn_5$ should transform to IM3 solid solution, but the decomposition process was not complete. It would take a considerable amount of time for all of the $CaZn_5$ to transfer to IM3 compound due to the sluggish decomposition process. From this key sample, it is found that IM3 has 4.5 at.% solubility in the ternary where the limiting compositions of this solid solution are $Al_{24.6}Ca_{25.1}Zn_{50.3}$ and $Al_{20.1}Ca_{23.9}Zn_{56.0}$ respectively.

The solubility of IM2 compound has been determined from KS6, KS7, KS9 and KS10. The microstructures and xrd patterns of these key alloys are depicted in Figure 4.16, 4.17, 4.18 and 4.19. The maximum solubility of IM2 has been determined with the approximate composition $Al_{40}Ca_{20}Zn_{40}$ in the Zn-rich side, which is consistent with the reuslts obtained from diffusion couples. The maximum solubility of the IM4 phase has been detected from KS9 with the composition $Al_{43.5}Ca_{33.4}Zn_{23.1}$,which is similar to the results obtained from the diffusion couples. Among the binary phases, the maximum solubility of $CaZn_5$ has been determined from KS6 to be 9.6 at% of Al with the composition $Al_{9.6}Ca_{17.2}Zn_{73.2}$. Another binary compound $CaZn_2$ has a solid solubility of 31.1 at% Al with the composition $Al_{31.1}Ca_{33.4}Zn_{35.6}$, All of the binary compounds showing extended solid solubility in the ternary show good agreement with the results

determined from the diffusion couples. The XRD patterns of KS6 to KS9 are given in from Figure 4.16 to Figure 4.21. However, inspite of a considerable amount of affort has been used to prepare an IM3-phase dominent sample, the attempts were not successful probably due to the peritectic reaction from binary $CaZn_5$ to IM3 compound. From the experiments, it has been observed that the formation of IM3 phase is quite sluggish and the annleaing time and temperature was not high enough for thecompletion of the peritectic reaction. Hence it has been difficult to obtain a sample very richof IM3 phase. The compositions of the equilibriating phases from KS5 to KS12 are shown is Figure 4.22 along with equiibrium tie lines.

Table 4.3.2-1: Chemical composition of key alloys from ICP and the equilibrium phases

Key alloys	Composition from ICP (at.%)	Phases from EPMA	Phase composition	Phases from XRD
KS5	$Al_{20.2}Ca_{29.6}Zn_{50.2}$	IM3	$Al_{24.6}Ca_{25.1}Zn_{50.3}$	Not available
			$Al_{20.1}Ca_{23.9}Zn_{56.0}$	
		IM4	$Al_{45.3}Ca_{33.3}Zn_{21.4}$	
		$CaZn_5$	$Al_{8.8}Ca_{17.5}Zn_{73.7}$	
KS6	$Al_{21.4}Ca_{20.7}Zn_{57.9}$	IM2	$Al_{40.6}Ca_{20.2}Zn_{39.2}$	IM2
		IM3	$Al_{21.8}Ca_{25.7}Zn_{52.5}$	IM3
		$CaZn_5$	$Al_{9.6}Ca_{17.2}Zn_{73.2}$	$CaZn_5$
KS7	$Al_{24.7}Ca_{27.1}Zn_{48.2}$	IM2	$Al_{40.1}Ca_{20.3}Zn_{39.6}$	IM2
		$CaZn_2$	$Al_{31.1}Ca_{33.4}Zn_{35.6}$	$CaZn_2$
		IM3	$Al_{20.6}Ca_{25}Zn_{54.4}$	IM3
		IM4	$Al_{45.3}Ca_{33.5}Zn_{20.1}$	IM4
KS8	$Al_{25.3}Ca_{28.4}Zn_{46.3}$	IM3	$Al_{20.4}Ca_{25.5}Zn_{54.1}$	IM3
		$CaZn_2$	$Al_{40.5}Ca_{20.5}Zn_{39}$	$CaZn_2$
KS9	$Al_{38.1}Ca_{29.3}Zn_{32.6}$	IM2	$Al_{20.1}Ca_{25.8}Zn_{55.1}$	IM2
		IM3	$Al_{28.3}Ca_{33.6}Zn_{38.1}$	IM3
		IM4	$Al_{43.5}Ca_{33.4}Zn_{23.1}$	IM4
		$CaZn_5$	$Al_{8.6}Ca_{17.2}Zn_{74.2}$	$CaZn_5$
KS10	$Al_{41.1}Ca_{31.3}Zn_{27.6}$	IM3	$Al_{21.9}Ca_{26.4}Zn_{51.7}$	Not available
		IM4	$Al_{47.9}Ca_{33.6}Zn_{18.5}$	
		$CaZn_2$	$Al_{31.9}Ca_{33.7}Zn_{34.4}$	
KS11	$Al_{41.1}Ca_{31.3}Zn_{27.6}$	IM2	$Al_{38.8}Ca_{19.6}Zn_{41.6}$	Not available
		IM3	$Al_{21.1}Ca_{26.1}Zn_{53.8}$	
		IM4	$Al_{49.3}Ca_{33.2}Zn_{17.5}$	
		$CaZn_5$	$Al_{8.3}Ca_{16.5}Zn_{75.1}$	
KS12	$Al_{12.5}Ca_{17.5}Zn_{70}$	IM2	$Al_{38.8}Ca_{19.6}Zn_{41.6}$	IM2
		IM3	$Al_{21.1}Ca_{26.1}Zn_{53.8}$	IM3
		$CaZn_5$	$Al_{8.3}Ca_{16.5}Zn_{75.1}$	$CaZn_5$

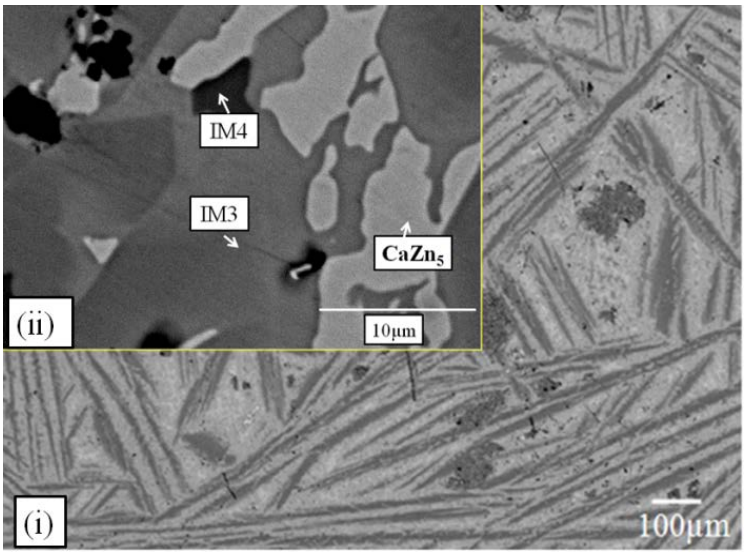

Figure 4.15: Microstructure of KS5 (i)general (ii)Magnified

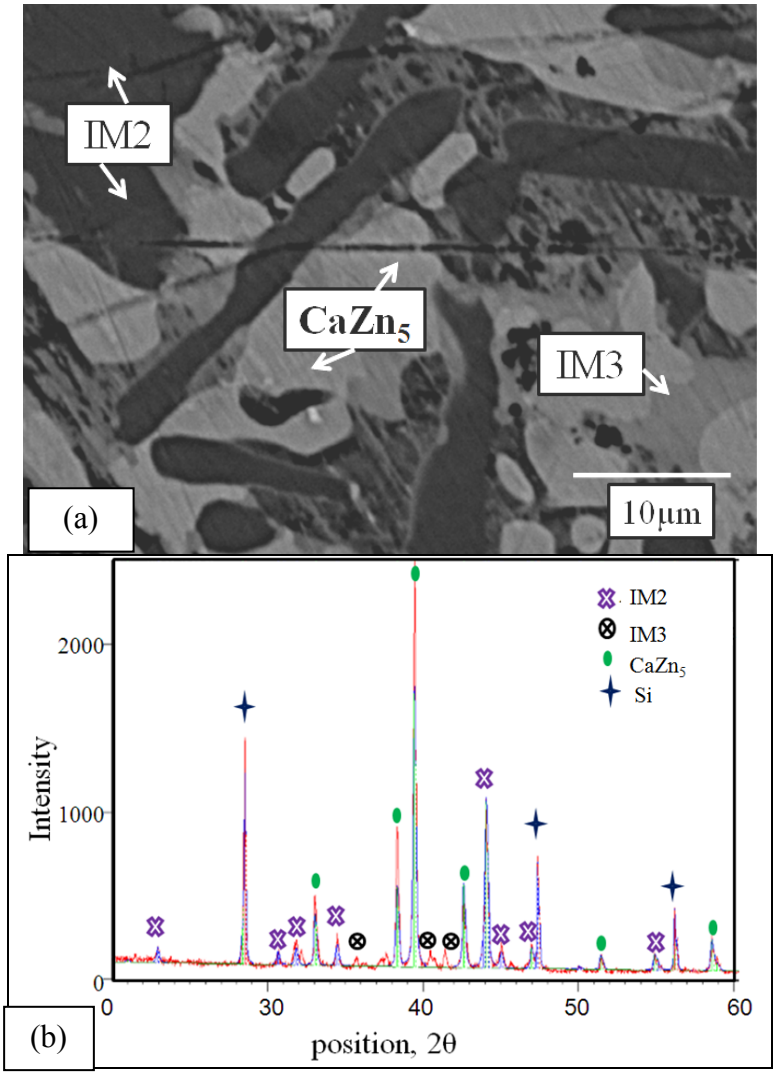

Figure 4.16: (a) Microstructure and (b) XRD pattern of KS6

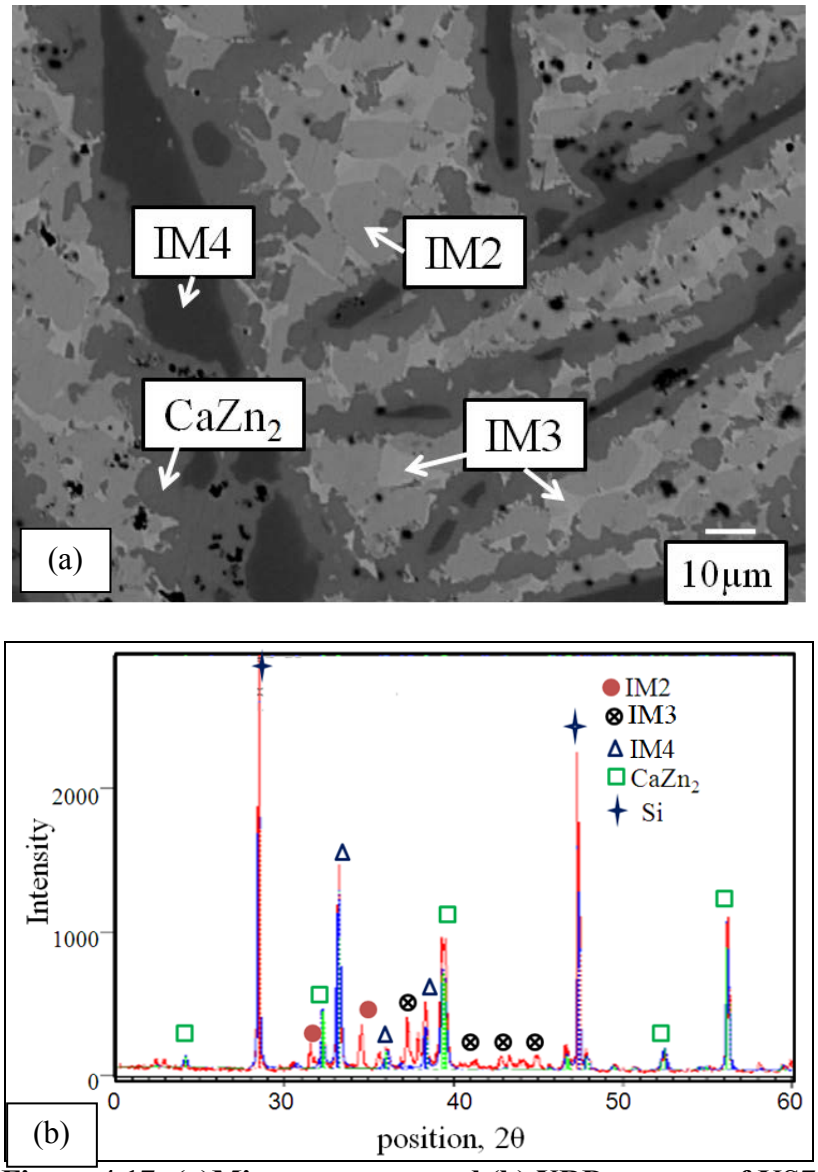

Figure 4.17: (a)Microstructure and (b) XRD pattern of KS7

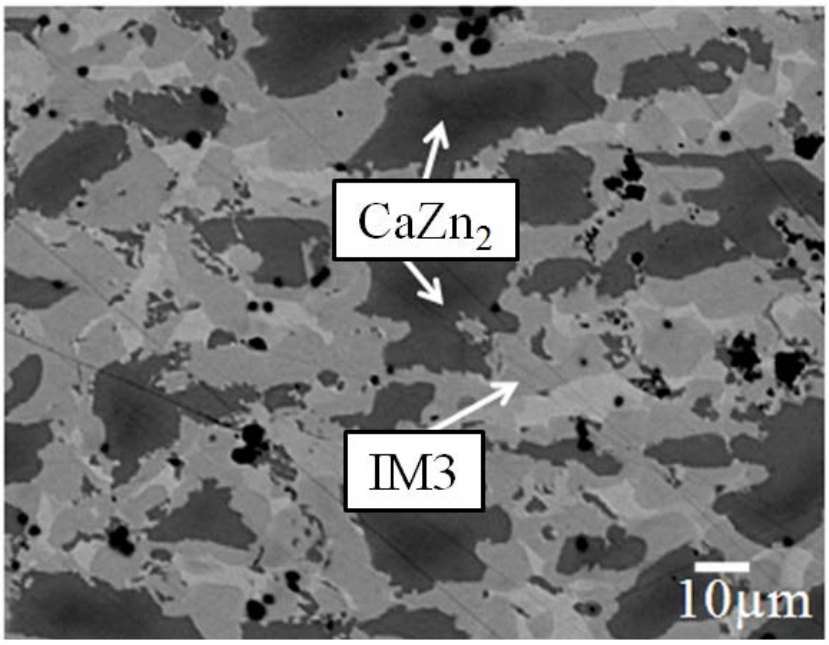

(a)

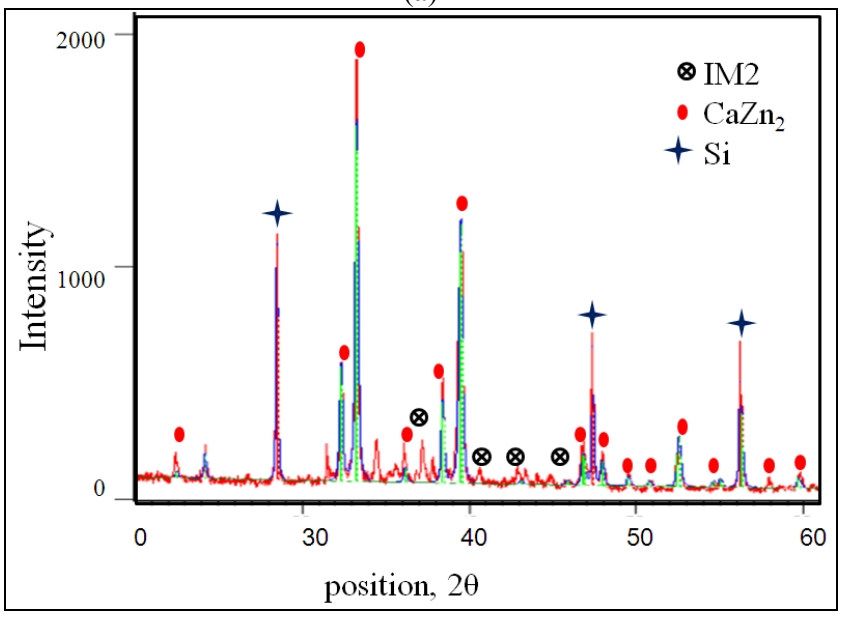

(b)

Figure 4.18: (a) Microstructure and (b) XRD pattern of KS8

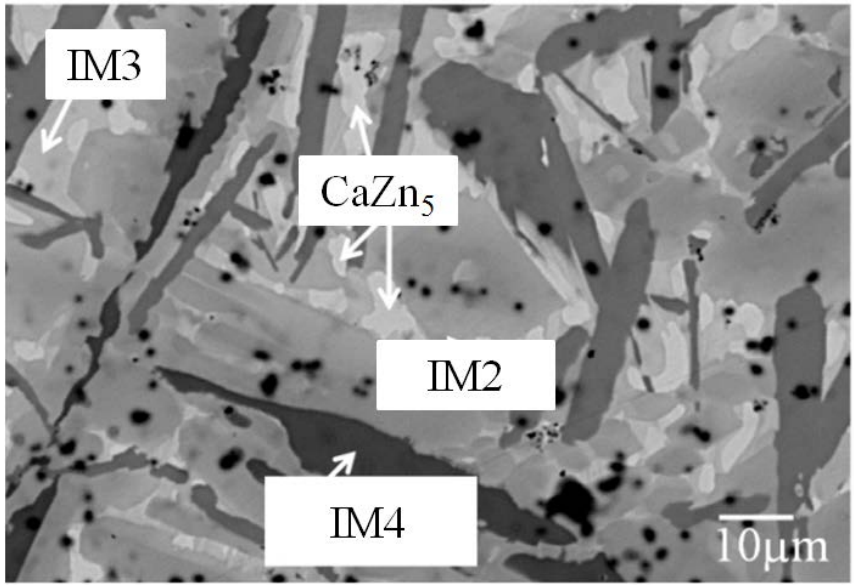

(a)

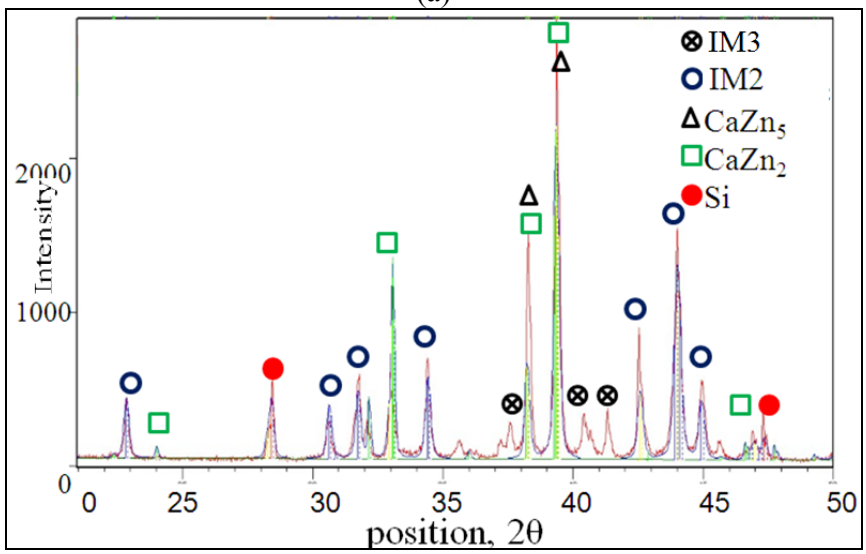

(b)

Figure 4.19: (a) Microstructure and (b) XRD pattern of KS9

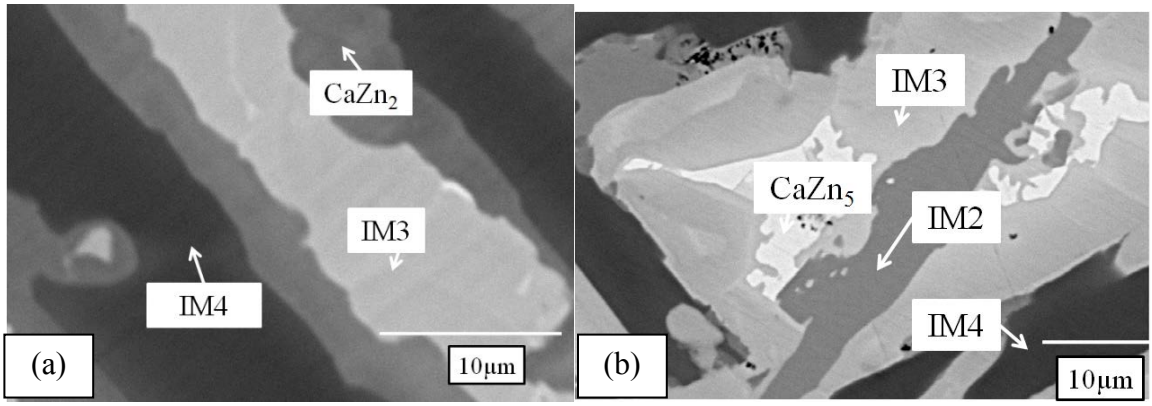

Figure 4.20: Microstructures of (a) KS10 (b) KS11

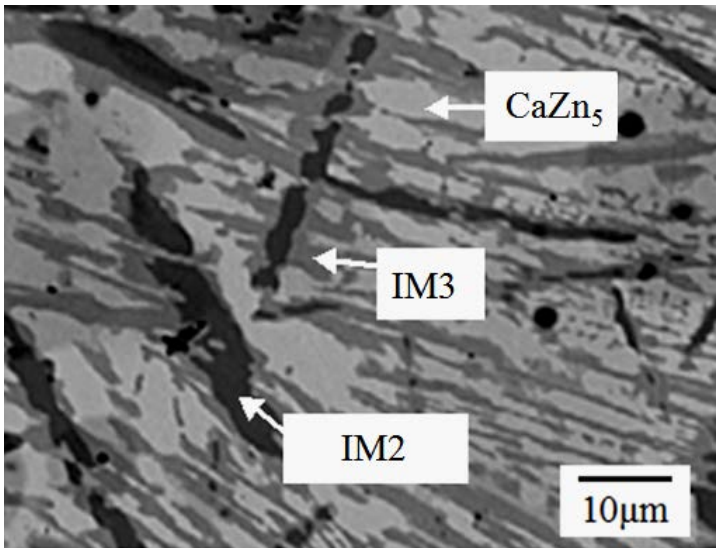

(a)

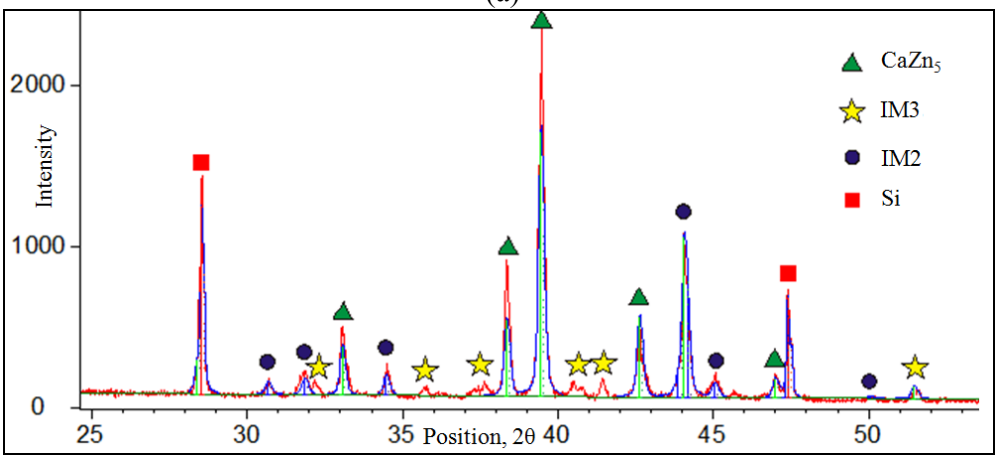

(b)

Figure 4.21: (a) Microstructure and (b) XRD pattern of KS12

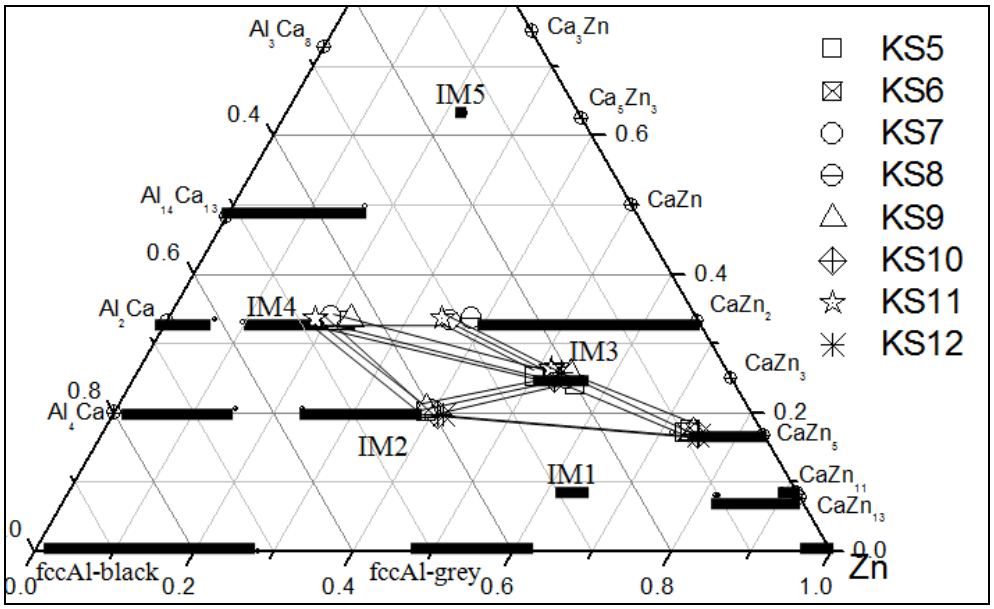

Figure 4.22: Phase equilibriums and homogeneity ranges of different phases obtained from KS5 to KS12

4.3.3 Homogeneity ranges and phase relationship between IM4, IM5, $Al_{14}Ca_{13}$, Al_2Ca and $CaZn_2$ phases

4 key alloys have been prepared to study the phase relationships and homogeneity ranges of IM4, IM5, $Al_{14}Ca_{13}$, Al_2Ca and $CaZn_2$ phases. The actual compostions of these alloys have been measured by ICP and tabulated in Table 4.3.3-1.

Table 4.3.3-1: Chemical composition of key alloys from ICP and the equilibrium phases

Key alloys	Composition from ICP (at.%)	Phases from EPMA	Phase composition	Phases from XRD
KS13	$Al_{36.4}Ca_{36.3}Zn_{27.3}$	IM4	$Al_{43.5}Ca_{33}Zn_{23.5}$	IM4
		IM5	$Al_{18}Ca_{62}Zn_{20}$	
		$CaZn_2$	$Al_{31}Ca_{33.3}Zn_{35.7}$	$CaZn_2$
KS14	$Al_{50.8}Ca_{37.1}Zn_{12.1}$	$Al_{14}Ca_{13}$	$Al_{38.1}Ca_{49.5}Zn_{12.4}$	Not available
		Al_2Ca	$Al_{60.7}Ca_{33.4}Zn_{5.9}$	
		IM4	$Al_{58}Ca_{33}Zn_9$ to $Al_{43.5}Ca_{33}Zn_{23.5}$	
		$CaZn_2$	$Al_{31.2}Ca_{33.4}Zn_{35.4}$	
KS15	$Al_{42.7}Ca_{47.2}Zn_{10.1}$	IM4	$Al_{54.5}Ca_{34.3}Zn_{11.2}$	IM4
		$Al_{14}Ca_{13}$	$Al_{37}Ca_{49}Zn14$	$Al_{14}Ca_{13}$
		IM5	$Al_{18.6}Ca_{62}Zn_{19.4}$	
KS16	$Al_{33.2}Ca_{50.9}Zn_{15.9}$	IM4	$Al_{55.4}Ca_{34.3}Zn_{10.3}$	Not available
		$Al_{14}Ca_{13}$	$Al_{36.3}Ca_{49}Zn_{18.5}$	
		IM5	$Al_{19.3}Ca_{63}Zn_{17.7}$	

The key sample (KS13) has been prepared and annealed at 350ºC for 1 weekto determine the solubility limit of $CaZn_2$and IM4 at 350ºC. The sample has been found to be consisting of three phases: IM4, IM5 and $CaZn_2$. It is expected that $Al_{14}Ca_{13}$would form between IM4 and IM5, but the annealing time was not adequete owing to the sluggish formation of this compound. It is observed from Figure 4.23(a) that $CaZn_2$ is a peritectic phase of IM4. A line scan was performed to determine the homogeniety ranges of IM4

and $CaZn_2$. The compositional profile of the30μm line scan with 10 EPMA points is presented in Figure 4.24(b). The maximum solubility of $CaZn_2$ was determined to be 31 at%. Al by EPMA where Al substitutes for Zn, which is consistent with the liturature [94, 95]. The solubility limitin the Zn-rich side of IM3 was determined by EPMA to be 43.5 at% Al through least-squares approximation at the interface of IM4 and $CaZn_2$. Hence the composition of IM4was obtained to be $Al_{43.5}Ca_{33}Zn_{23.5}$ from the EPMA line scan. The XRD pattern of KS13 is illustrated in Figure 4.23(c). The XRD data was analyzed by Rietveld method. IM5 is not detected in the XRD pattern due to its small relative amount in this alloy. KS14 was prepared to determine the homogeneity ranges of Al_2Ca and IM4. The sample was annealed for 5 weeks at 350ºC and analyzed by EPMA. The microstructure is presented in Figure 4.24(a) and (b). The microstructure of KS14 reveals that the sample contains four different phases, which indicates that the sample is not in global equilibrium owing to the two peritectic phases: IM4 and $CaZn_2$. The Al_2Ca compound forms at 1075ºC [94], then the ternary solid solution IM4 forms peritectically from Al_2Ca and after that $CaZn_2$ compound forms peritectically from IM4 solid solution [94]. During solidification, Al_2Ca solid solution precipitates as a primary phase. After heat treatment at 350ºC for 5 weeks, Al_2Ca should transform to IM4 solid solution, but the decomposition process was not complete. It would take a considerable amount of time for all of the Al_2Ca to transfer to IM4 phase. However due to the relatively low heat treatment temperature and the thermal stability of Al_2Ca, solid-state decomposition process is very sluggish. Complete equilibrium must be very difficult to obtain in this sample. Nonetheless, this sample is used to determine the phase relations between and the solubility limits of the constituent phases assuming that local equilibrium is achieved

between the adjacent phases. EPMA line scan (Figure 4.24(c)) was carried out to determine the homogeneity ranges of the Al_2Ca and IM4 compounds at 350ºC in Figure 4.24(b). The region between $CaZn_2$ and Al_2Ca grains is considered as a micro-diffusion couple with a local equilibrium between the layers. The result shows Al_2Ca has a maximum solubility of 5.9 at% Zn. IM4 phase has a homogeneity range from $Al_{58}Ca_{33}Zn_9$ to $Al_{43.5}Ca_{33}Zn_{23.5}$ and $CaZn_2$ phase has a maximum solubility of 31 at% Al. The results are consistent with those of KS13 and show close agreement with the values reported in the literature [94, 95]. KS15 and KS16 were prepared to investigate the new phase IM5 and the homogeneity ranges of $Al_{14}Ca_{13}$. From both samples, IM5 was found to be a congruent melting compound with the chemical composition $Al_9Ca_{31}Zn_{10}$. This phase contains approximately 62%. Figures 4.25(a) and (b) demonstrate the morphology of the phases contained in the key samples KS15 and KS16, respectively. The homogeneity range and crystal structure of $Al_{14}Ca_{13}$ in the KS15 and KS16 were determined using EPMA and XRD. The solid solubility limit was found to be 18 at% Zn. The XRD pattern of KS15 was analyzed using Rietveld method in combination with Pearson's crystallographic database [100], as presented in Figure 4.19(c). It was found from Rietveld analysis that the peak positions of $Al_{14}Ca_{13}$ solid solution shifted to a higher 2θ angle with decreasing Al content. The unit cell parameters of the $Al_{14}Ca_{13}$ solid solution decrease compared with the binary $Al_{14}Ca_{13}$ compound [12] due to the Zn substitution for Al atoms which has a larger atomic radius, as shown in Table 4.3.3-2. The results obtained from KS13 to KS16 are summarized in Figure 4.26.

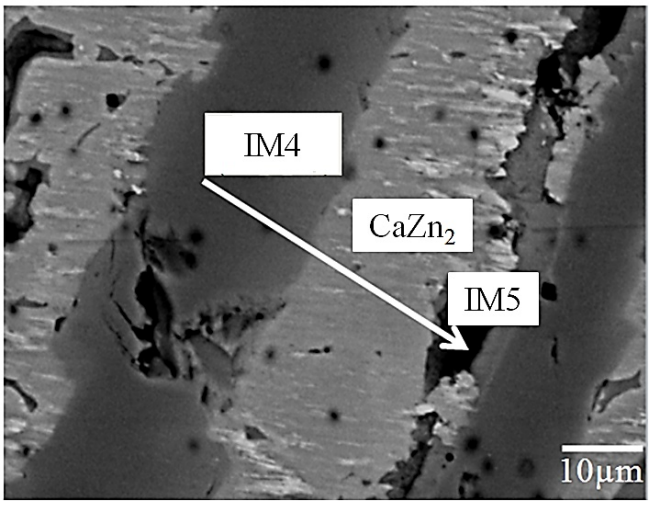

(a)

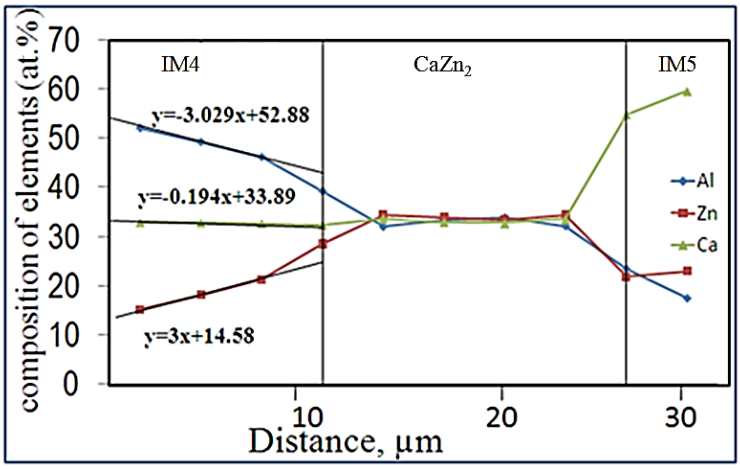

(b)

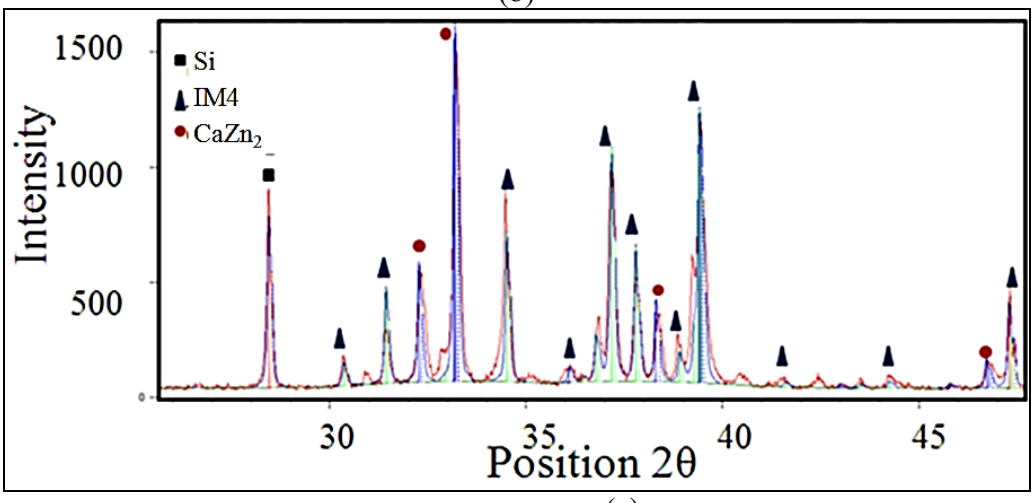

(c)

Figure 4.23: (a) The microstructure, (b) EPMA line scan profile, (c) the XRD pattern of KS13

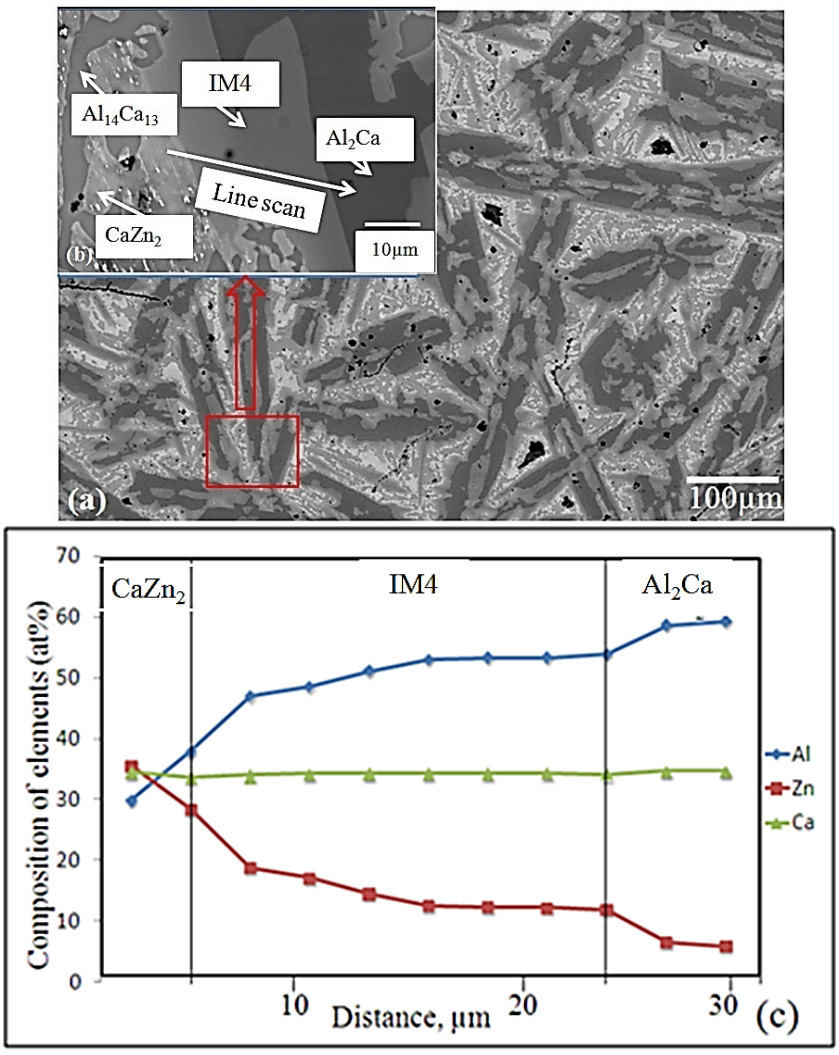

Figure 4.24: (a) Microstructure of KS14 after 5 weeks annealing at 350ºC, (b) higher magnified microstructure with EPMA line scan, (c) EPMA line scan profile.

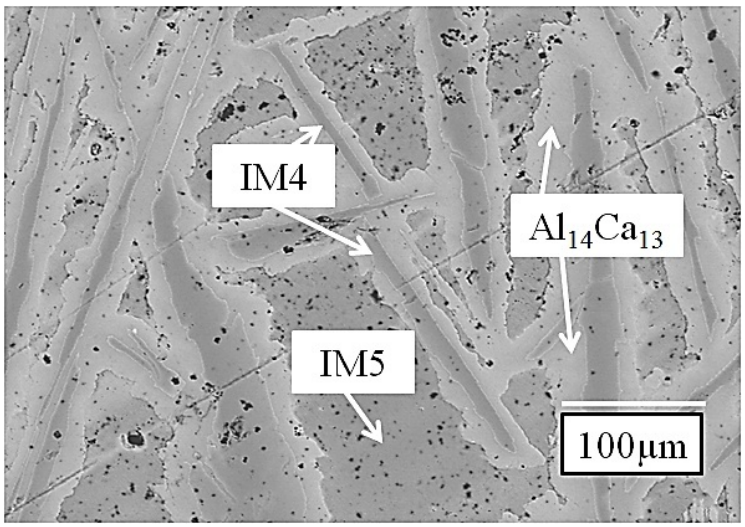

(a)

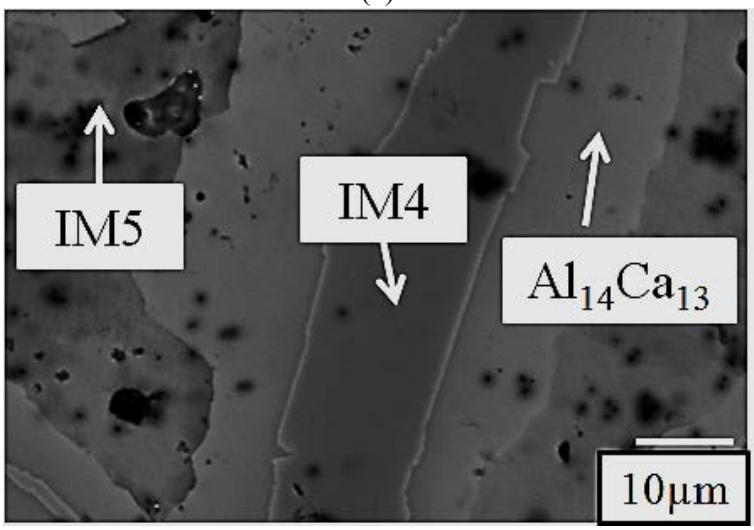

(b)

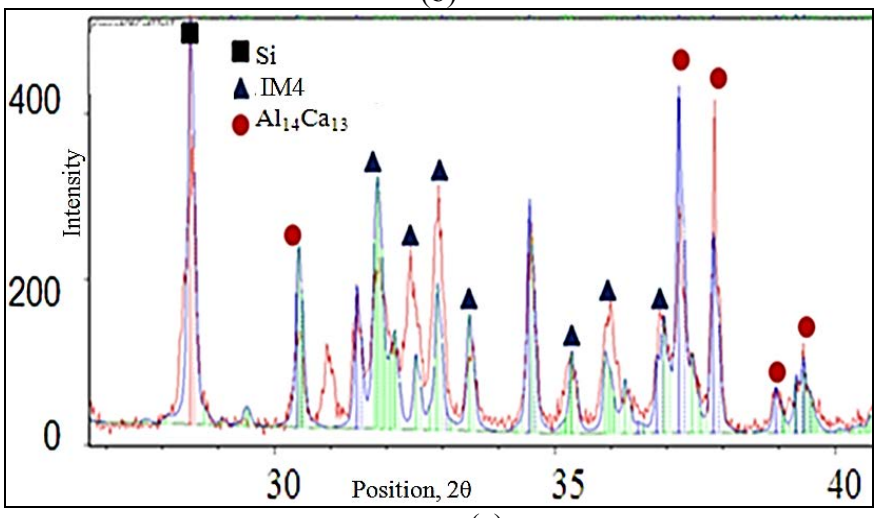

(c)

Figure 4.25: (a) The microstructure of KS15, (b) the microstructure of KS16, (c) the XRD pattern of KS15

Table 4.3.3-2: The comparison of the unit cell parameters for the $Al_{14}Ca_{13}$ binary compound

Unit cell parameter (Å)	a	b	c
This work	15.362	9.919	9.612
[28]	15.551	9.873	9.614

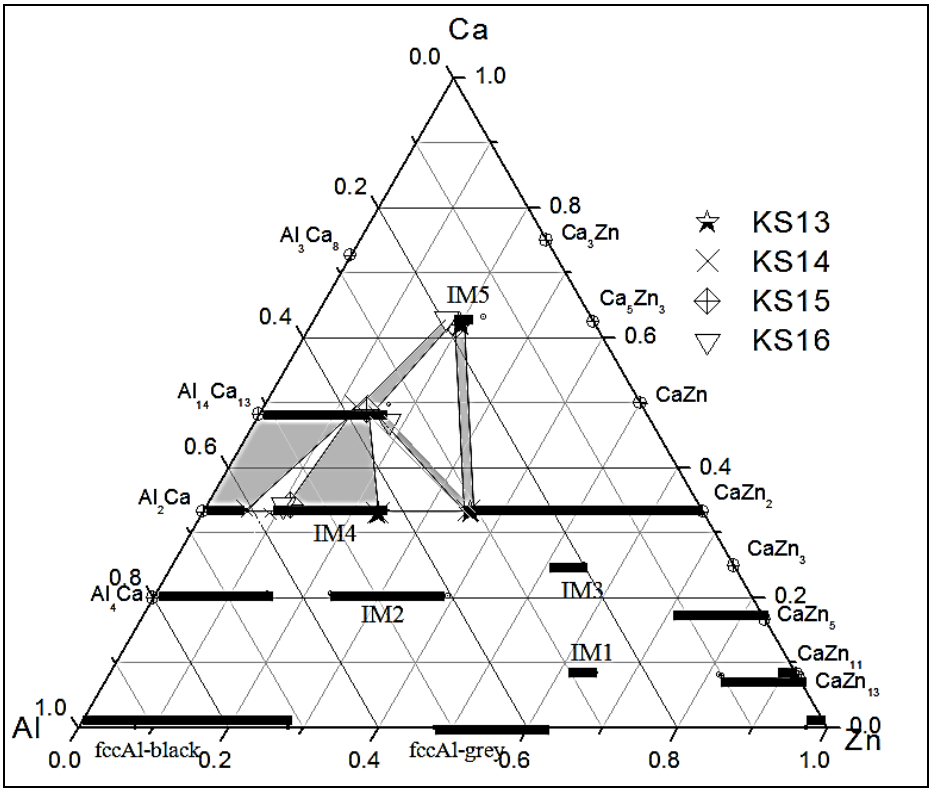

Figure 4.26: Phase equilibriums and homogeneity ranges of different phases obtained from KS13 to KS16

4.3.4 The phase relationship between $CaZn_3$ and $CaZn_2$

One more key alloy has been designed to check the homogeneity ranges of $CaZn_3$ and phase relation between $CaZn_3$ and $CaZn_3$. The actual composition for KS17 has been determined to be $Al_{20.7}Ca_{19.8}Zn_{59.5}$ from ICP. From this key alloy, the solubility of $CaZn_3$ has been found to be 6.3 at% Al at the composition $Al_{6.3}Ca_{27.2}Zn_{66.5}$ and the phase is in equilibrium with $CaZn_2$. The microstructure of this key alloy is illustrated in Figure 4.27.

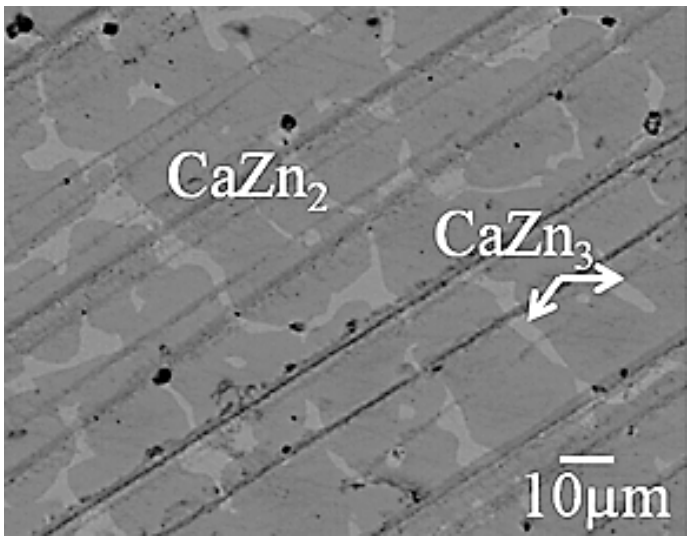

Figure 4.27: Microstructure of KS17

4.4: The Al-Ca-Zn isothermal section at 350°C

The isothermal section of the Al-Ca-Zn ternary system has been constructed at 350^{o}C as shown in Figure 4.28(a) based on the results obtained from 5 diffusion couples and 26 key alloys. The phase diagram has been compared with the isothermal section drawn using the thermodynamic database constructed by Wasiur-Rahman [19] as illustrated in Figure 4.28(b). The results obtained have also been compared with the experimental data from the literature. Since this study was carried out at lower temperature than reported in the literature, direct comparison was not possible. Therefore, the pseudobinary Al_2Ca-$CaZn_2$ phase diagram was constructed using data of Söderberg et al. [95] and the current experimental data. As illustrated in Figure 4.29, this work is in excellent agreement with the data of [95].

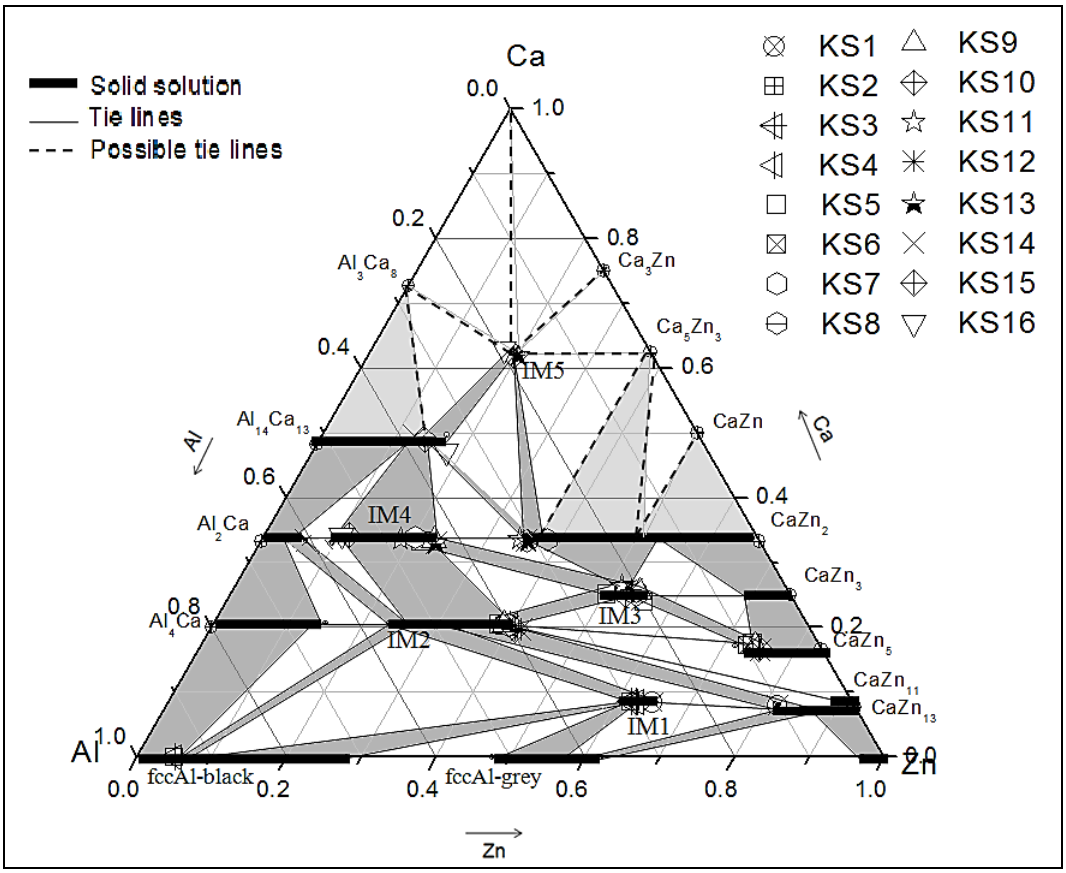

(a)

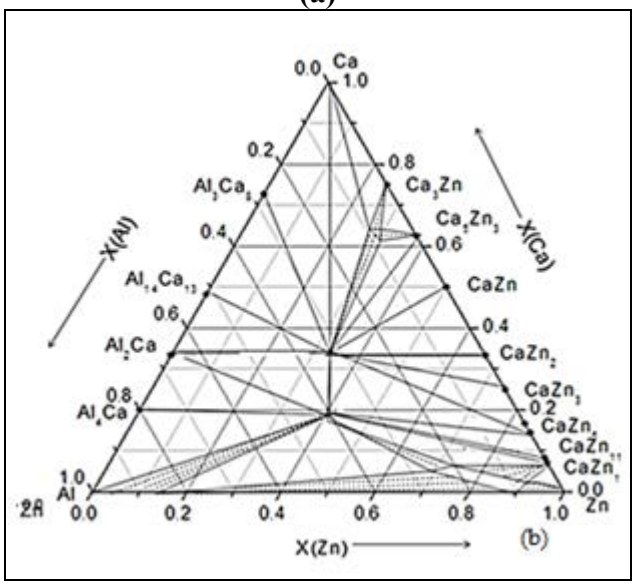

(b)

Figure 4.28: (a) The isothermal section of the Al-Ca-Zn system at 350ºC based on the current experimental work, (b) The isothermal section of the Al-Ca-Zn system based on the thermodynamic database of Wasiur-Rahman [19]

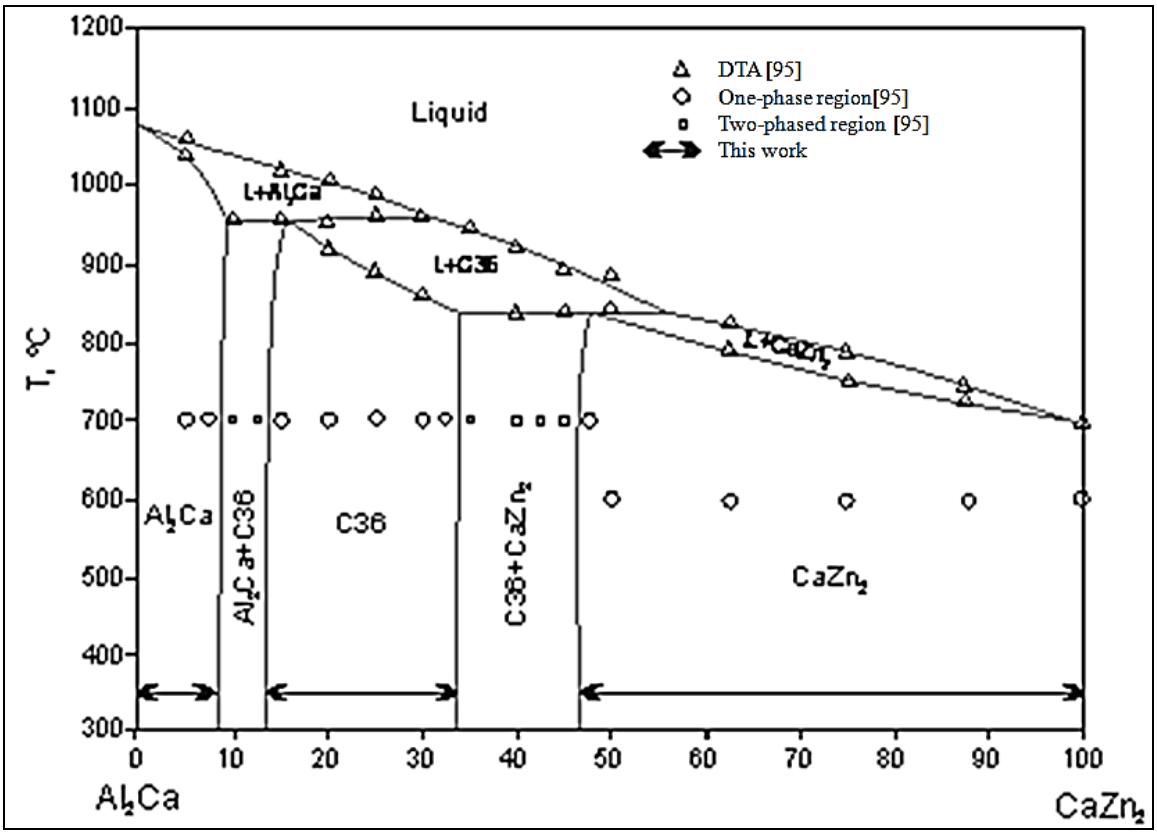

Figure 4.29: The pseudobinary Al_2Ca-$CaZn_2$ phase diagram constructed using data of Söderberg et al. [95] and experimental data from this work.

CHAPTER 5

CONCLUSION

5.1. Concluding remarks

A combination of diffusion couple technique and selected equilibrated key alloys have been used to construct the Al-Ca-Zn isothermal section at 350ºC. Phase relations, homogeneity ranges and crystallographic information have been determined for binary and ternary compounds using EPMA and XRD techniques. The new ternary compounds IM1, IM3 and IM5 have been studied for the first time and their homogeneity ranges at 350^{o}C have been determined. The formula of IM1 compound is $Al_xCa_{8.4}Zn_y$ ($26 \leq x \leq 29$, $62 \leq y \leq 65$at 350ºC) at 350°C. It has cubic structure with $Pm\bar{3}m$ (221) space group and $BaHg_{11}$ prototype. The composition and homogeneity ranges of previously reported two ternary compounds; IM2 and IM4 at 350^{o}C have also been studied and compared with the literature. Among the binary compounds, $Al_{14}Ca_{13}$, Al_2Ca, Al_4Ca, $CaZn_2$, $CaZn_3$, $CaZn_5$, $CaZn_{11}$ and $CaZn_{13}$ have extended solubility in the ternary system.

5.2 Contribution

The significant contributions of the present work are summarized below:

- Detailed investigation has been carried out throughout the whole compositional range of the Al-Ca-Zn system at 350^{o}C and possible phases, phase relationships and tie lines have been identified. These findings have substantially improved the

understanding of the Al-Ca-Zn Al-Ca-Zn system and will be helpful to improve the thermodynamic model of this system.

- Five ternary compounds have been confirmed in this work; among them, only two were previously known. This discovery will be very useful for the design of certain alloys for industrial applications.

- The solid solubility and crystal structure of the new ternary compound IM1 has been determined and confirmed by means of EPMA and XRD for the first time in this work.

5.2 Future works

- Additional experimental work is necessary to determine the crystal structure information of the new ternary compounds IM2 and IM3. To obtain the crystal structure of IM2, longer annealing time of the alloys containing this compound IM2 is recommended.

- DSC experiments are needed to determine the melting points of the ternary compounds.

REFERENCES

[1] D. Uffelmann, Aluminium Alloy for Superplastic Forming, *ATZproduktionworldwide*, Edition 2010-02.Retrieved from http://www.atzonline.com/index.php;do=show/site=a4e/sid=12294570014d0aabbc6f3dc569162208/alloc=3/id=11160

[2] L. Chappuis; K. Zengen, New Ideas for Aluminium Parts, *ATZautotechnology*, Edition 2004-02. Retrieved from http://www.atzonline.com/index.php;do=show/site=a4e/sid=1657738624d214b18e0f95509209016/alloc=3/id=2155

[3] G. Piatti, G. Pellegrini, R. Trippodo, The tensile properties of of a new superplastic aluminium alloy: Al-Al_4Ca eutectic, *Journal of Materials Science*, Vol. 11, Issue 1, 1976, pp. 186-190

[4] D.M. Moore, L.R. Morris, A new superplastic aluminum sheet alloy, *Material Science and Engineering*, Vol. 43,Issue 1, 1980, pp. 85-92.

[5] M.T. Perez-Prado, J. Ibanez, M.C. Cristina, M.A. Morris-Munoz, O.A. Ruano, G. Gonzalez-Doncel, Texture Evolution of the Tetragonal Al_3CaZn Phase in Al-5%Ca-5%Zn Superplastic Sheet Alloy after Annealing and Deformation, *Materials Transactions*, Vol. 40, Issue 9, 1999, pp. 1011-1014.

[6] V.A. Shvets, V.O. Lavrenko, V.M. Talash, Experience of application of protectors made of Al-Zn-Ca alloys, *Journal of Materials Science*, Vol. 42, Issue 4, 2006, pp. 563-565.

[7] D. Wenwen, S. Yangshan, M. Xuegang, X. Feng, Z. Min, W. Dengyun, Microstructureand mechanical properties of Mg–Al based alloy with calcium and rare earth additions, *Materials Science and Engineering*, Vol. 356, Issue 1-7, 2003, pp. 1-7.

[8] Y.A. Chang, S. Chen, F. Zhang, X. Yan, F. Xie, R. Schmid-Fetzer, W.A. Oates, Phase Diagram Calculation: Past, Present and Future, *Progress in Materials Science*, Vol.49, 2004, pp.313-345.

[9] L. Donski, Alloys of Calcium with Zinc, Cadmium, Aluminum, Thallium, Lead, Tin, Bismuth, Antimony and Copper, *Zeitschrift Für Anorganische und Allgemeine Chemie,* Vol. 57, 1908, pp. 185-193.

[10] K. Matsuyama, On the Equilibrium diagram of the Al-Ca system, Scientific Reports, Tohoku University, Vol. 17, 1928, pp.783-789.

[11] D. Kevorkov, R. Schmid-Fetzer, The Al-Ca system, Part 1: Experimental Investigation of Phase equilibria and crystal structures, *Zeitschrift Für Metallkunde***,** Vol. 92, 2001, pp. 946-952.

[12] B. Huang, J. D. Corbett, Two new binary Calcium-Aluminum compounds: $Ca_{13}Al_{14}$, with a novel Two-Dimensional aluminum network, and Ca_8Al_3, and Fe_3Al-Type, *Inorganic Chemistry*, Vol. 37, 1998, pp. 5827-5833.

[13] H. Nowotny , E. Wormnes , E. Mohrnheim , Investigation on the Al-Ca, Mg-Ca and Mg-Zr Systems, *Zeitschrift Für Metallkunde*, Vol. 32, 1940, pp. 39-42.

[14] M. Notin, J. C. Gachon, J. Hertz, Thermodynamic data for calcium-based alloys from a new galvanic method, *CALPHAD (Computer Coupling of Phase Diagrams and Thermochemistry)*, Vol. 6, Issue1, 1982, pp. 49-56.

[15] D. Kevorkov, R. Schmid-Fetzer, A. Pisch, F. Hodaj and C. Colinet., The Al-Ca system, Part 2: Calorimetric Measurements and Thermodynamic Assessment, *Zeitschrift Für Metallkunde*, Vol. 92, 2001, pp. 953-958.

[16] M. Aljarrah and M. Medraj, Thermodynamic Assessment of the Phase Equilibria in the Al-Ca-Sr System using the Modified Quasichemical Model, *Journal of Chemical Thermodynamics*, Vol. 40, No. 4, 2008, pp.724-734.

[17] F. Sommer, J.J. Lee and B. Predel, Thermodynamic Investigation of Liquid Al- Ca, Al-Sr, Mg-Ni and Ca-Ni Alloys, *Zeitschrift fur Metallkunde*, Vol.74, 1983, pp.100-104.

[18] Y.O. Esin, V.V. Litovski, S.E. Demin, M.S. Petrushevski, Enthalpies of Formation of Aluminum-Strontium and Barium-Silicon Melts, *Russian Journal of Physics and Chemistry*, Vol.59, 1985, pp. 446.

[19] S. Wasiur-Rahman, Thermodynamic Modeling of the (Mg, Al)-Ca-Zn Systems, M.A.Sc Thesis in Mechanical and Industrial Engineering, 2008, Concordia University: Montreal, QC, Canada.

[20] K. T. Jacob, S. Srikanth, Y. Waseda, Activities, concentration fluctuations and complexing in liquid Ca-Al alloys, *Transactions of the Japan Institute of Metals*, Vol.29, 1988, pp. 50-59.

[21] E. Schürmann, C.P. Fünders, H. Litterscheidt, Vapor pressure of Ca above Ca-Si, Ca-Al and Ca-Al-Si alloys, *Arch. Eisenhuttenews*., Vol. 46, 1975, pp. 473-476.

[22] K. Ozturk, L.Q. Chen, Z.-K.Liu, Thermodynamic Assessment of the Al-Ca Binary System Using Random Solution and Associate Models, *Journal of Alloys and Compounds*, Vol. 340, No.1-2, 2002, pp.199-206.

[23] S. Wasiur-Rahman, M. Medraj, A thermodynamic description of the Al-Ca-Zn ternary system, *CALPHAD (Computer Coupling of Phase Diagrams and Thermochemistry)*, Vol. 30, 2009, pp. 584-598.

[24] R. Paris, Ternary Alloys, *Publications Scientifiques et Techniques du minist'ere de L'Air, Ministère de L'Air*, No.45, 1934, pp. 1-86.

[25] A.F. Messing, M.D. Adams and R.K. Steunenberg, Contribution to the Phase Diagram Calcium-Zinc, *Transactions of the ASM.*, Vol. 56, 1963, pp. 345-350.

[26] V.P. Itkin and C.B. Alcock, The Ca-Zn System, *Bulletin of Alloy Phase Diagrams*, Vol. 11, Issue 4, 1990, pp. 328-333.

[27] G. Bruzzone, E. Franceschi and F. Merlo, M_5X_3 Intermediate Phases Formed by Ca, Sr and Ba, *Journal of the Less-Common Metals*, Vol. 60, 1978, pp. 59-63.

[28] M.L. Fornasini and F. Merlo, $CaZn_3$: a structure with mixed $BaLi_4$- and $CeCu_2$-like ordering, *Acta Crystallograpica*, Vol. B36, 1980, pp. 1739–1744.

[29] J.A.A. Ketelaar, The Crystal Structure of Alloys of Zinc with the Alkali and Alkaline Earth Metals and of Cadmium with Potassium, *Journal of Chemical Physics*, Vol. 5, 1937, pp. 668.

[30] A. Iandelli and A. Palenzona, Zinc-rich phases of the rare earth zinc alloys, *Journal of the Less-Common Metals*, Vol. 12, 1967, pp. 333–343.

[31] W. Haucke, The Crystal Structure of $CaZn_5$ and $CaCu_5$, *Zeitschrift für Anorganische und Allgemeine Chemie*, Vol. 244, 1940, pp.17-22.

[32] M. Wendorff and C. Röhr, Zink-reiche Erdalkalimetall-Verbindungen AZn_5 und AZn_{11}: Kristallstrukturen und chemische Bindung, *Zeitschrift für Naturforschung*, Vol. 62b, 2007, pp.1549–1562.

[33] G.E.R. Schulze and J. Wieting, The Structural Characteristics of The $CaZn_2$ Lattice, *Zeitschrift für Metallkunde*, Vol. 52, 1961, pp. 743-746.

[34] M.L. Fornasini, F. Merlo and K. Schubert, Crystal structures of Ca_3Zn and CaZn, *Journal of the Less-Common Metals,* Vol. 79, 1981, pp. 111-119.

[35] H.W. King, Temperature-dependent Allotropic Structures of the Elements, *Bull. Alloy Phase Diagrams*, Vol. 3, 1982, pp. 275-276.

[36] H.W. King, Pressure-dependent Allotropic Structures of the Elements, *Bull. Alloy Phase Diagrams*, Vol. 2, 1981, pp. 401-402.

[37] C.O. Brubaker and A. Zi-Kui Liu, Computational thermodynamic assessment of the Ca–Zn system, *CALPHAD (Computer Coupling of Phase Diagrams and Thermochemistry)*, Vol. 25, Issue 3, 2001, pp. 381–390.

[38] H. Okamoto and T. B. Massalski, Thermodynamically improbable phase diagrams. *Journal of Phase Equilibria*, Vol. 12, Issue 2, 1991, pp. 148–168.

[39] P.J. Spencer, A.D. Pelton, Y-B Kang, P. Chartrand, C.D. Fuerst, Thermodynamic assessment of the Ca–Zn, Sr–Zn, Y–Zn and Ce–Zn system, *CALPHAD (Computer Coupling of Phase Diagrams and Thermochemistry)*, Vol. 32, Issue 2, 2008, pp. 423-431.

[40] S. Wasiur-Rahman and M. Medraj, Critical assessment and thermodynamic modeling of the binary Mg–Zn, Ca–Zn and ternary Mg–Ca–Zn systems, *Intermetallics*, Vol. 17, Issue 10, 2009, pp. 847-864.

[41] P. Chiotti and R.J. Hecht, Thermodynamic Properties of the Calcium-Zinc System, *Transactions of the Metallurgical Society of AIME*, Vol. 239, 1967, pp. 536-542.

[42] J. Delcet and J.J. Egan, Thermodynamics of Liquid Ca-Zn Alloys, *Metalallurgical Transactions B*, Vol. 9B, Issue 4, 1978, pp.728-729.

[43] C.T. Heycock, F.H. Neville, The freezing points of alloys containing zinc and another metal, *Journal of the Chemical Society Transactions*, Vol. 71,1897, pp. 383-398.

[44] T. Isihara, On the equilibrium diagram of the aluminum-zinc system, *Science, Reports of the Tohoku Imperial University*, Vol. 13, 1924, pp. 18-21.

[45] T. Tanabe, Studies in the aluminum-zinc system, *Journal of the Institute of Metals*, Vol. 32, 1924, pp. 415-427.

[46] M.L.V. Gayler, M. Haughton, E.G. Sutherland, The constitution of aluminum-zinc alloys of high purity: The nature of the thermal change of 443^{o}C, *Journal of the Institute of Metals*, Vol. 63, 1938, pp.123-147.

[47] E. Pelzel, H. Schneider, Contribution to the understanding of Zn alloys, *Zeitschrift für Metallkunde*, Vol. 35, 1943, pp. 124-127.

[48] T. Morinaga, On the equilibrium diagram of the aluminum-zinc system, *Nippon Kinzoku Gakkaishi*, Vol. 3, 1939, pp. 216-221.

[49] E. Butchers, W. Hume-Rothery, On the constitution of aluminum-magnesium-manganese-zinc alloys: The solidus, *Journal of the Institute of Metals*, Vol. 71, 1945, pp. 291-311.

[50] E. Pelzel, The positions of the liquidus and solidus curves in the Al-Zn system from 30 to 70 wt.% Al, *Zeitschrift für Metallkunde*, Vol. 40, 1949, pp. 134-136.

[51] I.S. Solet, H.W.S. Clair, Liquidus temperatures and liquid densities of zinc-aluminum alloys, *Bureau of Mines Report of Investigations 4553*, 1949, pp. 1-7.

[52] Q.F. Peng, F.S. Chen, B.S. Qi, Y.S. Wang, Measurement of aluminum-zinc phase diagram by acoustic emission during solidification, *Transactions of the American Foundrymen's Society*, Vol. 99, 1991, pp. 199-202.

[53] E. Gebhardt, Equilibrium experiments on the systems zinc-aluminum and zinc-aluminum-copper, *Zeitschrift für Metallkunde*, Vol. 40, 1949, pp. 136-140.

[54] E.C. Ellwood, The solid solutions of zinc in aluminum, *Journal of the Institute of Metals*, Vol. 80, 1951, pp. 217-224.

[55] H. Araki, Y. Minamino, T. Yamane, K. Azuma, Y.S Kang, Y Miyamoto, Partial phase diagrams of the aluminum-rich region of the aluminum-zinc system at 0.1 MPa and 2.1 GPa, *Journal of Materials Science Letters*, Vol. 11, Issue 3, 1992, pp. 181-183.

[56] W.L Fink, L.A. Willey, Equilibrium relations in aluminum-zinc alloys of high purity, II, *Transactions of the Metallurgical Society of AIME*, Vol. 12, 1936, pp. 244-260.

[57] M. Simerska, P. Bartuska, The X-ray diffraction and electron microscopic investigation of stable and metastable equilibria in Al-rich Al-Zn alloys, *Czech Journal of Physics*, Vol. B24, 1974, pp. 553-559.

[58] G. Borelius, L.E. Larsson, Kinetics of precipitation in aluminum-zinc alloys, *Arkivför Matematik, Astronomioch Fysik*, Vol. 35A, Issue 13, 1948, pp. 1-14.

[59] A. Münster, K. Sagel, Miscibility gap and critical point of the aluminum-zinc system, *Zeitschriftfür Physikalische Chemie*, Vol. 7, 1956, pp. 267-295.

[60] H. Terauchi, N. Sakamoto, K. Osamura, Y. Murakami, Small angle X-ray critical scattering in an aluminum-zinc alloy with critical composition, *Transactions of the Japan Institute of Metals*, Vol. 16, Issue 7, 1975, pp. 379-383.

[61] J.M. Holender, J. Soltys, The studies of the eutectoidal decomposition of Al-59 at.% Zn at the temperature close to the critical temperature, *Diffusion and Defect Data-Solid State Data, Pt. A: Defect and Diffusion Forum*, Vol. 66-69, 1989, pp. 1461-1466.

[62] L.E. Larsson, Pre-precipitation and precipitation phenomena in the Al-Zn system, *Acta Metallurgica*, Vol. 15, 1967, pp. 35-44.

[63] W.M. Pierce, M.S. Palmerton, Studies on the constituent of binary zinc-based alloys, *Transactions of the Metallurgical Society of AIME*, Vol. 68, 1923, pp. 767-795.

[64] H. Auer, K.E. Mann, Magnetic investigation of the aluminum-zinc system, *Zeitschrift für Metallkunde*, Vol. 28, 1936, pp. 323-326.

[65] M.L. Fuller, R.L. Wilcox, Phase changes during aging of zinc-alloy die castings, II-Changes in the solid solution of aluminum in zinc and their relation to dimensional

changes, *Transactions of the Metallurgical Society of AIME*, Vol. 122, 1936, pp. 231-246.

[66] A. Burkhardt, Zinc alloys as a substitute material, *Zeitschrift für Metallkunde*, Vol. 28, Issue 10, 1936, pp. 299-308.

[67] K. Lohberg, X-ray determination of the solubility of aluminum and copper in zinc, *Zeitschrift für Metallkunde*, Vol. 32, 1940, pp. 86-90.

[68] W. Hoffman, G. Fahrenhost, Precipitation rates in high purity zinc-aluminum and zinc-copper alloys, *Zeitschriftfür Metallkunde*, Vol. 42, 1950, pp. 460-463.

[69] A. Pasternak, The solidsolubility of metals in lead and zinc, *Bulletin International de l'Academie Polonaise des Sciences et des Lettres*, *Classe des Sciences Mathematiques et Naturelles, Serie A: Sciences Mathematiques Serial A,* 1951, pp.177-192.

[70] J.L. Murray, The Aluminum-Zinc System, *Bulletin of Alloy Phase Diagrams*, Vol. 4, Issue 1, 1983, pp.55-73.

[71] S.A. Mey and G. Effenberg, A Thermodynamic Evaluation of the Aluminum-Zinc System, *Zeitschrift für Metallkunde*, Vol.77, Issue 7 1986, pp. 449-453.

[72] S.A. Mey, Re-evaluation of the Aluminum-Zinc System, *Zeitschrift für Metallkunde*, Vol.84, Issue 7, 1993, pp. 451-455.

[73] S.L. Chen and Y.A. Chang, A Thermodynamic Analysis of the Al-Zn System and Phase Diagram Calculation, *CALPHAD*, Vol.17, Issue 2, 1993, pp.113-124.

[74] P.S Rudman and B.L Averbach, X-ray measurements of local atomic arrangements in aluminum-zinc and in aluminum-silver solid solutions, *Acta Metallurgica*, Vol. 2, Issue 4, 1954, pp. 576-582.

[75] F.E. Wittig, G. Keil, Heats of mixing of binary liquid aluminum-B-metal alloys (zinc, cadmium, indium, thallium, tin, lead and bismuth), *Zeitschrift für Metallkunde*, Vol. 54, Issue 10, 1963, pp. 576-590.

[76] J.E. Hilliard, B.L. Averbach, M. Cohen, Thermodynamic properties of solid Aluminum-zinc alloys, *Acta Metallurgica*, Vol. 2, 1954, pp. 621-631.

[77] H. Corsepius, A. Münster, On the thermodynamic properties of solid aluminum-zinc alloys, *Zeitschrift für Physikalische Chemie*, Vol. 22, 1959, pp. 1-19.

[78] R.E. Wittig, L. Schoffl, Heat of formation in the aluminum-zinc system at 330, 370 and 430^{o}C, *Zeitschrift für Metallkunde*, Vol. 51, 1960, pp. 700-707.

[79] R.A. Connell, D.B. Downie, The enthalpies of formation of α-phase Al-Zn alloys, *Metal Science Journal*, Vol. 7, 1973, pp. 12-14.

[80] G. Batalin, E.A. Beloborodova, The activity of Al in the liquid, *Russian Metallurgy*, Vol. 4, 1968, pp. 121-125.

[81] B. Predel, U. Schallner, On the thermodynamic properties of binary aluminum alloys containing gallium and zinc, *Zeitschrift für Metallkunde*, Vol. 60, Issue 11, 1969, pp. 869-877.

[82] J. Sebkova, M. Beranek, Application of the EMF method for measurement of aluminum activities in liquid aluminum alloys, *Sbornik Vysoke Skoly Chemicko-Technologicke v Praze, B: Anorganicka Chemie a Technologie*, Vol. B18, 1974, pp. 217-225.

[83] G.J. Lutz, A.F. Voigt, A radioactive tracer dew point method for measuring vapor pressures of binary alloys, the zinc-aluminum system, *Journal of Physical Chemistry*, Vol. 67, Issue 12, 1963, pp. 2795-2799.

[84] P. Bolsaitis, P.M. Sullivan, The activity of zinc in liquid Zn-Al alloys from isopiestic measurements, *Transactions of the Metallurgical Society of AIME*, Vol. 245, 1969, pp. 1435-1438.

[85] A. Yazawa, Y.K. Lee, Thermodynamic studies of the liquid aluminum alloy systems, *Transactions of the Japan Institute of Metals*, Vol. 11, Issue 6, 1970, pp. 411-418.

[86] W. Ptak, L. Zabdyr, Determination of thermodynamic properties of aluminum-zinc solid solutions by EMF measurements, *Archiwum Hutnictwa*, Vol. 16, Issue 3, 1971, pp. 253-267.

[87] R.E. Miller, J.L. Straalsund, D.B. Masson, The effect of electron concentration on the thermodynamic properties of two alloy phases in the Al-Zn-Ag system, *Metallurgical Transactions*, Vol. 3, 1971, pp. 545-550.

[88] V. Piacente, V.D. Paolo, G. D'Ascenzo, The activity of zinc in solid Al-Zn alloys, *Thermochimica Acta*, Vol. 16, 1976, pp. 63-68.

[89] T. Takahashi, N. Asano, Thermodynamic studies of solid aluminum-zinc alloys, Niihama Kogyo Koto SenmonGakko Kiyo, Rikogaku-hen, Vol. 18, 1982, pp. 78-84.

[90]]N. Kono, Y. Tsuchida, S. Muromachi and H. Watanabe, Study of the Al-Ca-Zn ternary phase diagram, *Light Metals*, Vol. 35, 1985, pp.574-580.

[91] G. Cordier, E. Czech and H. Schafer, $CaAl_2Zn_2$, The First Example of an "Inverse" $ThCr_2Si_2$ Structure, *Zeitschrift für Naturforschung, Teil B: Anorganische Chemie, Organische Chemie*, Vol. 39B, Issue 12,1984, pp.1629-1632.

[92] I.N. Ganiev, M. S. Shukroev and K.M. Nazarov, Effect of phase composition on the electrochemical behavior ofAluminum-Zinc-Calcium alloys, *Zhurnal Prikladnoi Khimii*, Vol. 68, Issue 10, 1995, pp.1646-1649.

[93]I.N. Gantsev, K.M. Nazarov, M.M. Khakdodov and N.I. Gantseva, Interaction of binary eutectics in Al Zn-Ca (Sr, Ba) Systems, *Evtektika V, Mizhnarodna Konferentsiya, Dnepropetrovsk*, National Metallurgical Academy of Ukraine, Dnepropetrovsk, Ukraine, 2000, pp.56-58.

[94] M. Pani, L. Fornasini, D. Mazzone and F. Merlo, Structural features of intermetallic phases in the Ca-Zn-Al system, *Zeitschrift für Kristallographie*, Vol. 224, 2009, pp.397–406

[95] K. Söderberg, M. Bostrom, Y. Kubota, T. Nishimatsu. R. Niewa, U. Häussermann, Y. Grin, and O. Terasaki, Crystal structures and phase stability in pseudobinary $CaAl_{2-x}Zn_x$, *Journal of Solid State Chemistry*, Vol. 179, Issue 8, 2006, pp. 2690–2697.

[96] M. Pani, L. Fornasini and F. Merlo,The $CaAg_2$—$CaZn_2$—$CaAl_2$ pseudoternary system: crystal structures and structural stability, *Zeitschrift für Kristallographie*: Vol. 222, Issue 5, 2006, pp. 218-225.

[97] K. Söderberg, Y. Kubota, N. Muroyama, D. Grüner, A. Yoshimura and O. Terasak, Electron charge distribution of $CaAl_{2-x}Zn_x$: Maximum entropy method combined with Rietveld analysis of high-resolution-synchrotron X-ray powder diffraction data, *Journal of Solid State Chemistry*, Vol. 181, Issue 8, 2008, pp. 1998-2005.

[98] A.A. Kodentsov, G.F. Bastin, and F.J.J. van Loo, The Diffusion Couple Technique in Phase Diagram Determination, *Journal of Alloys and Compounds*, Vol. 320, Issue 2, 2001, pp. 207-217.

[99] Y. Zhang, D. Kevorkov, F. Bridierand M. Medraj, Experimental study of the Ca–Mg–Zn system using diffusion couples and key alloys, *Science and Technology of Advanced Materials*, Vol. 12,2011, 025003.

[100] Inductively Coupled Plasma Atomic Emission Spectrometer (ICP-AES), Analytical Chemistry Laboratory Manual, Concordia College, 2012. Retrieved from http://www.cord.edu/dept/chemistry/analyticallabmanual/experiments/icpaes/intro.html

[101] John Goodge, Electron Probe Micro-analyzer (EPMA), Integrating Research and Education, Carleton College, 2012. Retrieved from http://serc.carleton.edu/research_education/geochemsheets/techniques/EPMA.html

[102] Celeste Morris, Bradley Sieve, Heather Bullen, Introduction to X-Ray Diffraction. Retrieved from http://www.asdlib.org/onlineArticles/ecourseware/Bullen_XRD

[103] H. Putz, K. Brandenburg, Pearson's Crystal Data, Crystal Structure Database for Inorganic Compounds, CD-ROM software version 1.3.